U.S. DEPARTMENT OF ENERGY

PNNL-19018

Prepared for the
U.S. Nuclear Regulatory Commission
under a Related Services Agreement
with the U.S. Department of Energy
Contract DE-AC05-76RL01830

Technical Letter Report

An Evaluation of Ultrasonic Phased Array Testing for Reactor Piping System Components Containing Dissimilar Metal Welds

JCN N6398, Task 2A

AA Diaz
AD Cinson
SL Crawford
MT Anderson

November 2009

Pacific Northwest
NATIONAL LABORATORY

Proudly Operated by Battelle Since 1965

DISCLAIMER

PACIFIC NORTHWEST NATIONAL LABORATORY
operated by
BATTELLE
for the
UNITED STATES DEPARTMENT OF ENERGY
under Contract DE-AC05-76RL01830

Printed in the United States of America

Available to DOE and DOE contractors from the
Office of Scientific and Technical Information,
P.O. Box 62, Oak Ridge, TN 37831-0062;
ph: (865) 576-8401
fax: (865) 576-5728
email: reports@adonis.osti.gov

Available to the public from the National Technical Information Service,
U.S. Department of Commerce, 5285 Port Royal Rd., Springfield, VA 22161
ph: (800) 553-6847
fax: (703) 605-6900
email: orders@ntis.fedworld.gov
online ordering: http://www.ntis.gov/ordering.htm

This document was printed on recycled paper.
(9/2003)

PNNL-19018

Technical Letter Report

An Evaluation of Ultrasonic Phased Array Testing for Reactor Piping System Components Containing Dissimilar Metal Welds

JCN N6398, Task 2A

AA Diaz
AD Cinson
SL Crawford
MT Anderson

November 2009

Prepared for the
U.S. Nuclear Regulatory Commission
under the U.S. Department of Energy
Contract DE-AC05-76RL01830

Pacific Northwest National Laboratory
Richland, Washington 99352

Executive Summary

Research is being conducted for the U.S. Nuclear Regulatory Commission at the Pacific Northwest National Laboratory to assess the effectiveness and reliability of advanced nondestructive examination (NDE) methods for the inspection of light-water reactor components. The scope of this research encompasses primary system pressure boundary materials including dissimilar metal welds (DMWs), cast austenitic stainless steels (CASS), piping with corrosion-resistant cladding, weld overlays, inlays and onlays, and far-side examinations of austenitic piping welds. A primary objective of this work is to evaluate various NDE methods to assess their ability to detect, localize, and size cracks in steel components that challenge standard and/or conventional inspection methodologies. This interim technical letter report (TLR) provides a summary of a technical evaluation aimed at assessing the capabilities of phased-array (PA) ultrasonic testing (UT) methods as applied to the inspection of small-bore DMW components that exist in the reactor coolant systems (RCS) of pressurized water reactors (PWRs). Operating experience and events such as the circumferential cracking in the reactor vessel nozzle-to-RCS hot leg pipe at V.C. Summer nuclear power station, identified in 2000, show that in PWRs where primary coolant water (or steam) are present under normal operation, Alloy 82/182 materials are susceptible to pressurized water stress corrosion cracking (PWSCC) (NRC 2008b, 2009). The extent and number of occurrences of DMW cracking in nuclear power plants (domestically and internationally) indicate the necessity for reliable and effective inspection techniques. The work described herein was performed to provide insights for evaluating the utility of advanced NDE approaches for the inspection of DMW components such as a pressurizer (PZR) surge nozzle DMW, a shutdown cooling pipe DMW, and a ferritic (low-alloy carbon steel)-to-CASS pipe DMW configuration.

In this study, a set of flaws, including both thermal fatigue cracks and electrical discharge machining (EDM) notches that were hot isostatically pressed (HIP'ed) were inserted into five DMW mock-up specimens. The DMW specimens used in this study were either salvaged from a cancelled plant that had never been in an operational state, or were fabricated from new and/or vintage materials. PA-UT flaw responses from these cracks were used to evaluate detection and characterization performance. The PA-UT examination approach used on the DMW component mock-ups focused on acquiring data as a function of inspection frequency (2.0 MHz, 1.5 MHz, and 1.0 MHz), inspection angle (30° to 70° in 1° increments), and by employing both raster and line-scan data acquisition. Data were acquired from both sides of the welds; however, the focus in this document is to evaluate inspection performance by assessing the data taken from the austenitic side of the DMW configuration, as this is the side where an inspector typically has access in the field. The data analyses conducted here provide quantitative information regarding detection and sizing performance against the true state. Additional metrics used for these analyses included signal-to-noise ratio (SNR) and root-mean-square error (RMSE) for length and depth sizing. Also, a comparison of detection and sizing performance for line-scan versus raster-scan data was also conducted to determine if inspection performance is significantly enhanced by performing more rigorous and time-consuming raster scans over simple line scans. Finally, a qualitative assessment of the effect of angular flaw tilt (from the normal to the inner-diameter [ID] surface) on detection and flaw characterization performance was conducted.

The detection and sizing data showed that all of the implanted cracks in all five DMW mock-up specimens were detected from the austenitic side of the DMWs. While most of the data were acquired at inspection frequencies of 1.5 and 2.0 MHz, it was shown that 1.0-MHz data also provided suitable penetration and resolution for effective flaw detection and sizing, without compromising data quality or results. The results reported here show that longitudinal mode, transmit-receive matrix PA probes over a fairly wide frequency range can provide optimal and effective sound fields for detection and characterization of circumferential and axial flaws in smaller-bore DMW components. The flaw depths

chosen for the implanted thermal fatigue cracks (TFCs) and HIP'ed EDM notch cracks employed in this study ranged from approximately 10% through-wall to 95% through-wall. Flaw lengths ranged from approximately 19.1 mm (0.75 in.) to 72.4 mm (2.85 in.). This set of flaw dimensions (depths and lengths) provided a wide spectrum of sizes from which to assess the inspection performance and evaluate resolution and sensitivity of the PA-UT approach in these components. Approximately 75% of the flaws were positioned in the Inconel 82/182 buttering of the DMWs, while approximately 25% of the flaws were positioned in the weld material.

Signal-to-noise values were consistently acceptable (> 10 dB), spanning both raster- and line-scan data at both 1.5- and 2.0-MHz frequencies, indicating that flaw detection was not an issue. SNRs were generally above 12 dB, corresponding to a factor of 4-to-1. The data show that flaws are detectable at frequencies up to 2.0 MHz in these DMW mock-up specimens, even in the subject DMW configurations containing CASS pipe segments, where grain sizes can be as large as 41 mm (1.61 in.), with the nominal wall thickness of approximately 33 mm (1.3 in.). The higher frequency (2.0-MHz probe) was able to detect tip-diffracted energy from some of the cracks in these DMW mock-ups. Out of 24 total cracks evaluated in this study, 10 of these cracks were implanted at an angle (tilt) to the normal of the ID surface of the component, ranging from +2° to +30° from the normal. In reviewing the data provided, there was no correlation to either degradation or enhancement of flaw detection or flaw characterization performance as a function of flaw tilt. In addition, access limitations became a critical issue with specimen 9C-034, where the weld crown precluded effective coverage by limiting data acquisition with the necessary inspection angles to consistently detect and characterize the implanted flaws. From a review of the results, it can be shown that weld crown removal can indeed significantly improve ultrasonic inspection results by providing a scanning surface that enhances probe coupling and allows suitable access for volumetric weld coverage.

Results show that all flaw-length sizing fell completely within the American Society of Mechanical Engineers (ASME) Code-allowable limit while depth sizing cumulative error was outside (over) the Code-allowable value. With regard to length sizing, raster data sets better defined the flaw responses and provided greater circumferential accuracy. The raster scanned data appeared to perform better than with the finer circumferential step size in the line scan data. The 2.0-MHz raster data also outperformed the 1.5-MHz data. When the material supports a higher frequency, the resolution will be improved as the data indicate. For depth sizing, the very upper portions of the flaws nearest the outer-diameter (OD) surface were not detected. By including the four deepest flaws in the root mean square error (RMSE) calculations (three 75% TW flaws and one 95% TW flaw), cumulative sizing results for all the inspections do not pass the ASME Code RMSE acceptance limit of 3.2-mm (0.125-in.). However, if these four deeper data points are removed from the analyses, RMSE values for the 1.5-MHz raster and line scan data are: 2.9 mm, and 2.4 mm, respectively. Under these conditions, the 1.5-MHz line scan and raster data would be within the ASME Code-acceptable 3.2-mm limit for depth sizing.

In conclusion, based upon the results of this work, state-of-the-art phased-array inspection approaches are rapidly evolving and the capability to detect cracks in DMW components where the wall thickness is generally less than 50 mm (2.0 in.) has been demonstrated here. While additional questions remain to be answered, PA ultrasonic approaches, coupled with advanced signal processing technologies, are showing the capability to successfully address this challenging inspection issue.

Acronyms and Abbreviations

ASME	American Society of Mechanical Engineers
BW	bandwidth
BWR	Boiling Water Reactor
CASS	cast austenitic stainless steel
CCSS	centrifugally cast stainless steel
CE	Combustion Engineering
dB	decibels
DMW	dissimilar metal weld
EDM	electrical discharge machining
EPRI	Electric Power Research Institute
HIP	Hot Isostatic Press
ID	inner diameter
ISI	inservice inspection
LWR	light water reactor
MRP	Materials Reliability Program
NDE	nondestructive examination
NPP	nuclear power plant
NRC	U.S. Nuclear Regulatory Commission
OD	outer diameter
PA	phased array
PA-UT	phased array ultrasonic testing
PNNL	Pacific Northwest National Laboratory
PWR	pressurized water reactor
PWSCC	pressurized water stress corrosion cracking
PZR	pressurizer
RCS	reactor coolant system
RIS	Regulatory Issue Summary
RMSE	root mean square error
RT	radiographic testing
SAFT	synthetic aperture focusing technique
SCSS	statically cast stainless steel
SNR	signal-to-noise ratio
SS	stainless steel
TFC	thermal fatigue crack
TLR	technical letter report
TRL	transmit-receive longitudinal

UT	ultrasonic testing
WNP-3	Washington Nuclear Power Unit 3
WSS	wrought stainless steel

Contents

Executive Summary iii
Acronyms and Abbreviations v
1.0 Introduction 1.1
2.0 Background and Objectives 2.1
3.0 Scope of PA-UT Evaluations 3.1
4.0 The DMW Inspection Challenge 4.1
5.0 Phased-Array Probes and Focal Law Development 5.1
5.1 Ultrasonic Probe Details 5.1
5.2 Focal Law Development 5.1
5.3 2.0-MHz TRL Probe 5.2
5.4 1.5-MHz TRL Probe 5.4
5.5 1.0-MHz TRL Probe 5.6
5.6 Focal Law and Probe Information for Specimen 8C-032 ..... 5.8
6.0 Data Acquisition Set-Up and Configuration 6.1
6.1 Phase Array Data Acquisition 6.1
6.2 Phased-Array Data Acquisition on Specimen 8C-032 ..... 6.3
7.0 Specimens and Flaws Evaluated in this Study 7.1
7.1 DMW Specimen 8C–032 ..... 7.1
7.2 DMW Specimen 9C–023 ..... 7.4
7.3 DMW Specimen 8C–091 ..... 7.7
7.4 DMW Specimen 9C–034 ..... 7.10
7.5 DMW Specimen 8C-036 ..... 7.14
8.0 Data Analysis and Results 8.1
8.1 Specimen 8C-032 ..... 8.1
8.2 DMW Specimen 9C-023 ..... 8.4
8.3 DMW Specimen 8C-091 ..... 8.6
8.4 DMW Specimen 9C-034 ..... 8.10
8.4.1 With Weld Crown 8.10
8.4.2 Weld Crown Removed 8.11
8.5 DMW Specimen 8C-036 ..... 8.14
8.5.1 8C-036 After HIP 8.14
8.6 Summary of Results 8.17
9.0 Discussion and Conclusions 9.1
10.0 References 10.1
Appendix A – Dissimilar Metal Weld Specimen 8C-032 Phased-Array Data A.1
Appendix B – Dissimilar Metal Weld Specimen 9C-023 Phased-Array Data B.1

Appendix C – Dissimilar Metal Weld Specimen 8C-091 Phased-Array Data C.1
Appendix D – Dissimilar Metal Weld Specimen 9C-034 Phased-Array Data D.1
Appendix E – Dissimilar Metal Weld Specimen 8C-036 Phased-Array Data.....E.1

Figures

4.1 Digital Photograph Illustrating Geometry, Grain Growth and Orientation, ID/OD Contour, Metallurgical Interfaces and Other Inspection Challenges Provided by a Standard PWR Steam Generator Nozzle DMW Configuration 4.1

4.2 LEFT: WNP-3 Surge Line Section Showing the Location of the Pipe Cut to Produce DMW Specimen 9C-034 ..... 4.3

5.1 The ZETEC Advanced Phased Array Calculator is Useful for Generating Focal Laws and Simulating the Sound Field for the Focal Law to Determine Beam Characteristics 5.2

5.2 2.0 MHz, Phased-Array Probe, Originally Developed for Inlays, Onlays, and Overlays 5.3

5.3 Un-normalized Beam Simulations for the 2.0-MHz PA Probe at 45° Incidence in the DMW Specimen, Using a Half-Path Focus at 50 mm 5.3

5.4 1.5-MHz TRL Probe Originally Designed for Wrought Stainless Steel Welds 5.4

5.5 Normalized Simulations of the Beams Created by the 1.5-MHz TRL Arrangement for 30°, 45°, and 60° 5.5

5.6 Beam Simulations for the 1.5 MHz PA Probe at 45° Incidence in the DMW Specimen, Using a Half-Path Focus at 50 mm 5.5

5.7 1.0 MHz, Phased-Array Probe, Originally Developed for Inlays, Onlays, and Overlays 5.6

5.8 Un-normalized Beam Simulations for the 1.0-MHz PA Probe at 45° Incidence in the DMW Specimen, Using a Half-Path Focus at 50 mm 5.7

6.1 Photograph of the DMW Specimen 9C-034 Configured for Standard PA-UT with the ZETEC Manual Scanner Attached Directly onto the Specimen Being Examined 6.1

6.2 Photographs of the DMW Specimen 8C-036 ..... 6.2

6.3 Data Acquisition System and Laboratory Workstation 6.2

7.1 Photographs of the DMW Mock-up Specimen 8C-032 ..... 7.2

7.2 Side View Illustration of All Four Thermal Fatigue Cracks Implanted into DMW Mock-Up Specimen 8C-032 ..... 7.3

7.3 End View Illustration of All Four Thermal Fatigue Cracks Implanted into DMW Mock-Up Specimen 8C-032 ..... 7.4

7.4 Photographs of the DMW Mock-up Specimen 9C-023 ..... 7.5

7.5 Side View Illustration of All Four Thermal Fatigue Cracks Implanted into DMW Mock-up Specimen 9C-023 ..... 7.6

7.6 End View Illustration of All Four Thermal Fatigue Cracks Implanted into DMW Mock-up Specimen 9C-023 ..... 7.7

7.7 Photographs of the DMW Mock-up Specimen 8C-091 ..... 7.8

7.8 Side View Illustration of All Four Cracks Implanted into DMW Mock-up Specimen 8C-091 ..... 7.9

7.9 End View Illustration of All Four Cracks Implanted into PZR CASS Specimen 8C-091 ..... 7.10

7.10 Photographs of the Original OD Surface of DMW Mock-up Specimen 9C-034 ..... 7.11

7.11 Photographs of the OD Surface of DMW Mock-up Specimen 9C-034 after Weld Crown Removal 7.11

7.12 Photographs of the ID Surface of DMW Mock-up Specimen 9C-034 Depicting Various ID Surface and Weld Geometries 7.12
7.13 Side-View Illustration of All Four Thermal Fatigue Cracks Implanted into DMW Mock-Up Specimen 9C-034 ..... 7.13
7.14 End-View Illustration of All Four Thermal Fatigue Cracks Implanted into DMW Mock-up Specimen 9C-034 ..... 7.14
7.15 Photographs of DMW Mock-up Specimen 8C-036 ..... 7.15
7.16 Side-View Illustration of All Four Thermal Fatigue Cracks Implanted into DMW Mock-up Specimen 8C-036 ..... 7.16
7.17 Side-View Illustration of the Two Circumferentially HIP'ed EDM Notches Implanted into DMW Mock-up Specimen 8C-036..... 7.17
7.18 Side-View Illustration of the Two Axially HIP'ed EDM Notches Implanted into DMW Mock-up Specimen 8C-036..... 7.17
7.19 End-View Illustration of All Eight TFCs and HIP'ed EDM Cracks Implanted into DMW Mock-up Specimen 8C-036..... 7.18
8.1 Flaw 2 from DMW Specimen 8C-032 at 1.5 MHz 8.2
8.2 Flaw 3 from Specimen 8C-032 at 2 MHz on the Top and at 1.5 MHz on the Bottom..... 8.2
8.3 Length Sizing Results on Specimen 8C-032 ..... 8.3
8.4 Depth Sizing Results on Specimen 8C-032..... 8.3
8.5 Flaw 1 Data on Specimen 9C-023, Obtained from the WSS Side at 1.5 MHz 8.4
8.6 Flaw 1 Data on Specimen 9C-023, Obtained from the WSS Side at 1.5 MHz 8.5
8.7 Data from Flaw 2 in Specimen 9C-023, Obtained from the WSS Side at 1.5 MHz 8.5
8.8 Flaw 4 in Specimen 9C-023, from the WSS Side of the Weld at 1.5 MHz..... 8.6
8.9 Flaw 2 in Specimen 8C-091 at 1 MHz 8.7
8.10 Flaw 2 in Specimen 8C-091 at 1.5 MHz 8.8
8.11 Flaw 2 in Specimen 8C-091 at 2 MHz 8.8
8.12 Length Sizing Results on Specimen 8C-091 ..... 8.9
8.13 Depth Sizing Results on Specimen 8C-091..... 8.9
8.14 Specimen 8C-091 Flaw 2 on the Left, an EDM Notch, and Flaw 3 on the Right, a TFC 8.10
8.15 Specimen 9C-034 Flaw 2 at 1.5 MHz as Observed from the CASS Side of the Weld was Detected Before Weld Crown Removal at 60°..... 8.11
8.16 Specimen 9C-034 Flaw 3 at 1.5 MHz and 55° as Observed from the CASS Side of the Weld, with a Marginal Detection Before Weld Crown Removal..... 8.11
8.17 Specimen 9C-034 Flaw 2 at 1.5 MHz as Observed from the CASS Side of the Weld After Weld Crown Removal was Detected..... 8.12
8.18 Specimen 9C-034 Flaw 2 at 2 MHz as Observed from the CASS Side of the Weld After Weld Crown Removal was Detected..... 8.12
8.19 Specimen 9C-034 Flaw 3 at 1.5 MHz as Observed from the CASS Side of the Weld After Weld Crown Removal was Detected..... 8.13
8.20 Specimen 9C-034 Flaw 3 at 2 MHz as Observed from the CASS Side of the Weld After Weld Crown Removal was Detected..... 8.13
8.21 Length Sizing Results on Specimen 9C-034 ..... 8.14

8.22 Depth Sizing Results on Specimen 9C-034 ..... 8.14
8.23 Data Acquired at 2 MHz from Flaw 2 as Observed from the WSS Safe End Side of the Weld 8.15
8.24 Data Acquired at 1.5 MHz from Axial Flaw 8 in Specimen 8C-036 ..... 8.16
8.25 Length Sizing Results on Specimen 8C-036 ..... 8.16
8.26 Depth Sizing Results on Specimen 8C-036 ..... 8.17

Tables

5.1 Ultrasonic Transducer Physical Specifications 5.1
5.2 Theoretical Focal Spot Dimensions for all Probes Used in this Study 5.8
7.1 Summary Table Depicting True-State Dimensions and Locations of All Flaws in All Five DMW Mock-Up Specimens Examined in This Study 7.19
8.1 Summary DMW Length Sizing Data 8.18
8.2 Summary DMW Depth Sizing Data 8.19
8.3 DMW Signal to Noise Ratio Summary 8.19

1.0 Introduction

This document is a technical letter report (TLR) summarizing confirmatory research and laboratory evaluations of phased-array (PA) ultrasonic testing (UT) on reactor coolant system (RCS) components containing dissimilar metal welds (DMWs). The technical evaluations described here were conducted on a set of smaller bore DMW mock-ups representing various component configurations where Alloy 600/82/182 material was used in conjunction with either wrought steel or cast austenitic stainless steel (CASS) piping components. This work was performed at the Pacific Northwest National Laboratory (PNNL) in Richland, Washington. The effort was conducted as part of a funded program sponsored by the U.S. Nuclear Regulatory Commission (NRC) titled, "Reliability of Nondestructive Examination for Nuclear Power Plant Inservice Inspection," under Task 2 of JCN N6398. This TLR is submitted as an Operating Plan Milestone deliverable for Task 2.

The general focus of this research effort is to determine the effectiveness and reliability of advanced nondestructive examination (NDE) methods on light-water reactor (LWR) components containing DMWs and other coarse-grained components that encompass CASS. In addition, DMWs and CASS components with corrosion-resistant cladding, weld overlays, inlays and onlays, as well as far-side examinations of austenitic piping welds, are also considered in this program. The specific goal of the work reported here is to assess the effectiveness and reliability of various NDE methods to detect and characterize (localize and size) cracks in components containing DMWs that exist in the Class 1 primary pressure boundary of commercial light-water nuclear reactors.

The work described here was performed to provide insights for evaluating the utility of advanced NDE approaches for the inspection of smaller-bore DMW components, such as a pressurizer (PZR) surge nozzle DMW, a shutdown cooling pipe DMW, and a ferritic (low-alloy carbon steel)-to-CASS pipe DMW configuration. This interim TLR describes recent findings and provides a detailed status of the work conducted on DMW inspectability using phased-array ultrasonic-testing (PA-UT) methods at PNNL to date. Work is continuing relative to DMW inspectability issues and a final NUREG/CR report summarizing all DMW work is planned.

Section 1 provides a programmatic introduction to the work described here. Section 2 of this report describes the project background and technical objectives. Section 3 provides a description of the scope of work as it pertains to this evaluation for PA inspection capability. Section 4 provides a discussion of the DMW inspection problem as it relates to the propagation of ultrasonic energy in buttered welds and through coarse-grained microstructures, as well as information pertaining to access limitations and geometrical considerations for the various specimens used in this study. Section 5 describes the various probes and probe configurations used, modeling of the probe configurations to generate expected performance information, and issues associated with PA focal law development. Section 6 provides a description of the data acquisition set-up and experimental approach employed in this work, while Section 7 describes the various DMW specimens used in these laboratory studies, including details regarding flaw location, size, and true-state dimensions. Section 8 provides discussions of the data analysis process and results from PA examinations of the DMW mock-up specimens. Section 9 includes a technical discussion and conclusions from the work presented here. And finally, Section 10 identifies references cited in this TLR.

2.0 Background and Objectives

Since 1977, PNNL has conducted advanced NDE research under the sponsorship and guidance of the NRC to evaluate state-of-the-art technical approaches for inspecting nuclear reactor components that pose significant challenges to conventionally employed inspection methods used in the nuclear industry (Taylor 1984; Diaz et al. 1998; Anderson et al. 2007; Diaz et al. 2008). This work recently has focused on assessing the viability and effectiveness of phased-array ultrasonic NDE methods applied from the outside pipe surface where the material composition is detrimental to performing effective inspection and component configurations affect probe placement. Regarding ultrasonic methods, PNNL's strategy has been to evaluate advanced phased-array ultrasonic testing methods (often in the lower-frequency regime < 2 MHz) to assess the viability in using longer-wavelength inspection techniques that are inherently less sensitive to the effects of the component geometries, surface conditions, and coarse-grained microstructures present in many DMW and CASS configurations; while at the same time, maintaining suitable resolution to effectively detect, localize, and size flaws in these materials (Anderson et al. 2003; Anderson et al. 2007).

The main objectives of the overall effort for Task 2 in JCN N6398 are focused on assessing the effectiveness of new techniques and methods that allow for the consistent and reliable inspection of coarse-grained materials having complex geometrical conditions. PNNL is tasked with determining if certain NDE techniques (e.g., phased-array UT, synthetic aperture focusing technique [SAFT]-UT) can reliably and effectively detect and characterize flaws on the far side of austenitic welds, the far side of DMWs, and either side of CASS components; and identify problem areas that have resulted in the failure of NDE methods to detect flaws in areas such as control rod drive housings. This includes inspection applications where there are components with corrosion-resistant cladding and weld overlays, inlays, and onlays as well. These techniques should allow for discrimination between coherent ultrasonic energy scattered from grain boundaries (metallurgical or geometric reflectors) and cracks (e.g., discontinuities) in these traditionally challenging steel components.

Inservice inspection (ISI) requirements dictate that piping welds in the primary pressure boundary of LWRs be subject to a volumetric examination based on the requirements of Section XI of the American Society of Mechanical Engineers (ASME) Boiler and Pressure Vessel Code (ASME 2008). This volumetric examination may be either radiographic (RT) or ultrasonic (UT); but because background radiation and access limitations typically preclude the use of RT, UT is used to examine DMW components within the RCS of pressurized-water reactors (PWRs). A variety of inspection challenges exist that need to be addressed to demonstrate effective and reliable UT inspections of DMWs. Over the past many years, PNNL has focused much of its laboratory and field-based research toward addressing the prevalent inspection issues associated with detection and characterization of flaws through coarse-grained microstructures in CASS components. As PNNL has documented recent technical progress with the inspection of smaller-bore CASS components (Diaz et al. 2008), specific (and technically related) inspection challenges associated with DMWs have emerged. In some DMW configurations where CASS piping is used, inspection from the far-side (through the CASS parent material, weld, and Inconel buttering) is required because, for example, component configuration precludes adequate placement of probes on the other side of the weld. In the United States, the nuclear industry has coordinated its response to cracking in Alloy 600/82/182 materials via the Materials Reliability Program (MRP), and while this program has evaluated key issues regarding cracked DMW scenarios, the NRC has funded PNNL to conduct confirmatory research to review the work conducted by industry groups (NRC 2008a,

b). In October 2008, the NRC generated a Regulatory Issue Summary (RIS) 2008-25, *Regulatory Approach for Primary Water Stress Corrosion Cracking (PWSCC) of Dissimilar Metal Butt Welds in Pressurized Water Reactor Primary Coolant Piping* (NRC 2008b). This RIS was issued to inform nuclear power plant (NPP) licensees of the regulatory approach for ensuring the integrity of DMWs containing Alloy 82/182 in PWRs. This issuance documents the NRC's stance, perspective, and summary evaluation of the MRP-139 (EPRI 2005) inspection guidelines and MRP's actions to mitigate welds to address PWSCC (the primary mechanism for cracking in Alloy 600/82/182 materials used in DMWs). Finally, PNNL has been guided by the NRC to evaluate the data and results obtained through the PNNL confirmatory research program to determine the need for any additional changes/modifications to the ASME Code, based upon technical findings, and thereby recommend changes that should be considered for implementation.

The work reported here focuses on smaller-bore, thinner-walled (< 2-in. wall thickness) DMW component designs that exist in PWRs, such as ferritic vessel nozzles-to-safe-end-to-stainless steel RCS loop piping. This evaluation was initiated because optimum frequencies and ultrasonic PA inspection parameters have yet to be established to examine the various DMW component configurations and relatively challenging inspection conditions. This TLR provides the results and conclusions from newly acquired ultrasonic PA data on five DMW mock-up specimens using a range of inspection frequencies—2.0 MHz, 1.5 MHz, and 1.0 MHz, respectively. These mock-up specimens were fabricated to include both circumferentially and axially oriented flaw types, including implanted thermal fatigue cracks (TFCs) and electrical discharge machining (EDM)-initiated hot isostatically pressed (HIP'ed) cracks. This work is expected to provide insights and data to support modifications to, or development of new, ASME Code rules for improved inspections of component configurations with DMWs and allow for new performance-demonstration processes for DMWs to be established.

3.0 Scope of PA-UT Evaluations

The scope of the work reported here was defined by NRC guidance and is focused toward evaluating UT inspection capabilities in smaller-bore components (< 2-in. wall thickness) containing DMWs that exist in the Class 1 primary pressure boundary of commercial light-water nuclear reactors. PNNL was tasked with acquisition and procurement of materials, fabrication of flawed specimens, design and procurement of specialized PA probes, and conducting data acquisition and analysis on five DMW mock-up specimens. The materials chosen for mock-up fabrication are representative of existing DMW component configurations in PWRs. In addition, these mock-ups were designed and fabricated to accurately reflect the physical dimensions and conditions (inner diameter [ID]- and outer diameter [OD]-surface conditions, weld geometry, etc.) of in-field DMW components. The materials comprising these components include ferritic (low-alloy carbon steels), wrought stainless steel (WSS), centrifugally cast stainless steel (CCSS), and Alloy 82/182 material. The mock-ups have dimensions of approximately 30.5- to 35.5-cm (12- to 14-in.) OD and approximately 33-mm (1.3-in.) wall thickness. This thickness is representative of typical DMWs in PZR surge lines (Westinghouse and Combustion Engineering [CE] plants), and various safe-ends in CE-designed plants. The technical evaluation reported here included PA-UT examinations on circumferentially oriented, implanted/fabricated TFCs and EDM-initiated HIP'ed cracks, of which two cracks were oriented in the axial plane of the pipe, parallel to the flow direction. The experimental design included an evaluation of PA-UT detection, localization, and sizing performance as a function of frequency and other critical inspection parameters.

The work consisted of design and sound field assessments for various PA probes, probe configurations, and wedges; development of specific PA focal laws; and use of a state-of-the-art data acquisition system (DYNARAY) for implementing examinations. The primary focus of the work reported in this TLR includes:

- Lower-frequency PA-UT examination of DMW component mock-ups
  - As a function of inspection frequency (2.0 MHz, 1.5 MHz, and 1.0 MHz),
  - As a function of inspection angle (30° to 70° in 1° increments),
  - As a function of both raster and line scan data acquisition, and
  - From both sides of the weld (however, the TLR focuses on data taken from the austenitic pipe side of the DMW configuration, as this is typical for inspection access in the field).

The data analysis portion of this work provides evaluation and results as a function of each individual specimen, gives quantitative information regarding detection and sizing performance against the true state, and assesses the capabilities of PA-UT for effective flaw localization/ positioning versus true state. Metrics used for the analysis included signal-to-noise ratio (SNR), root-mean-square error (RMSE), and true-state values for flaw length, depth, and axial and circumferential location on the specimen mock-ups.

4.0 The DMW Inspection Challenge

Welds used to join low-alloy ferritic components to stainless steel components are defined as dissimilar metal welds. The DMW components fabricated as mock-ups for this evaluation were designed to simulate actual DMW configurations that reside within the reactor pressure boundaries of primarily PWRs, but also simulate certain nozzle-to-safe-end configurations in boiling-water reactors (BWRs); for example, recirculation riser pipe to jet pump nozzles. The pipe side of these component configurations typically include either wrought steel or CASS, where a variety of butt welds (full-penetration welds) containing Alloy 82/182 materials were used in the fabrication and joining processes of these components (Ammirato 2001; Mayinger and Metzner 2001; NRC 2008b). DMW components come in a wide variety of designs and configurations, and are fabricated from an array of materials that are typically predicated by the components being joined. In PWRs, they include pressurizer surge, spray, safety and relief nozzle welds, as well as safe-end-to-stainless steel pipe butt welds in the reactor coolant, safety injection, and shutdown cooling systems. Typically, DMWs contain multiple boundaries and multiple material types that affect the propagation of the ultrasonic field from the austenitic pipe side. A standard PWR steam generator nozzle DMW configuration consists of the carbon steel nozzle parent material, buttering, a weld, a wrought safe-end, another weld, and the pipe parent material, as shown in Figure 4.1. The inspection challenge is defined by these complex configurations including metallurgical interfaces, microstructural variations, and ID/OD geometry/access issues. Variations in the actual geometries and dimensions of the welds and butterings are quite extensive in the field, as are the type of welding employed, the weld direction, repair processes, and other factors (Ammirato 2001). These issues essentially eliminate the possibility to evaluate and mock-up each type of DMW configuration. Therefore, this evaluation is based upon a limited set of DMW configurations and targets a set of five mock-up specimens designed to provide the foundation to better understand and assess the inspection challenges and technical issues pertinent to addressing inspection performance.

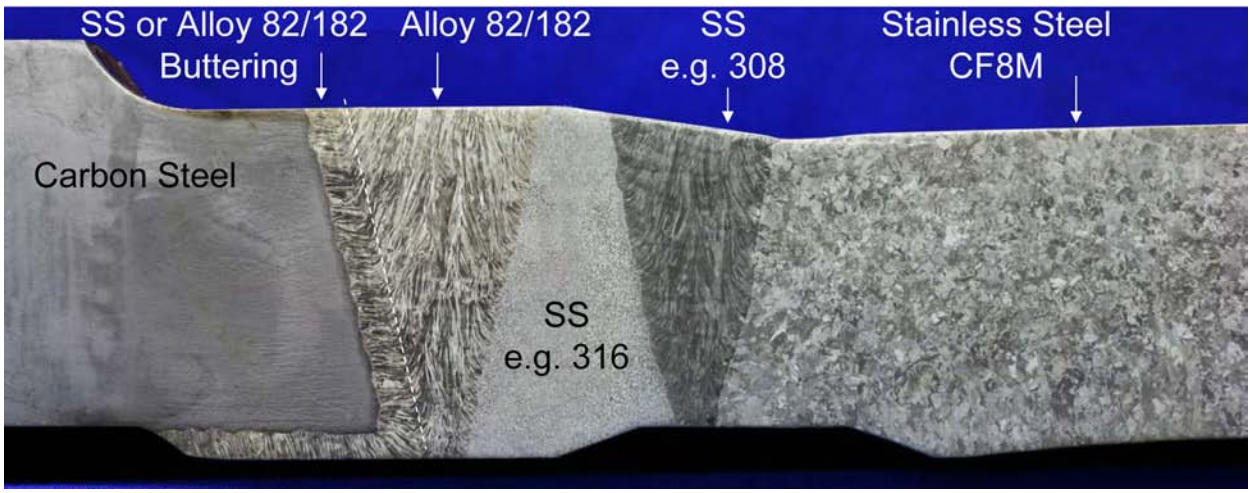

Figure 4.1. Digital Photograph Illustrating Geometry, Grain Growth and Orientation, ID/OD Contour, Metallurgical Interfaces and Other Inspection Challenges Provided by a Standard PWR Steam Generator Nozzle DMW Configuration

Operating experience and events have shown that in PWRs where primary coolant water (or steam) are present under normal operation, Alloy 82/182 materials are susceptible to PWSCC (NRC 2008b, 2009). For example, in 2000, cracking in the reactor vessel nozzle-to-RCS hot-leg DMW at V.C. Summer nuclear power station was identified. Five circumferential cracks in three DMWs were discovered on pressurizer piping at the Wolf Creek Generating Station in 2006. Internationally, cracking in DMW components has been detected at NPPs (of both PWR and BWR designs) in countries including Germany, Japan, France, and Sweden (Mayinger and Metzner 2001; Faidy et al. 2003; Hsiao et al. 2008; Kroning et al. 2008). The extent and number of occurrences of DMW cracking in NPPs indicate the necessity for reliable and effective inspection techniques.

PWSCC in DMWs typically occurs in the buttering (Alloy 82/182 material) or weld metal, where the challenges described earlier generally preclude the use of ultrasonic shear waves, thereby requiring the use of refracted longitudinal waves for detection and characterization of flaws. To complicate matters further, the ultrasonic responses can be affected by the ID surface contour (weld root, counterbore, etc.), the numerous metallurgical interfaces, the weld metal (especially if austenitic), and the variability in the complex configurations of DMWs (Ammirato 2001). In some cases, such as CE plants, DMW components include a CASS pipe, where the inspection access is limited and the sound field must pass through the coarse-grained microstructure of the CASS parent material as well. Alloying elements and casting processes used in the fabrication of CASS materials are responsible for its corrosion resistance and strength but also create complex and coarse-grained microstructures.

DMW components that reside in the reactor coolant system of PWRs are subject to periodic UT examinations, based on requirements found in the ASME Boiler and Pressure Vessel Code, Section XI, Rules for Inservice Inspection of Nuclear Power Plant Components. In addition, MRP-139 (EPRI 2005) provides industry guidance for the volumetric inspections of DMWs in PWRs (NRC 2008a, b). For ISI to be successful, service-induced flaws must be detected and repaired prior to becoming of such size that the integrity of a component is compromised. Flaw detection is the initial priority, and for UT this is accomplished by analyzing ultrasonic echo waveforms from reflections within the volume of inspected material that are potentially caused by service degradation. In DMW components containing CASS piping, the large size of the anisotropic grains relative to the acoustic pulse wavelength severely scatters and attenuates the sound field. Significant changes in acoustic velocity are also evident. Refraction and reflection of the sound beam occur at the grain boundaries, effectively skewing and/or partitioning the sound field, resulting in flaws being incorrectly identified, specific volumes of material not being examined, or both. To reduce the impact of the microstructure, metallurgical interfaces, complex internal and external geometries, and other factors that affect the inspection technique, the work reported here focuses on lower-frequency (1.0 kHz to 2.0 MHz) sound field propagation through the material as applied from the OD surface.

Most specimens evaluated in this study were acquired from piping components fabricated from wrought piping materials on hand at PNNL or directly salvaged from cancelled NPPs never brought to full operation. A few low-alloy carbon steel segments were procured from FlawTech. Thus, the microstructures of the CASS segments of pipe used to construct one of the DMW mock-ups are considered vintage microstructures and representative of those that would be typically found in similar NPPs built in the 1970s. One of the DMW mock-up specimens examined in this study (9C-034) was designed and fabricated using CASS PZR surge line piping from Washington Nuclear Power Unit 3 (WNP-3). The parent component, from which the pipe segment was extracted, is shown in Figure 4.2.

Figure 4.2. LEFT: WNP-3 Surge Line Section Showing the Location of the Pipe Cut to Produce DMW Specimen 9C-034. RIGHT: The Centrifugally Cast Pipe Microstructure is Displayed for DMW Mock-up 9C-034 (top and bottom).

The PZR surge-line segments used for fabricating the DMW mock-up consisted of a wide range of grain sizes overall, exhibiting rather large but considered average grain diameters. The long segment of PZR surge line from WNP-3 was sectioned, and a segment of this section used for fabrication of the DMW mock-up was sliced, polished, and chemically etched to bring out the microstructure. The dendritic (columnar) microstructure of DMW mock-up 9C-034 is shown in Figure 4.2. The micrograph illustrates the variability and range of grain sizes that can be found in PZR surge-line components. The WNP-3 specimen's average grain sizes were measured at 6.6 mm (0.26 in.) and the maximum grain diameter for the segments used reached 25.6 mm (1.01 in.) on the CASS pipe side of the DMW mock-up.

Overall grain diameters from the WNP-3 PZR segment ranged in size from approximately 0.5 mm (0.04 in.) to over 40 mm (1.6 in.) and grain diameter varied as a function of depth or spatial position in the material. At a 1.5-MHz inspection frequency, the corresponding wavelength in the CASS PZR surge-line material is approximately 3.8 mm (0.15 in.). Thus, it was anticipated that the wavelength at this inspection frequency (relative to the average grain diameters encountered) would experience significant scattering and attenuation as the sound field propagates through the material and into the DMW. However, the results from this evaluation show that this was not the case; and in fact, frequencies between 1.0 MHz and 2.0 MHz provided suitable penetration and resolution for flaw detection and characterization.

Austenitic piping used for the remaining specimens in this study was available from an inventory of wrought piping existing at PNNL.

5.0 Phased-Array Probes and Focal Law Development

5.1 Ultrasonic Probe Details

The samples were examined using three phased-array probes: a 2.0-MHz transmit-receive longitudinal (TRL) arrangement, a 1.5-MHz TRL probe, and a 1.0-MHz TRL probe. The 1.5-MHz transducer was chosen based on frequencies commonly used in reactor inspections of stainless steels. The additional 1.0- and 2.0-MHz probes were employed to more fully evaluate the entire frequency spectrum and provide data to better assess lower and higher frequency limits for inspecting the various DMW components. A set of custom wedges was fabricated for use in this study. Each set of wedges was curved to match the approximate 318-mm (12.5-in.) diameter of the DMW specimens. General specifications for the three models of transducers are described in Table 5.1.

Table 5.1. Ultrasonic Transducer Physical Specifications

Probe	1.0-MHz TRL	1.5-MHz TRL	2.0-MHz TRL
Active Aperture	40 mm (1.6 in)	35 mm (1.4 in)	22 mm (0.9 in)
Passive Aperture	20 mm (0.8 in)	17.5 mm (0.7 in)	11 mm (0.4 in)
Active Aperture Elements	10	10	10
Passive Aperture Elements	5	3	5

5.2 Focal Law Development

Before a phased-array probe can be used to perform an examination, a set of focal laws must be produced to control the firing of individual elements. The focal laws are inputs to the UltraVision control software, which determines specific elements to excite at specific times to allow for proper beam-forming in the material to be examined. The focal laws also contain details about the angles being generated, the focal point of the sound field, the delays associated with the wedge and electronics, and the orientation of the probe. PNNL uses a software package for producing focal laws known as the "ZETEC Advanced Focal Law Calculator (AFLC)" that has now been fully integrated into the UltraVision 3.1R9 software package used for this study. The AFLC performs two functions: (1) focal law generation and (2) simulation of the ultrasonic field produced by the probe when using the generated laws. The user enters the physical information about the PA probe, such as the number of elements and the sizes of the elements, and the wedge information, such as the wedge angle and the wedge size, into the program. The desired angles and focal distances are then entered, and the software generates the needed delays for each element to produce the desired beam steering and focusing in the material. The software beam simulation produces a simple image of the probe on the wedge, ray-tracing to show the focal depth and steering desired, and density mapping to enable the viewer to see how well the sound field responds for a particular angle and whether grating lobes exist that may be detrimental to the examination. Figure 5.1 shows an example of the ray tracing for a probe on the left with the sound field density mapping on the right. It should be noted that this simulation is performed in isotropic material; that is, the velocity of sound is maintained throughout any angle for a particular wave mode, which is not really the true state for all stainless steels, but enables the user to estimate sound field parameters and transducer performance for optimal array design and focal law development.

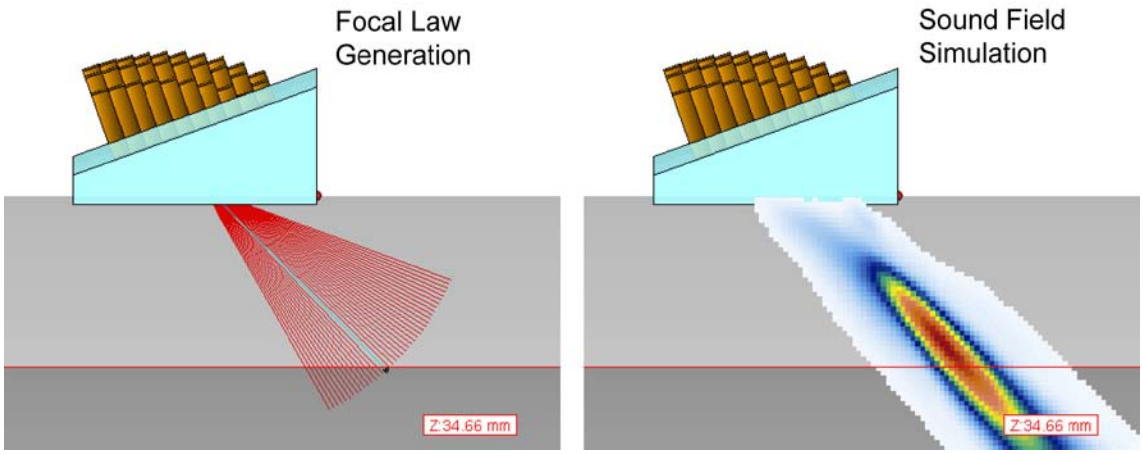

Figure 5.1. The ZETEC Advanced Phased Array Calculator is Useful for Generating Focal Laws (left) and Simulating the Sound Field for the Focal Law (right) to Determine Beam Characteristics

5.3 2.0-MHz TRL Probe

The 2-MHz TRL array was originally designed for evaluating inspection effectiveness of PA methods on components with inlays, onlays, and overlays (Figure 5.2). It consists of two 10-element by 5-element matrix arrays. One array is used for transmitting, the other for receiving ultrasonic signals. This probe has a 62% bandwidth (BW) at −6 decibels (dB) and an approximately 30-mm^2 (1.2-in.^{2}) footprint with a customized wedge for data collection in tight geometrical configurations. The probes were designed at PNNL and built by Imasonic®. This smaller size generally allows insonification of the far side of a specimen even with a weld crown present. The probe's nominal wavelength in stainless steel is 2.92 mm (0.11 in.) at its average center frequency of 2.0 MHz. Skew angles of ±20 degrees are possible with this array.

Specific focal laws were generated for the DMW specimens based on the thickness of each specimen and the width of the welds in each specimen. While a frequency of 2.0 MHz would normally be considered too high for use on some stainless steel specimens, inspection work at 1.5 MHz indicated that even at higher frequencies, detection and sizing of flaws in smaller bore piping could be achieved. To push the detection limits and determine whether microstructure-induced attenuation would dominate, a higher than conventional inspection frequency of 2.0 MHz was employed. Based on the focal laws and the results of the simulation, it was determined that the 2.0-MHz probe was capable of effectively insonifying the region surrounding the weld in the DMW samples. Example simulations of the 2.0-MHz beam using one set of focal laws are shown in Figure 5.3. The images are shown in an un-normalized configuration to highlight the −3 and −6-dB spot sizes for this particular angle (45º).

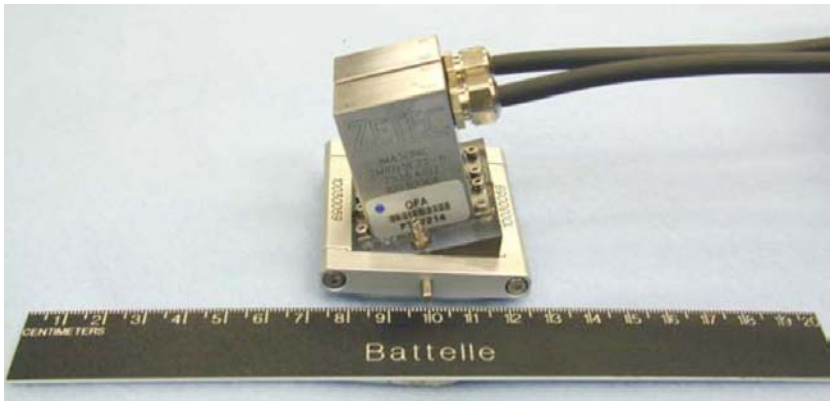

Figure 5.2. 2.0 MHz, Phased-Array Probe, Originally Developed for Inlays, Onlays, and Overlays

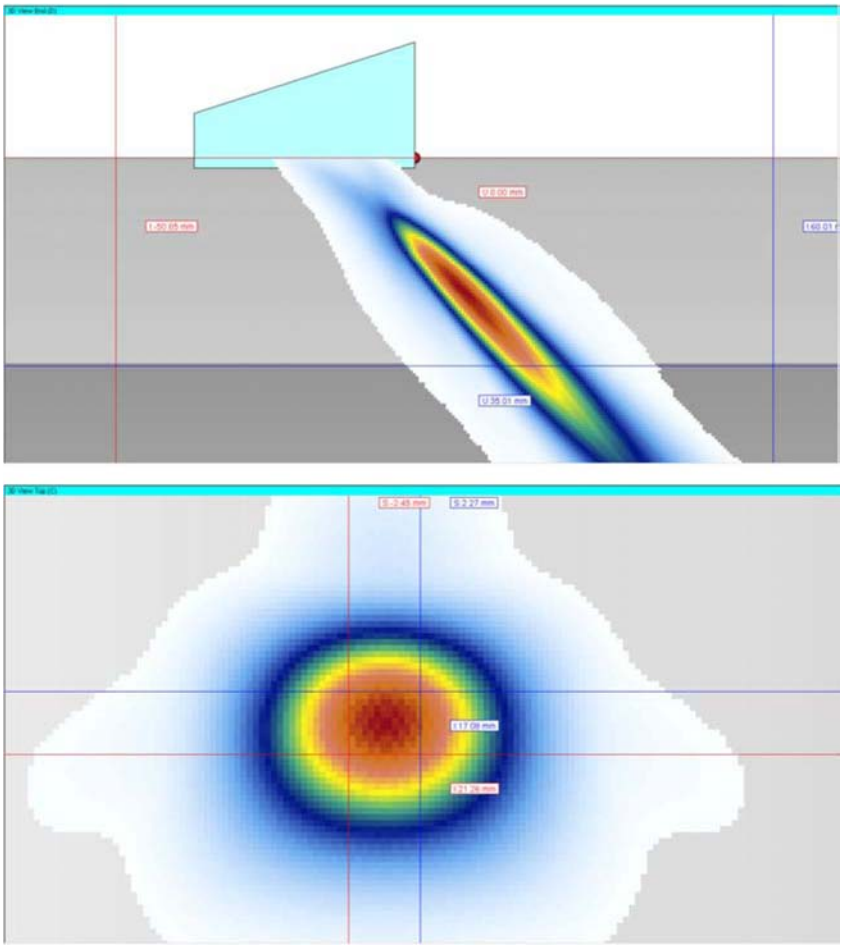

Figure 5.3. Un-normalized Beam Simulations for the 2.0-MHz PA Probe at 45° Incidence in the DMW Specimen, Using a Half-Path Focus at 50 mm (1.97 in.). Top: side-view of focused sound field at 45° incident angle in the part. Bottom: cross-sectional view of sound field at the focal spot, where cursors mark the −3 dB points.

The 2.0-MHz probe was found to produce a beam with a horizontal width of 4.72 mm (0.19 in.) by vertical width of 4.18 mm (0.16 in.) at 45° at the −3 dB points. The 2.0-MHz probe is able to provide an effective sound field at distances from almost directly under the probe to a distance approximately 45 mm (1.8 in.) in front of the wedge. As with the 1.5-MHz probe, the ability of the probe to accurately measure crack width and depth improves with proximity between the probe focal spot and the flaw, as this is the location of tightest focusing and highest sensitivity.

5.4 1.5-MHz TRL Probe

This 1.5-MHz TRL probe was originally designed by PNNL for examinations of WSS, and consists of two 1.5-MHz PA transducers mounted side-by-side on a Rexolite® wedge. The 1.5-MHz probes operated in the pitch-catch mode with wedges held together by an aluminum frame. The wedge dimensions were 49 × 50 mm (1.93 × 1.97 in.). Both transmit and receive probes were identical in design with a 10×3 element array, an active area of 35 × 17.5 mm (1.38 × 0.69 in.), and a greater than 60% bandwidth at −6 dB. The 1.5-MHz probe has been used in previous examinations of flaws on the near and far sides of austenitic welds in WSS. 1.5 MHz is, however, generally considered to be too high in frequency for examining CASS components, which have larger and more complex grain structures than WSS. The 1.5-MHz TRL probe was included in this study because the probe has proven effective in examining materials of similar thickness to the DMWs and provides a point of comparison for the other techniques. Skew angles of ±10 degrees are possible with this array. The probe is shown in Figure 5.4.

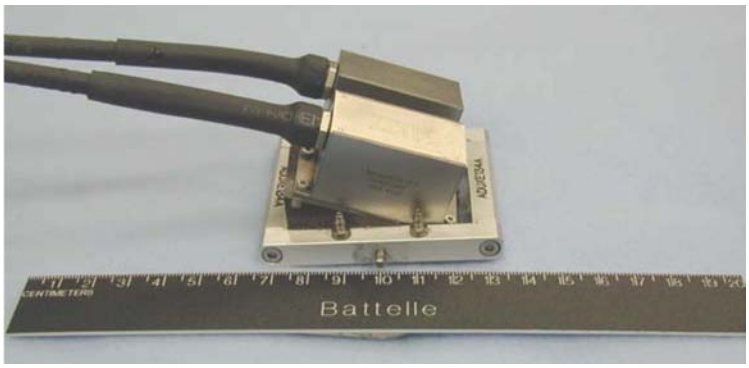

Figure 5.4. 1.5-MHz TRL Probe Originally Designed for Wrought Stainless Steel Welds

Specific focal laws were generated for the DMW specimens based on the thickness of the piping and the width of the weld. After the focal laws were developed, the ultrasonic field that would be produced by these laws was simulated to demonstrate that the probe and the focal laws are able to insonify the region of interest. The simulations indicated that the 1.5-MHz probe would be able to produce a well-focused beam at distances from directly below the probe to approximately 45 mm (1.8 in.) in front of the wedge. The probe produces a sound field that works best for detecting and sizing flaws on the near side of the weld, but it is also capable of detecting flaws from the far side of most welds in thinner materials, assuming that the microstructure allows the waves to form and propagate appropriately. Multiple focal laws were used in the examinations to obtain optimal results. Example simulations of the 1.5-MHz probe steered to 30°, 45°, and 60°, focused to a half path focus depth of 50 mm (1.97 in.), is shown in Figure 5.5. It is revealed that, by normalizing all the focal laws, the higher angle laws exhibit a lower

level of insonification thereby reducing the ability to detect and size flaws in that region. The wavelength for a 1.5-MHz probe is 3.8 mm (0.15 in.). From Figure 5.6, the 1.5-MHz probe was found to produce a beam with a horizontal width of 5.01 mm (0.20 in.) by vertical width of 3.81 mm (0.15 in.) at 45° at the −3 dB points. The focal spot sizes were generated using un-normalized simulations to produce theoretical spot sizes for the singular angle of 45º.

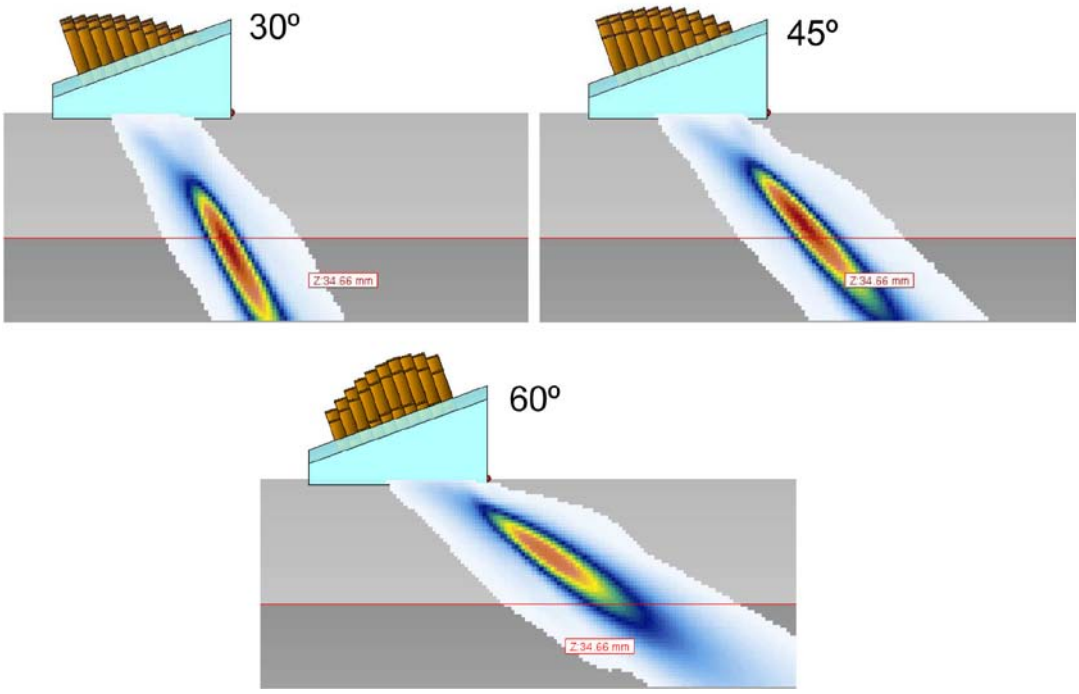

Figure 5.5. Normalized Simulations of the Beams Created by the 1.5-MHz TRL Arrangement for 30°, 45°, and 60°

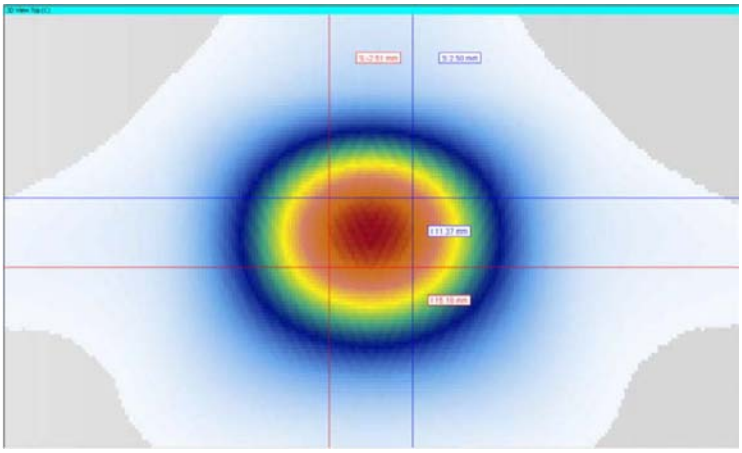

Figure 5.6. Beam Simulations for the 1.5 MHz PA Probe at 45° Incidence in the DMW Specimen, Using a Half-Path Focus at 50 mm (1.97 in.). This is a cross-sectional view of sound field at the focal spot, where cursors mark the −3 dB points.

5.5 1.0-MHz TRL Probe

The 1-MHz TRL array (Figure 5.7) was originally designed for evaluating inspection effectiveness of PA methods on components with inlays, onlays, and overlays. It consists of two 10-element by 5-element matrix arrays. One array is used for transmitting, the other for receiving ultrasonic signals. This probe has a 58% BW at −6 dB and an approximately 50-mm^2 (1.97 in.^{2}) footprint with a customized wedge for data collection in tight geometrical configurations. This probe size generally allows insonification of the far side of a specimen even with a weld crown present, but can be prohibitive if the weld crown is too large. The probe's nominal wavelength in stainless steel is 5.31 mm (0.21 in.) at its average center frequency of 1.1 MHz. Skew angles of ±20 are possible with this array.

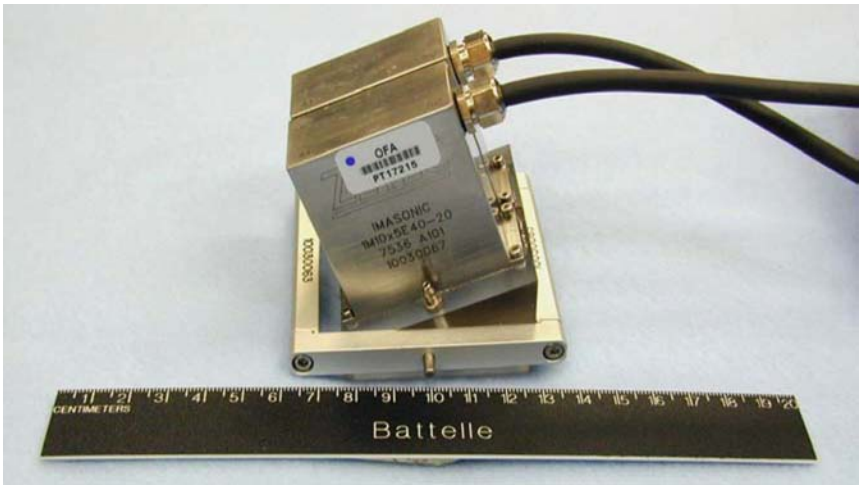

Figure 5.7. 1.0 MHz, Phased-Array Probe, Originally Developed for Inlays, Onlays, and Overlays

Specific focal laws were generated for the DMW specimens based on the thickness of each specimen and the width of the welds in each specimen. A frequency of 1.0 MHz was chosen to be the low end inspection frequency for this DMW study. Based on the focal laws and the results of the simulation, it was determined that the 1.0-MHz probe was capable of effectively insonifying the region surrounding the weld in the DMW samples. Again, examples of the un-normalized simulations of the 1.0-MHz beam using one set of focal laws are shown in Figure 5.8.

The 1.0-MHz probe was found to produce a beam with a horizontal width of 6.16 mm (0.24 in.) by vertical width of 4.94 mm (0.19 in.) at 45° at the – 3 dB points. The 1.0-MHz probe is able to provide an effective sound field at distances from almost directly under the probe to a distance approximately 45 mm (1.8 in.) in front of the wedge. The probes were designed at PNNL and built by Imasonic®. As with the 1.5-MHz probe, the ability of the probe to accurately measure crack width and depth improves with proximity between the probe focal spot and the flaw, as this is the location of tightest focusing and highest sensitivity.

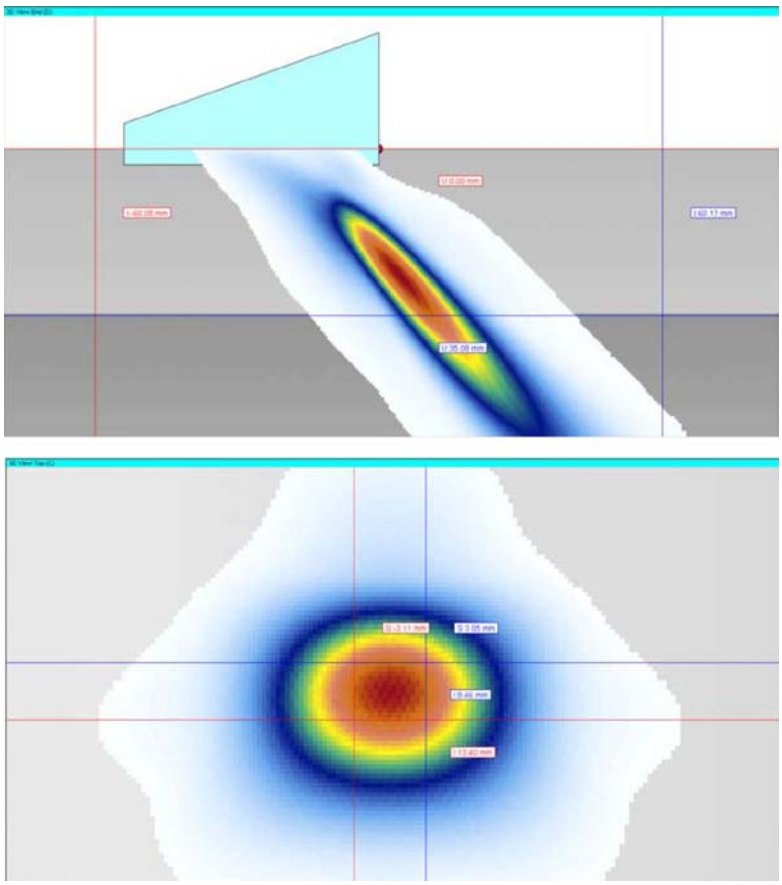

Figure 5.8. Un-normalized Beam Simulations for the 1.0-MHz PA Probe at 45° Incidence in the DMW Specimen, Using a Half-Path Focus at 50 mm (1.97 in.). Top: side-view of focused sound field at 45° incident angle in the part. Bottom: cross-sectional view of sound field at the focal spot, where cursors mark the −3 dB points.

The sound field dimensions at 30° were calculated at the ID surface rather than at the actual focal spot because the dimensions of the sound field extended past the ID for the 30° sound beam. The focal spot beyond the ID surface is not of interest. As anticipated, the sound field focal dimensions decrease with increasing frequency, and the focal spots are not symmetric. Focal laws were generated for each probe to insonify the weld region at a constant sound path from the probe (half-path focusing). The focal depth was set to 50 mm (1.97 in.). The spot size for the 1.5-kHz probe at 45° was 5.0 by 3.8 mm (0.20 in. by 0.15 in.). These were measured at the approximately −3 dB points. Table 5.2 provides the −3 dB and −6 dB spot size dimensions in both the horizontal and vertical planes for each probe at three primary angles of incidence (30°, 45° and 60°). The first dimension represents the primary axis of the probe and the second is the secondary axis of the probe; in this case, the circumferential direction. A smaller spot size will give a more accurate length measurement, assuming the entire crack is detected.

Table 5.2. Theoretical Focal Spot Dimensions for all Probes Used in this Study

Sound Field Spot Size for DMW Specimens								
PA Probe and Incident Angle	**-3dB point**				**-6dB point**			
	Horizontal		**Vertical**		**Horizontal**		**Vertical**	
1 MHz TRL	**mm**	**in.**	**mm**	**in.**	**mm**	**in.**	**mm**	**in.**
30 deg @ ID	5.89	0.23	3.46	0.14	12.49	0.49	7.95	0.31
45 deg	6.16	0.24	4.94	0.19	13.43	0.53	9.92	0.39
60 deg	5.61	0.22	7.4	0.29	12.57	0.49	15.36	0.60
1.5 MHz TRL								
30 deg @ ID	4.99	0.20	2.86	0.11	10.94	0.43	5.92	0.23
45 deg	5.01	0.20	3.81	0.15	10.72	0.42	7.86	0.31
60 deg	4.94	0.19	6.33	0.25	10.59	0.42	12.8	0.50
2 MHz TRL								
30 deg @ ID	4.2	0.17	2.62	0.10	10.11	0.40	5.79	0.23
45 deg	4.72	0.19	4.18	0.16	11.2	0.44	9.36	0.37
60 deg	4.02	0.16	2.4	0.09	9.98	0.39	6.49	0.26

5.6 Focal Law and Probe Information for Specimen 8C-032

This study on DMW specimens incorporates data previously acquired on a DMW specimen (8C-032) that has similar features and flaws as the other four samples. In the interest of time and redundancy, the decision was made to use the data already collected on this specimen and simply include the analysis results in this report. Note that only 1.5- and 2.0-MHz data were collected on this specimen using slightly different focus settings as well as an entirely different 2.0-MHz probe.

The same 1.5-MHz TRL probe as previously described was used for the inspection of this particular specimen. Instead of using a half-path focusing at 50 mm (1.97 in.), a half-path focusing at 45 mm (1.77 in.) was created using the Advanced PA Calculator 1.2R4 and implemented for the inspection of 8C-032. This focus setting yields a theoretical −3 dB spot size of 4.5 mm by 3.4 mm (0.18 in. by 0.13 in.) and a −6 dB spot size of 10.7 mm by 8.3 mm (0.42 in. by 0.33 in.) at an incidence angle of 45°, which is comparable to that of the half-path focusing at 50 mm used on the four other specimens in this study. Minimal changes in the spot size indicate that the previously collected data did properly insonify the regions of interest with enough energy to appropriately inspect this specimen.

At the time of data collection on this specimen, the 2.0-MHz 10×5 element non-integral probe (previously described) was not available and so the 2.0-MHz data collected on 8C-032 was acquired with a mini 2.0-MHz TRL. The 2.0-MHz TRL mini array was designed for near- and far-side applications in thinner pipe sections. It consists of two 2-element by 14-element matrix arrays. One array is used for transmitting, the other for receiving ultrasonic signals. The highly damped probe has a 70% BW at −6 dB and an approximately 25-mm^2 footprint with an integral wedge for data collection in tight geometrical configurations. This smaller size generally allows insonification of the far side even with a weld crown present. The probe's nominal wavelength in stainless steel is 3.0 mm at its average center frequency of 1.9 MHz. Skew angles of ±10 degrees are possible with this array. A focusing of half path 55 mm (2.17 in.) was used to collect 2.0-MHz data on this specimen. This focusing resulted in a theoretical spot size at −3 dB of 6.3 mm by 4.7 mm (0.25 in. by 0.19 in.) and at −6 dB of 14.2 mm by 11.4 mm (0.56 in. by 0.45 in.) at an incidence angle of 45°.

6.0 Data Acquisition Set-Up and Configuration

Phased-array data were acquired on specimens in the 305–356 mm (12–14 in.) diameter range using a manual track scanner. The laboratory setup for handling and data acquisition of the DMW specimens is described below.

6.1 Phase Array Data Acquisition

Set-up and laboratory configuration for PA-UT data acquisition on the DMW specimens required the use of the ZETEC manual-encoded scanner mounted either directly onto the pipe under inspection (preferred setup) as shown in Figure 6.1, or on an adjustable guide track or ring supported by a custom-designed floor-to-ceiling brace. The floor-to-ceiling brace was equipped with a translation slide providing additional control and degrees of freedom for movement both horizontally and vertically. This translation slide provided easy manipulation for fine-tuning of the guide-ring position, relative to the pipe specimen. The setup is shown in Figure 6.2 with the manual scanner on the guide-ring section. The probe is mounted on an extension arm that is adjustable along the pipe axis. Two encoders on the manual track scanner provide positional information in either or both the axial and circumferential directions for line and raster scanning.

Figure 6.1. Photograph of the DMW Specimen 9C-034 Configured for Standard PA-UT with the ZETEC Manual Scanner Attached Directly onto the Specimen Being Examined

Figure 6.2. Photographs of the DMW Specimen 8C-036. Left: Configured for standard PA-UT with the stainless steel safe end on the right and the carbon steel end on the left side of the photograph. Right: The guide ring, translation slide and floor-to-ceiling brace are shown to the right.

To establish adequate acoustic coupling between the probe wedge and the specimen surface, a flow loop was designed to pump water through nipple fixtures embedded on both sides of the wedge harness that direct the flow evenly over the surface of the specimen to be imaged. As the water couplant flowed off of the top of the specimen, it was collected in a tray, channeled back to the pump, and recycled. Data acquisition was accomplished using the low-frequency DYNARAY system for PA probes evaluated in this study. This commercially available system is equipped to accommodate a maximum of 256 channels from PA probes and requires the use of UltraVision 3.1R9 software. Its frequency-pulsing electronics drive probes in the 0.2–20 MHz range. Phased-array data were acquired over a range of inspection angles from 30° to 70°, in 1° increments. Both line (at multiple distances away from the weld center line) and raster data were collected on each flaw. The laboratory workstation and DYNARAY data acquisition system are shown in Figure 6.3.

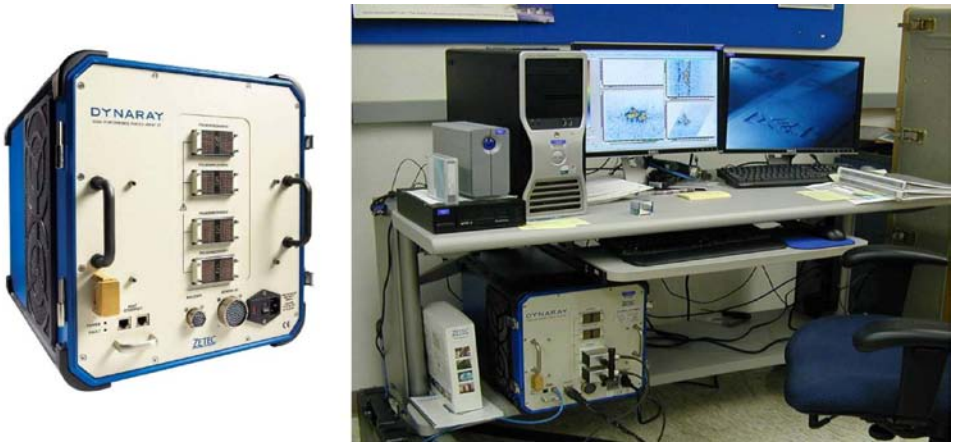

Figure 6.3. Data Acquisition System and Laboratory Workstation. Left: DYNARAY phased array data acquisition system (courtesy of ZETEC). Right: Laboratory workstation for both data acquisition and data analysis, with the DYNARAY system on the lower shelf.

6.2 Phased-Array Data Acquisition on Specimen 8C-032

The PNNL PA system used for data acquisition on 8C-032 consisted of a Tomoscan III 32-channel instrument, available off-the-shelf from ZETEC, Inc. The instrument can be programmed by developing focal laws to control up to 32 channels for transmission and reception of ultrasonic signals. It incorporates 12-bit logic and operates through a local Ethernet connection to a standard desktop computer. The UltraVision 2.1R4 software package was available and required to control the Tomoscan III system. Aside from the slightly different hardware and software, data acquisition on 8C-032 was collected as described in Section 6.1 via the use of the ZETEC manual track scanner and the adjustable ring track.

7.0 Specimens and Flaws Evaluated in this Study

The DMW mock-up specimens used in this evaluation were fabricated by FlawTech. If the specimen is already welded together prior to insertion of cracks, the FlawTech technique includes excavation of parent/weld material in the area targeted for implantation, and then subsequent insertion of the coupon containing the thermally induced fatigue crack. The flaw implantation vendor employs a unique proprietary process where heating/cooling under tension is used to initiate a TFC in a coupon. The number of cycles is controlled to obtain the desired crack depth and "roughness." After taking exact physical measurements, the flaw implant is seal welded in place to establish final location and size. The remaining weld groove is then filled with a standard welding procedure. The disadvantage is that the coupon is surrounded by weld metal that may potentially introduce additional UT reflectors, and in the event that the weld cannot be precisely located, the excavation "remnants" can indeed be detected with PA-UT. DMW mock-up specimens 8C-091 and 9C-023 were sent to FlawTech in an already assembled state. Only in the case of specimen 9C-023 did the excavation process for flaw implantation impact the ultrasonic responses. This is discussed in greater detail in Section 8.0.

The implanted TFCs and EDM-initiated HIP'ed cracks were specified to cover depths ranging from 10% through-wall to 95% through-wall with lengths ranging from 19.1 mm (0.75 in.) to 72.4 mm (2.85 in.) to provide a wide range of flaw dimensions. Some of the implanted cracks were introduced at a variable "tilt" angle from the 0 degree (normal) with the ID surface, with flaw tilt angles ranging from 0° to 30°. The flaw specifications defined in this evaluation provided a dimensionally diverse set of flaws (depth-wise in particular) across the set of five DMW mock-up specimens, effectively allowing the study to push the detection limits as well as the sizing limits for the PA approach. Depending on the particular mock-up, flaws were either specified to be implanted within the weld metal or within the Inconel 82/182 butter to minimize the potential for disturbing the parent material or introducing implantation anomalies that might result in reflection of coherent sound energy, and to simulate the weld area where PWSCC has been experienced.

7.1 DMW Specimen 8C–032

Specimen 8C-032 consists of a SA508 nozzle welded to a 316 stainless steel (SS) safe end welded to an A312 TP304L pipe. The individual sections were sent to FlawTech where four circumferentially oriented TFCs were implanted in the nozzle butter material (Inconel 82/182) as the nozzle was welded to the safe end. This DMW mock-up specimen is 347.4 mm (13.68 in.) in diameter at the flaw position, and is approximately 249.5 mm (9.82 in.) in length, with approximately 37.1-mm (1.46-in.) wall thickness at the flaw location within the DMW. Photographs of the mock-up are provided in Figure 7.1.

The four TFCs were inserted via a coupon-implant technique and were all circumferentially oriented flaws. A side-view illustration of the four flaws depicting flaw position relative to the DMW geometry and flaw depth is provided in Figure 7.2.

A full-circumferential view of all flaw positions and extents on specimen 8C-032 is shown in Figure 7.3. This pipe end-view depicts the circumferential extent (length) of the implanted ID surface-connected cracks, relative to the radial position along the pipe circumference.

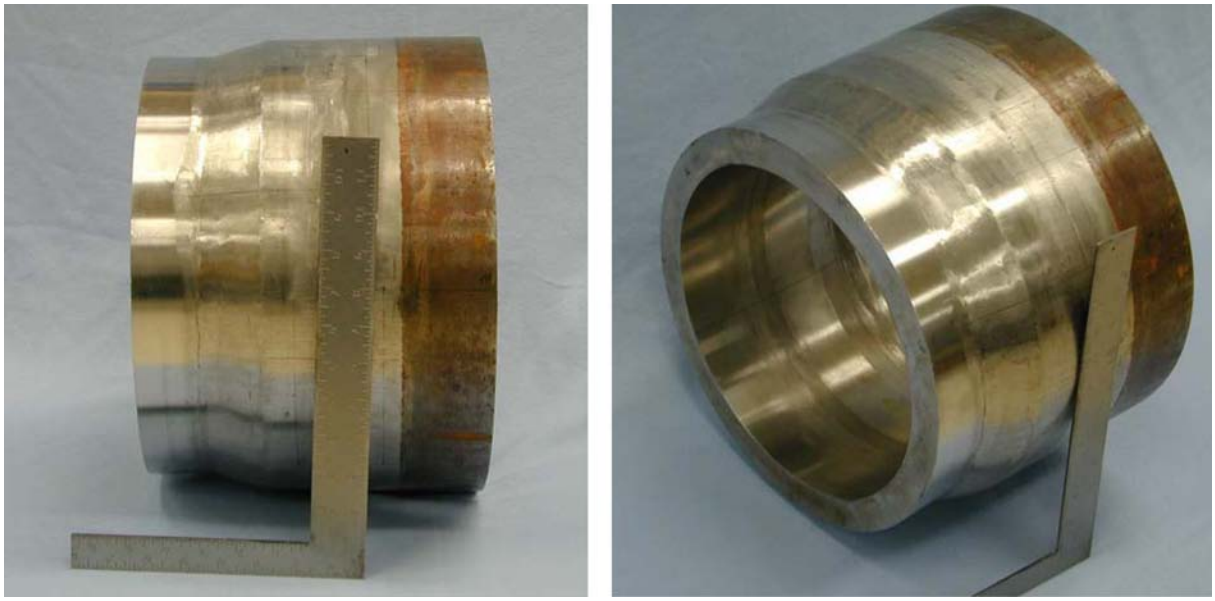

Figure 7.1. Photographs of the DMW Mock-up Specimen 8C-032

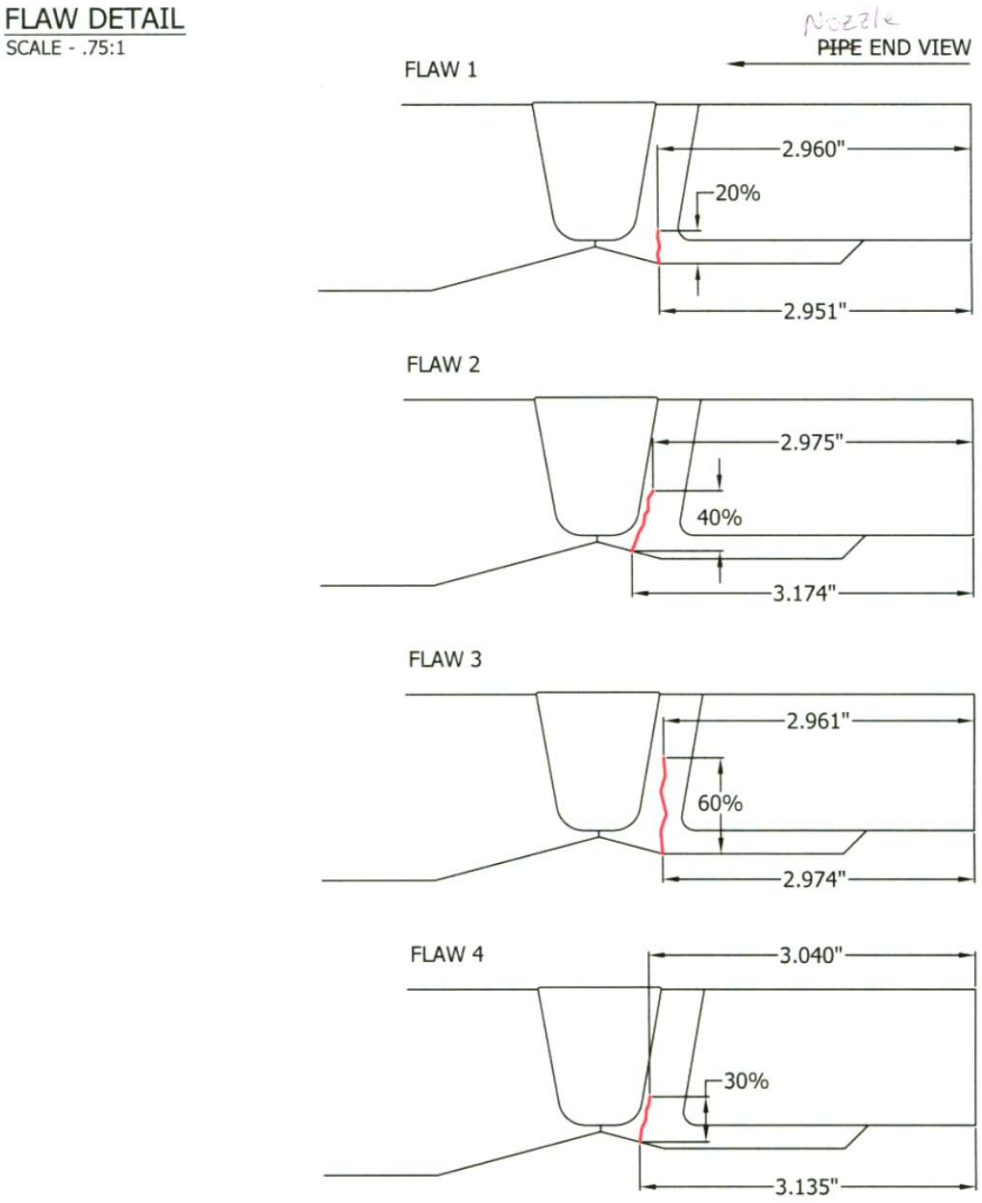

Figure 7.2. Side View Illustration of All Four Thermal Fatigue Cracks Implanted into DMW Mock-Up Specimen 8C-032

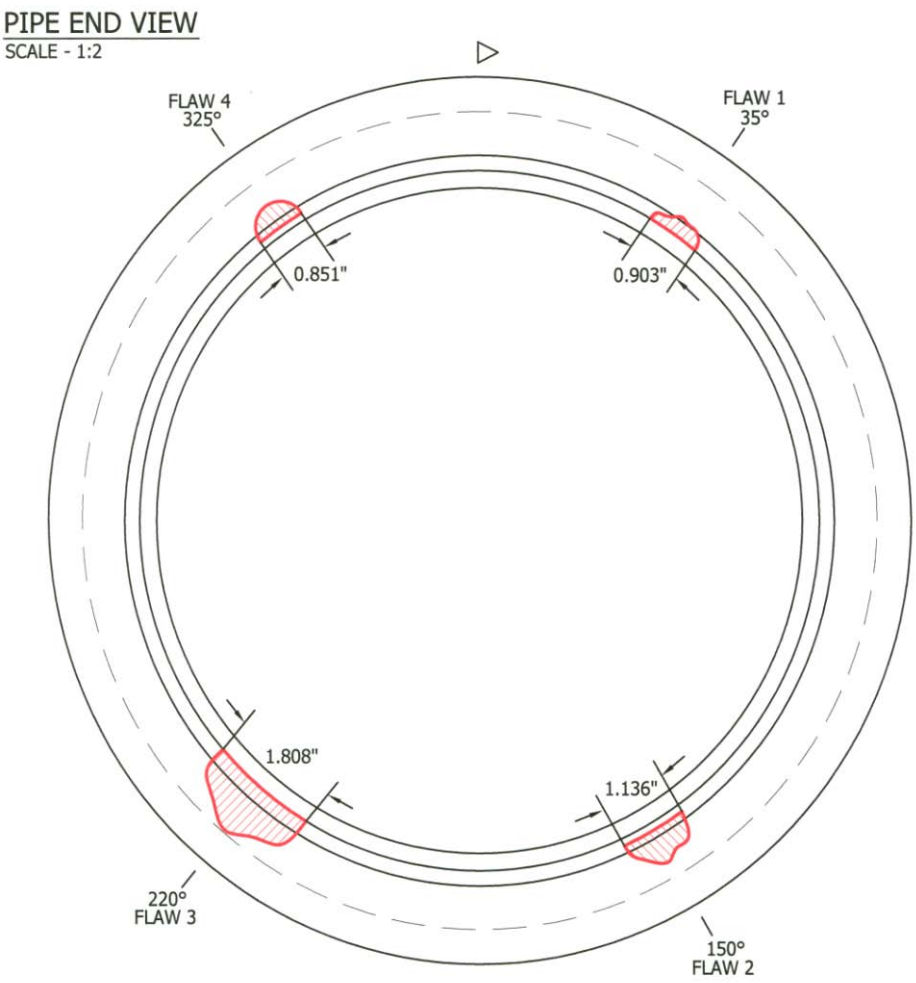

Figure 7.3. End View Illustration of All Four Thermal Fatigue Cracks Implanted into DMW Mock-Up Specimen 8C-032

7.2 DMW Specimen 9C–023

Specimen 9C-023 is a shutdown cooling pipe DMW salvaged from WNP-3 and consists of a ferritic (low-alloy carbon steel) nozzle with Inconel 82/182 buttering, and welded to a WSS pipe. This specimen was sent to FlawTech as an already-welded assembly so the TFCs were specified to be implanted into the weld region following an excavation process. The weld profile was not known so the axial position for flaw implantation in the weld/butter region was estimated. The flaw implantation required first excavating a region, then inserting the crack coupon, and adding weld filler material around the coupon. The excavation area is reported to be only 2.5 mm (0.100 in.) beyond the crack coupon. When the excavation area is in the weld or butter regions, it should not be ultrasonically visible because the filler material should be acoustically similar to the weld/butter material. This DMW mock-up specimen is 364.3 mm (14.34 in.) in diameter at the flaw position, and is approximately 281.0 mm (11.06 in.) in length, with approximately 36.1-mm (1.42-in.) wall thickness at the flaw location within the DMW. Photographs of the mock-up are provided in Figure 7.4.

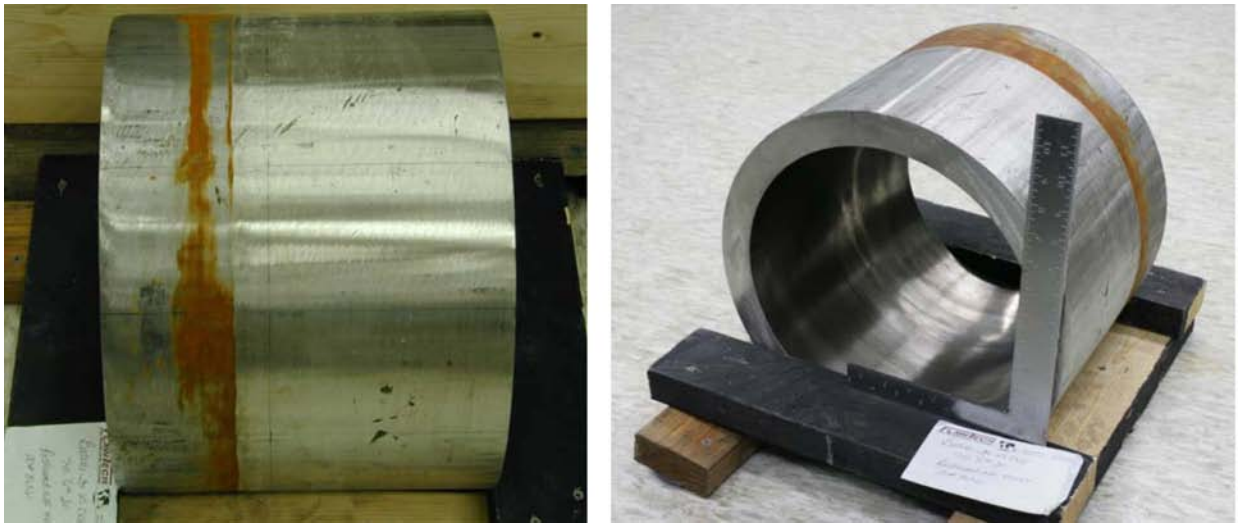

Figure 7.4. Photographs of the DMW Mock-up Specimen 9C-023

The four TFCs were inserted via a coupon-implant technique and were all circumferentially oriented flaws. A side-view illustration of the four flaws depicting flaw position relative to the DMW geometry and flaw depth is provided in Figure 7.5.

A full circumferential view of all flaw positions and extents on specimen 9C-023 is shown in Figure 7.6. This pipe end-view depicts the circumferential extent (length) of the implanted ID surface-connected cracks, relative to the radial position along the pipe circumference.

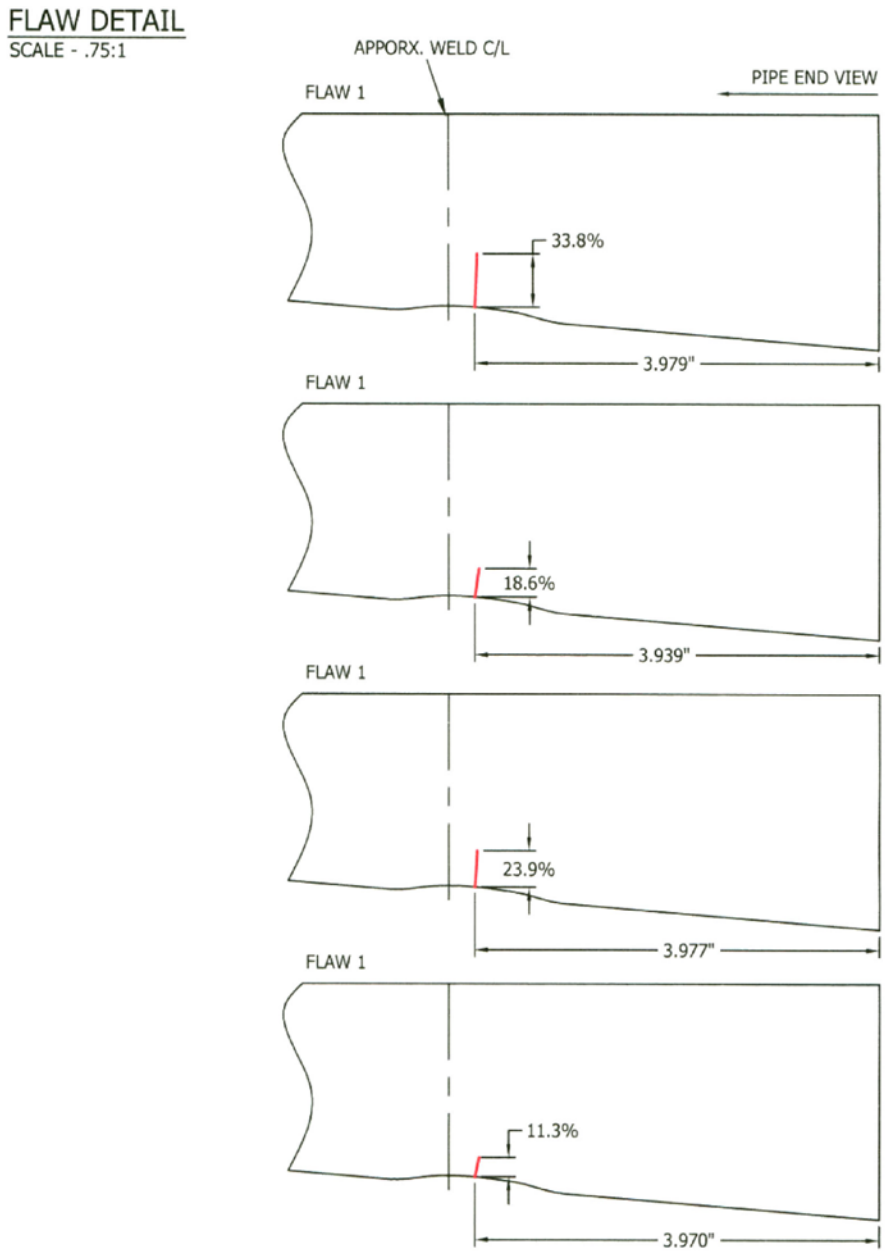

Figure 7.5. Side View Illustration of All Four Thermal Fatigue Cracks Implanted into DMW Mock-up Specimen 9C-023

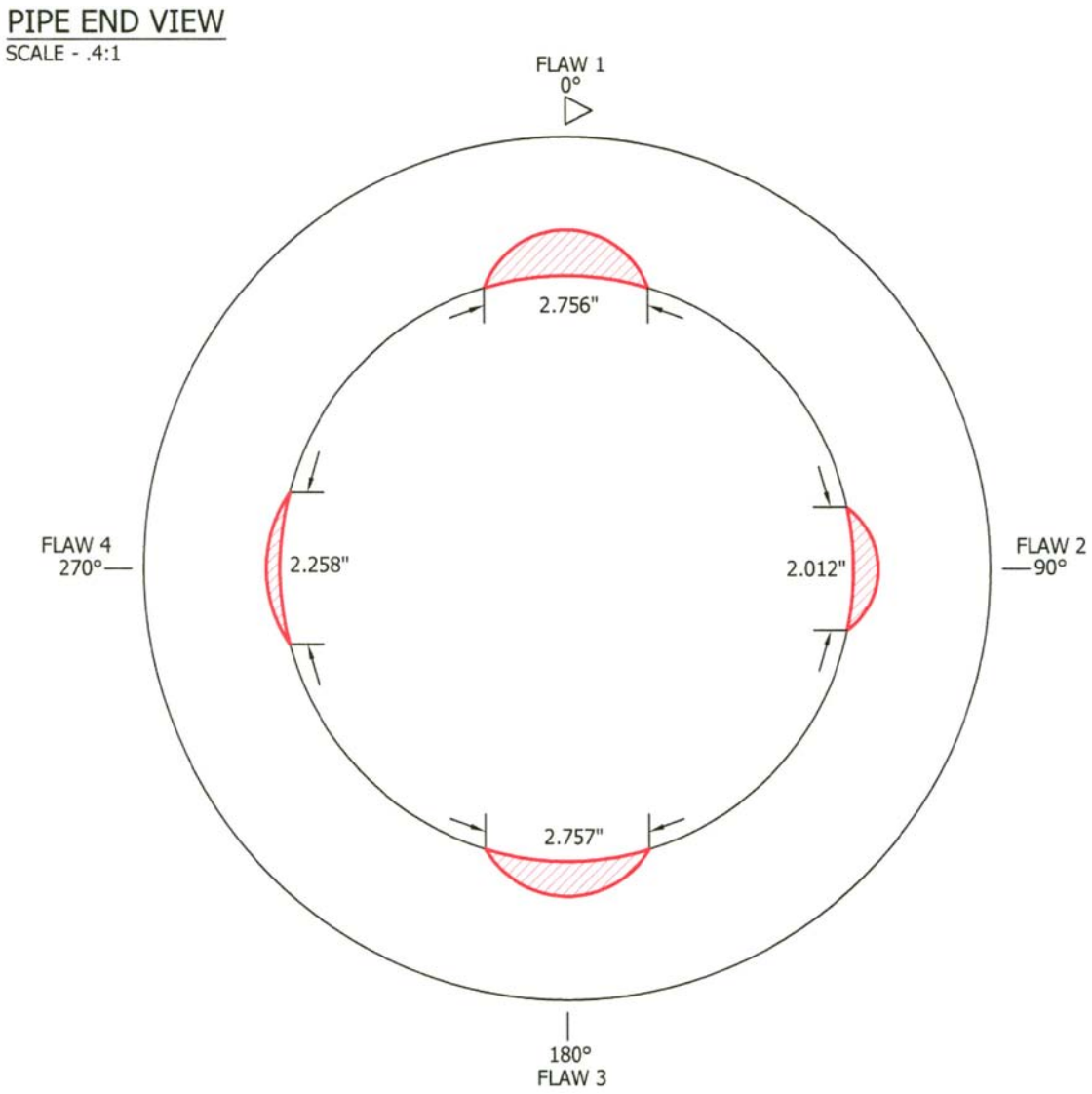

Figure 7.6. End View Illustration of All Four Thermal Fatigue Cracks Implanted into DMW Mock-up Specimen 9C-023

7.3 DMW Specimen 8C–091

Specimen 8C-091 is a DMW PZR surge nozzle specimen that was sent to FlawTech for flaw implantation in the already-assembled state. The assumed configuration for this specimen is a ferritic nozzle-to-Inconel 82/182 butter and weld-to-WSS PZR surge line pipe. The specimen contains two HIP'ed EDM notches and two TFCs placed in the butter region as best estimated because the actual weld dimensions are unknown.

FlawTech introduced two circumferentially oriented TFCs and two circumferentially oriented EDM-initiated HIP'ed cracks into the Inconel 82/182 butter material adjacent to the weld. This DMW mock-up specimen is 323.7 mm (12.75 in.) in diameter at the flaw position, and is approximately 608.1 mm (23.94 in.) in length, with approximately 39.4-mm (1.55-in.) wall thickness at the flaw location within the

DMW. The OD weld region was machined flat prior to the ultrasonic examinations because there was a large weld crown that prohibited full contact of the probe wedge with the specimen. The machining left a step approximately at the nozzle-to-weld OD interface (weld toe region on the nozzle side). Photographs of the mock-up are provided in Figure 7.7.

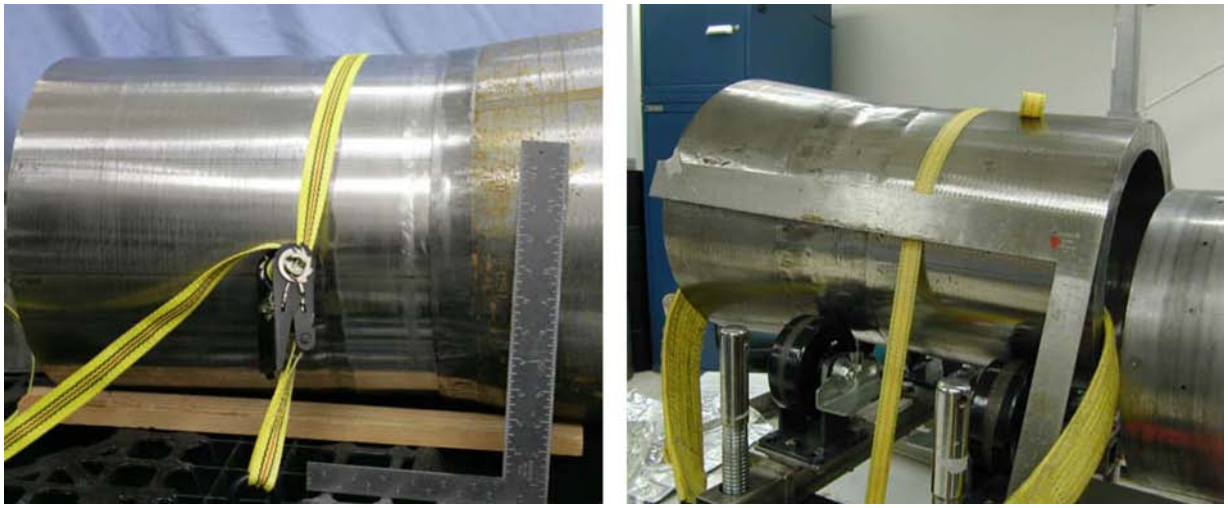

Figure 7.7. Photographs of the DMW Mock-up Specimen 8C-091

The two TFCs were inserted via an excavation and coupon-implant technique, while the other two cracks were initiated with EDM notches and subsequently HIP'ed. All cracks were circumferentially oriented in the buttering. A side-view illustration of the four flaws depicting flaw position relative to the DMW geometry and flaw depth is provided in Figure 7.8.

Figure 7.9 shows a full circumferential view of all flaw positions and extents on specimen 8C-091. This pipe end-view depicts the circumferential extent (length) of the implanted ID surface-connected cracks, relative to the radial position along the pipe circumference.

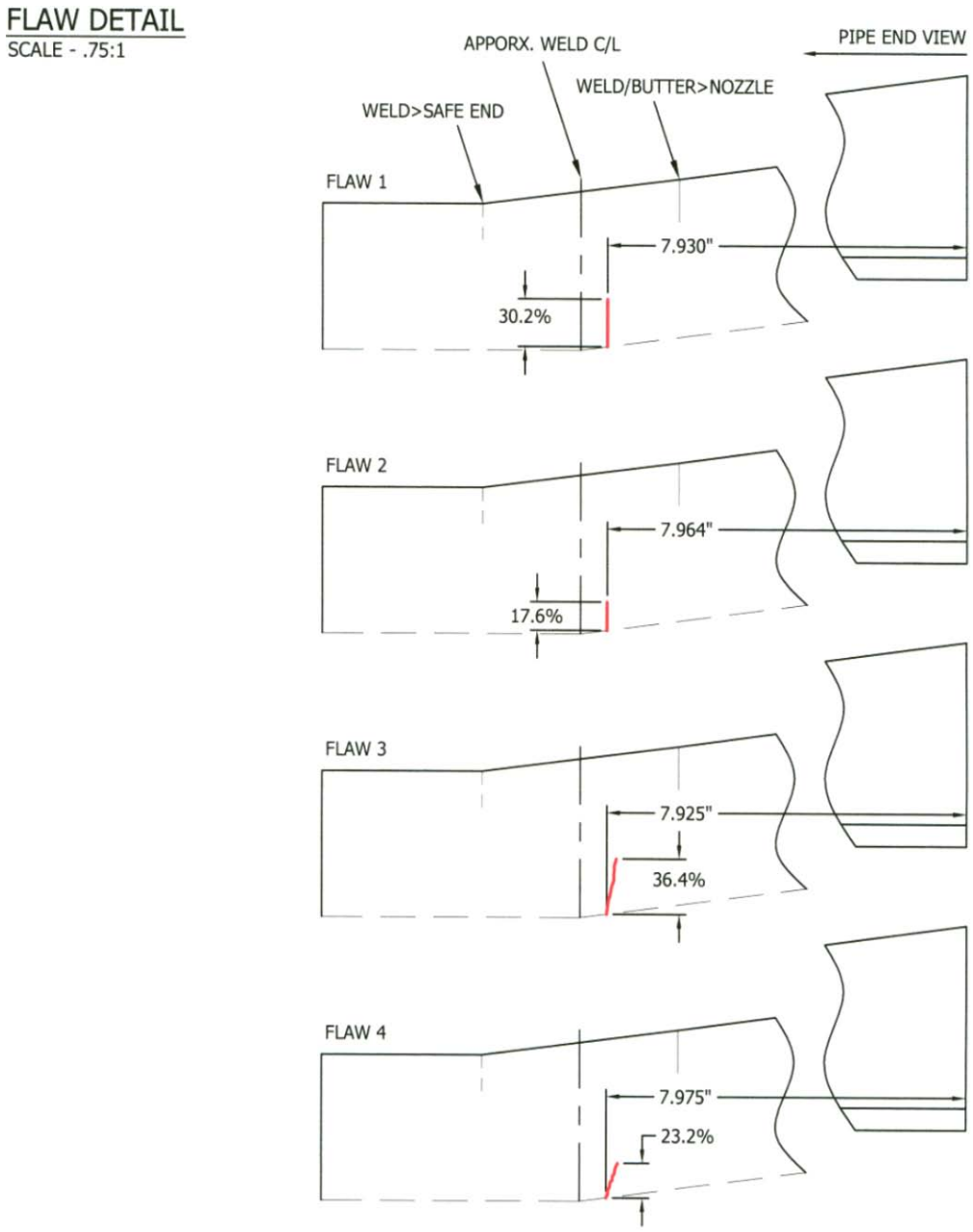

Figure 7.8. Side View Illustration of All Four Cracks (two TFC's and two HIP'ed EDM Notches) Implanted into DMW Mock-up Specimen 8C-091

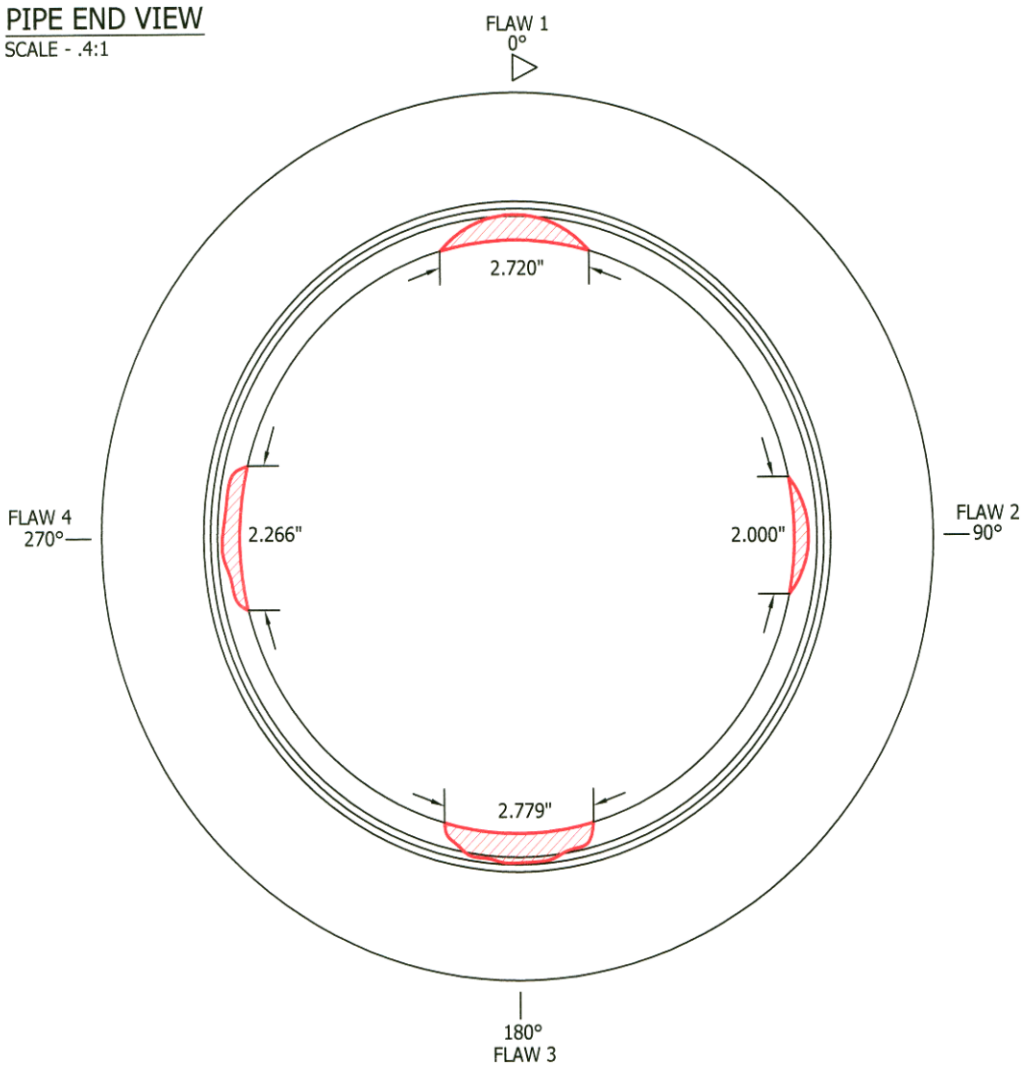

Figure 7.9. End View Illustration of All Four Cracks (two TFC's and two HIP'ed EDM Notches) Implanted into PZR CASS Specimen 8C-091

7.4 DMW Specimen 9C–034

Specimen 9C-034 contains a DMW between a 516 Gr70 carbon steel nozzle and a CASS pipe. The nozzle side butter and weld were fabricated from Inconel 82/182 material. Four TFCs were implanted in the weld butter region with flaw depths ranging from 13% to 31% through-wall. The flaws are vertical (i.e., no tilt) and are circumferentially oriented. The specimen was first ultrasonically examined with the weld crown in place. It was determined that the presence of the weld crown limited data acquisition, so the crown was removed and the specimen rescanned. Data were acquired from the CASS piping side of the weld. The CASS PZR surge-line pipe segment has an approximate 324-mm (12.75-in.) OD, and is approximately 31.8 mm (1.25 in.) in wall thickness. This pipe portion of the DMW specimen was cut from a longer segment of a CASS PZR surge line from WNP-3. The individual section of CASS pipe was sent to FlawTech where it was buttered and welded to a procured carbon steel nozzle segment and the four TFCs were simultaneously implanted into the specimen, eliminating any traces of excavation remnants. This DMW mock-up specimen is 324.9 mm (12.75 in.) in diameter at the flaw position, and is

approximately 584.2 mm (23.00 in.) in length, with approximately 34.8-mm (1.37-in.) wall thickness at the flaw location within the DMW. Digital photographs of the mock-up are provided in Figure 7.10 and Figure 7.11. These photos show a significant difference in surface condition and subsequent access and transducer coupling efficiency between the specimen with and without the weld crown.

Figure 7.10. Photographs of the Original OD Surface of DMW Mock-up Specimen 9C-034

Figure 7.11. Photographs of the OD Surface of DMW Mock-up Specimen 9C-034 after Weld Crown Removal

This specimen also exhibited significant ID surface conditions and geometry that, to some degree, impacted the ultrasonic responses from the PA-UT evaluations. The weld root was substantial, and can be seen in the photographs provided in Figure 7.12.

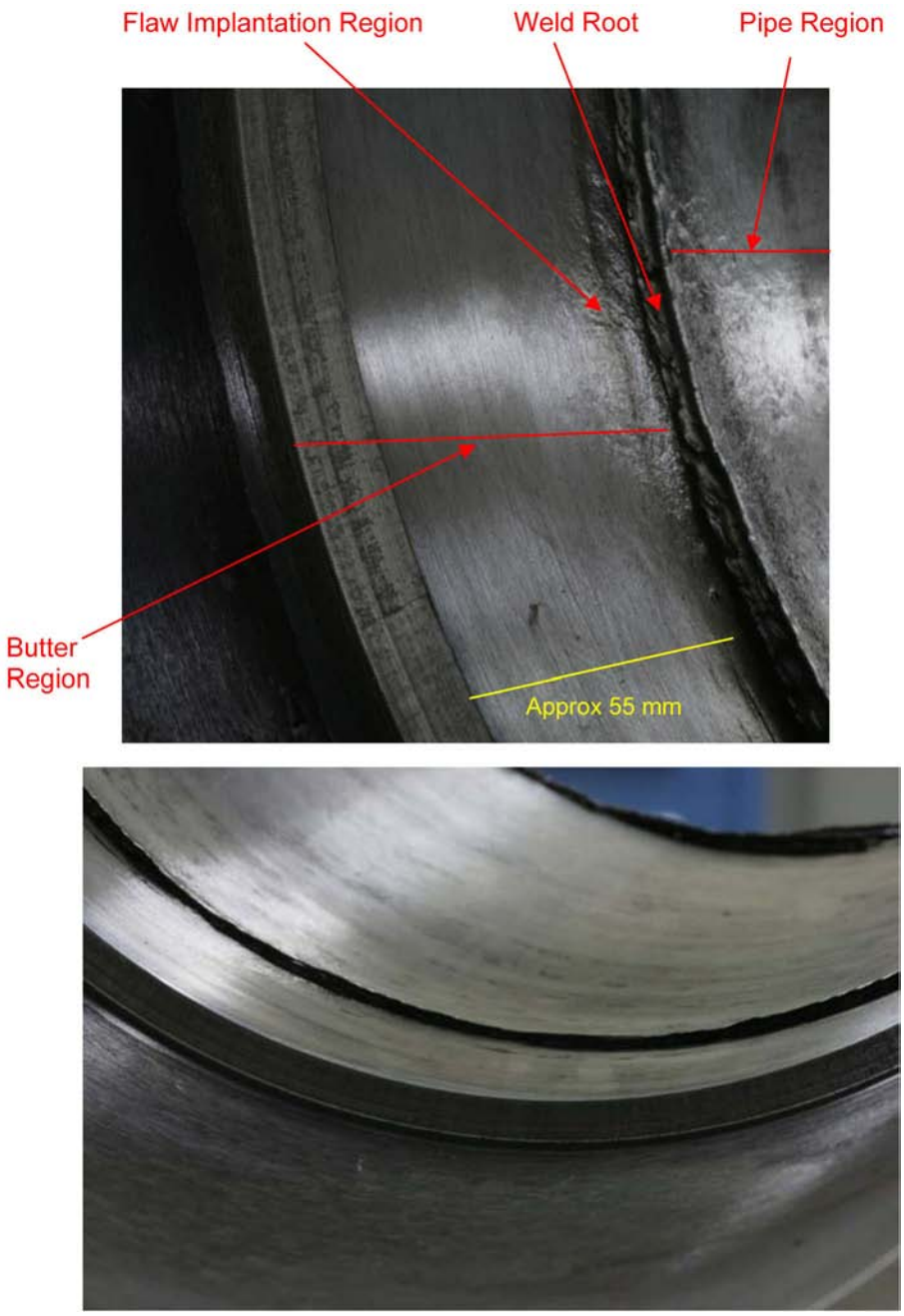

Figure 7.12. Photographs of the ID Surface of DMW Mock-up Specimen 9C-034 Depicting Various ID Surface and Weld Geometries

The four TFCs were inserted via a coupon-implant technique and were all circumferentially oriented flaws. A side-view illustration of the four flaws depicting flaw position relative to the DMW geometry and flaw depth is provided in Figure 7.13.

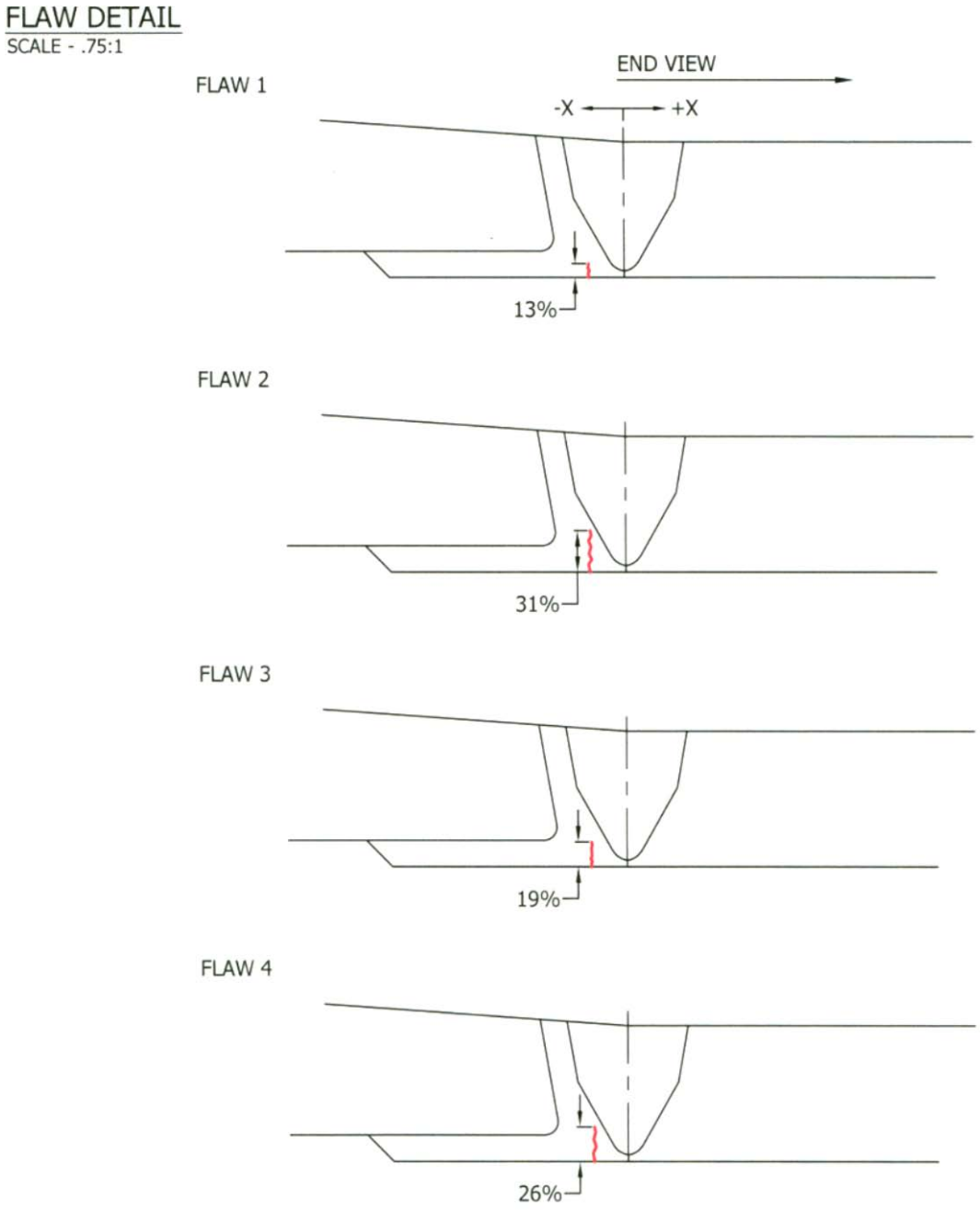

Figure 7.13. Side-View Illustration of All Four Thermal Fatigue Cracks Implanted into DMW Mock-Up Specimen 9C-034

Figure 7.14 shows a full circumferential view of all flaw positions and extents on specimen 9C-034. This pipe end-view depicts the circumferential extent (length) of the implanted ID surface-connected cracks, relative to the radial position along the pipe circumference.

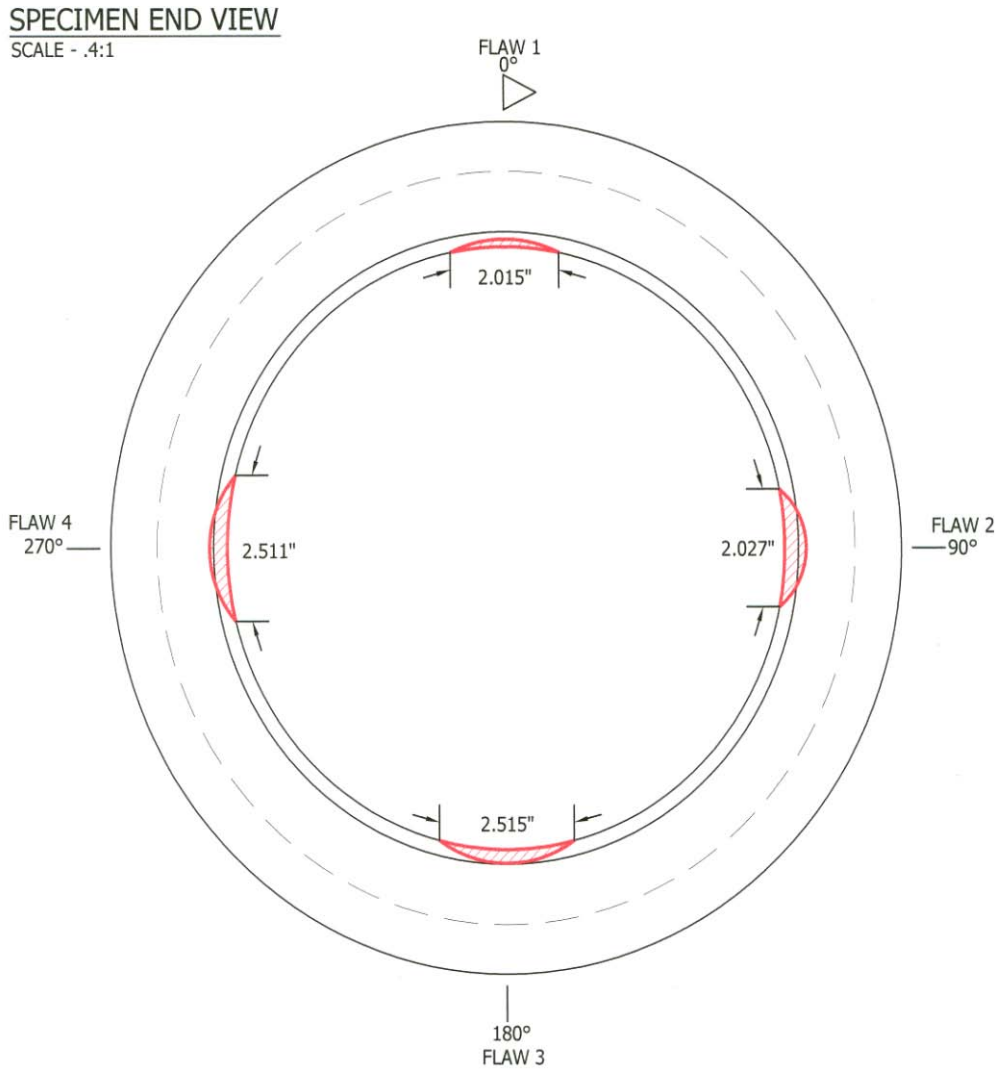

Figure 7.14. End-View Illustration of All Four Thermal Fatigue Cracks Implanted into DMW Mock-up Specimen 9C-034

7.5 DMW Specimen 8C-036

Specimen 8C-036 is a nozzle-to-stainless steel safe end-to-pipe DMW configuration. It contains four TFCs and four HIP'ed EDM notches. Two of the EDM notches are axially oriented while the other six flaws are circumferential in orientation. The individual sections were sent to FlawTech where the DMW specimen mock-up was buttered and welded and subsequently all six circumferential cracks were implanted in the Inconel 82/182 butter material while the two axial cracks spanned the butter and weld zones. This DMW mock-up specimen is 348.2 mm (13.71 in.) in diameter at the flaw position, and is approximately 241.0 mm (9.49 in.) in length, with approximately 37.8-mm (1.49-in.) wall thickness at the flaw location within the DMW. Photographs of the mock-up are provided in Figure 7.15.

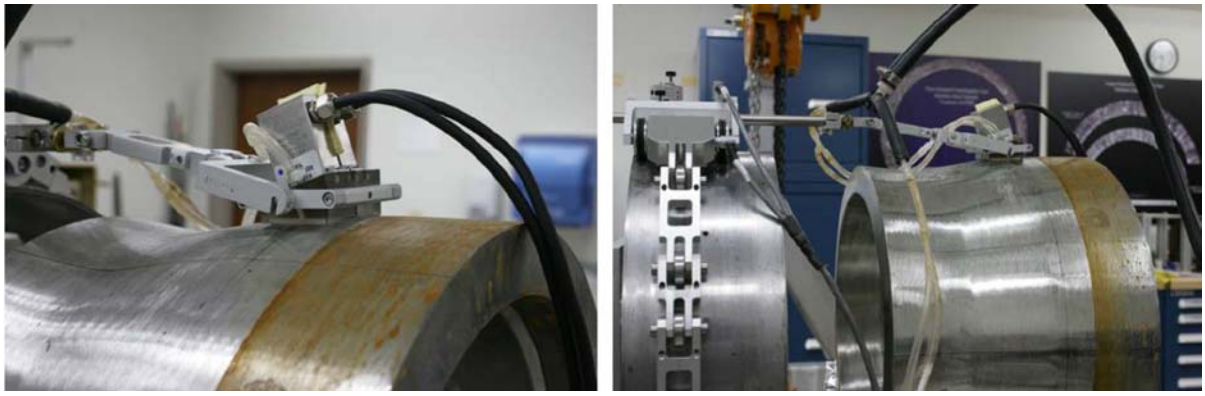

Figure 7.15. Photographs of DMW Mock-up Specimen 8C-036

A side-view illustration of the four flaws depicting flaw position relative to the DMW geometry and flaw depth is provided in Figure 7.16, while side views of the two circumferentially HIP'ed EDM notches and two axially HIP'ed EDM notches are provided in Figure 7.17 and Figure 7.18, respectively.

Figure 7.19 shows a full circumferential view of all flaw positions and extents on specimen 8C-036. This pipe end-view depicts the circumferential extent (length) of the implanted ID surface-connected cracks, relative to the radial position along the pipe circumference.

A summary of true-state flaw position, location, orientation, length, and depth (flaw height) for all five DMW mock-up specimens is provided in Table 7.1.

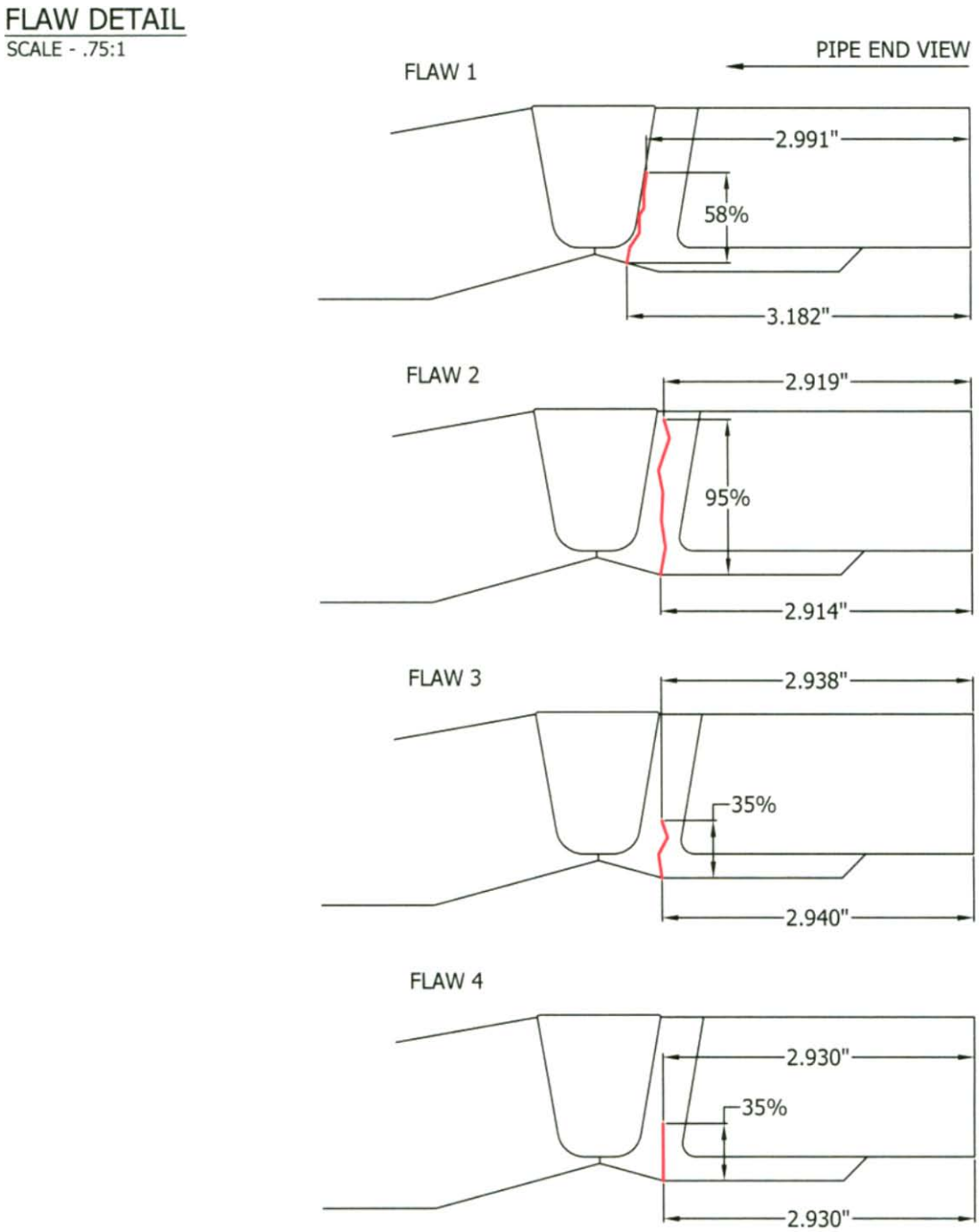

Figure 7.16. Side-View Illustration of All Four Thermal Fatigue Cracks Implanted into DMW Mock-up Specimen 8C-036

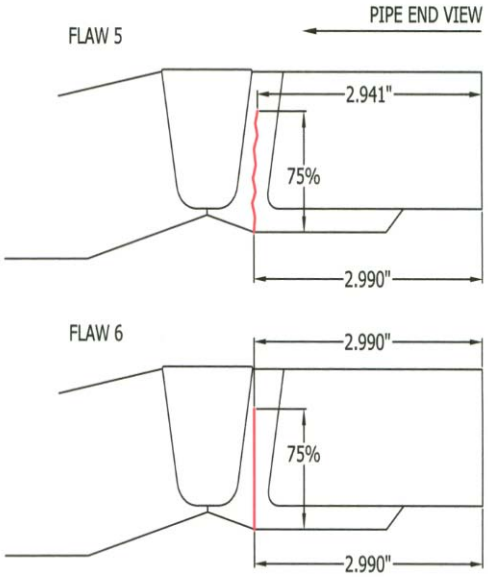

Figure 7.17. Side-View Illustration of the Two Circumferentially HIP'ed EDM Notches Implanted into DMW Mock-up Specimen 8C-036

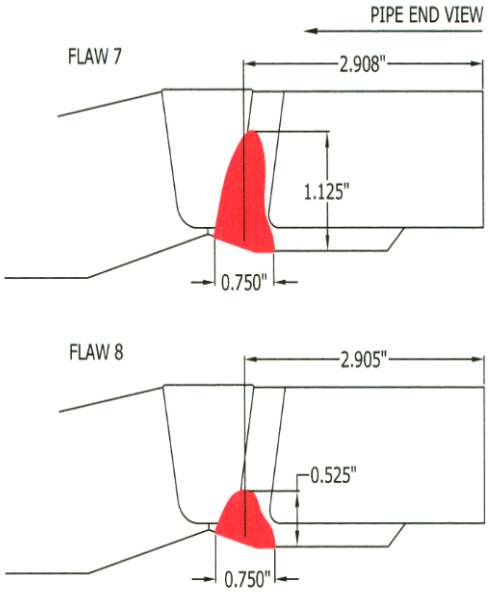

Figure 7.18. Side-View Illustration of the Two Axially HIP'ed EDM Notches Implanted into DMW Mock-up Specimen 8C-036

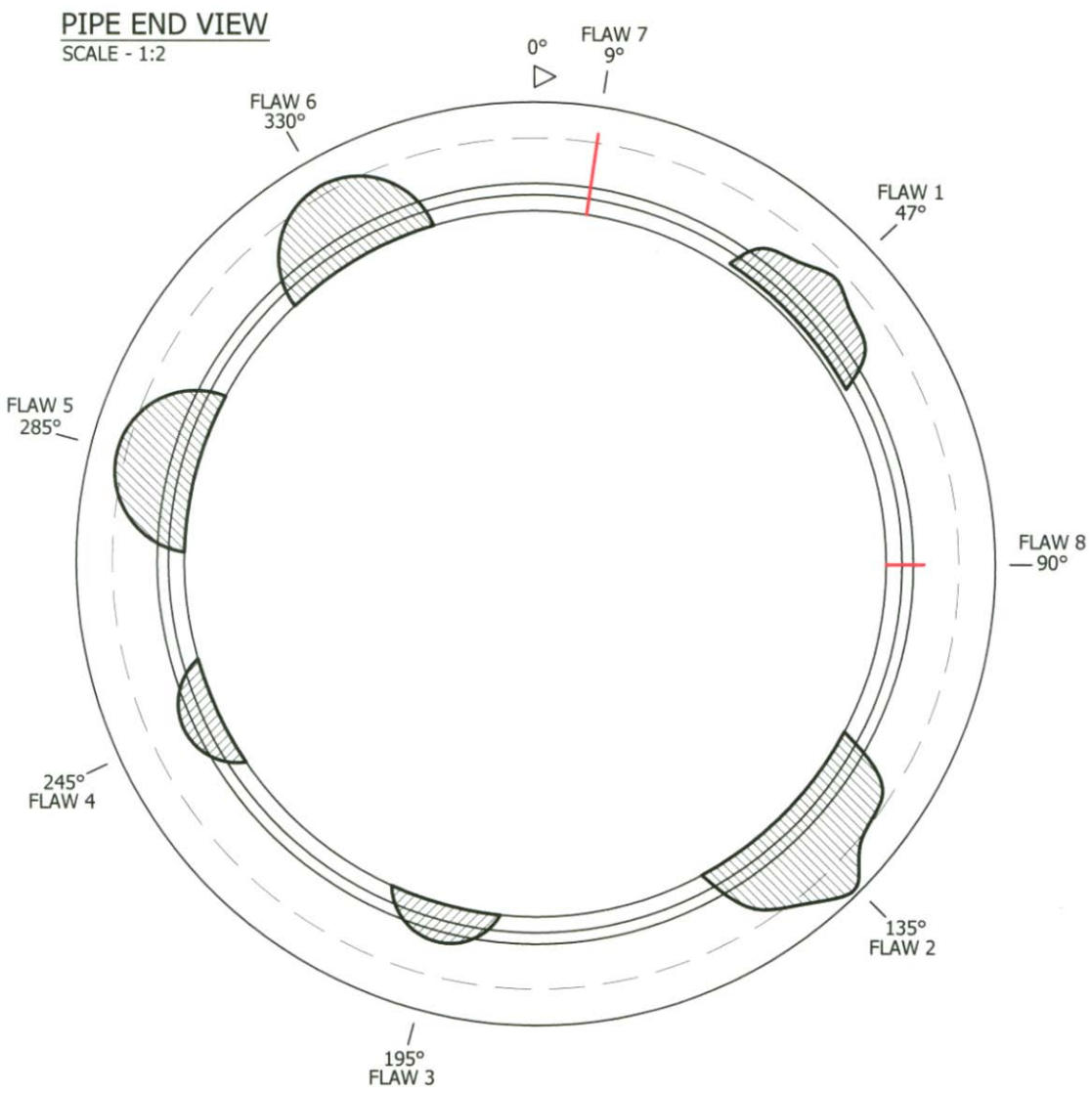

Figure 7.19. End-View Illustration of All Eight TFCs and HIP'ed EDM Cracks Implanted into DMW Mock-up Specimen 8C-036

Table 7.1. Summary Table Depicting True-State Dimensions and Locations of All Flaws in All Five DMW Mock-Up Specimens Examined in This Study

Flaw	Type	Length (mm/in)	Depth (mm/in)	Depth (%)	Tilt (deg)	Orientation
8C-032						
1	TFC	22.9 (0.903)	7.7 (0.302)	20	0	Circ.
2	TFC	28.9 (1.136)	14.4 (0.568)	40	19	Circ.
3	TFC	45.9 (1.808)	23.0 (0.904)	60	0	Circ.
4	TFC	21.6 (0.851)	10.8 (0.427)	30	13	Circ.
9C-023						
1	TFC	70.0 (2.756)	12.5 (0.491)	33.8	2	Circ.
2	TFC	51.1 (2.012)	6.7 (0.262)	18.6	8	Circ.
3	TFC	70.0 (2.757)	8.4 (0.332)	23.9	4	Circ.
4	TFC	57.4 (2.258)	4.1 (0.162)	11.3	12	Circ.
8C-091						
1	HIP'ed EDM	69.1 (2.720)	11.7 (0.459)	30.2	0	Circ.
2	HIP'ed EDM	50.8 (2.000)	7.0 (0.277)	17.6	0	Circ.
3	TFC	70.6 (2.779)	14.1 (0.556)	36.4	10	Circ.
4	TFC	57.6 (2.266)	9.2 (0.363)	23.2	19	Circ.
9C-034						
1	TFC	51.2 (2.015)	4.5 (0.179)	13	0	Circ.
2	TFC	51.5 (2.027)	10.7 (0.423)	31	0	Circ.
3	TFC	63.9 (2.515)	6.5 (0.255)	19	0	Circ.
4	TFC	63.8 (2.511)	9.2 (0.362)	26	0	Circ.
8C-036						
1	TFC	63.1 (2.483)	21.1 (0.830)	58	30	Circ.
2	TFC	72.4 (2.852)	36.2 (1.427)	95	0	Circ.
3	TFC	40.1 (1.579)	13.4 (0.528)	35	0	Circ.
4	HIP'ed EDM	40.0 (1.575)	13.3 (0.525)	35	0	Circ.
5	TFC	57.4 (2.260)	28.8 (1.132)	75	0	Circ.
6	HIP'ed EDM	57.2 (2.250)	28.6 (1.125)	75	0	Circ.
7	HIP'ed EDM	19.1 (0.750)	28.6 (1.125)	74.7	0	Axial
8	HIP'ed EDM	19.1 (0.750)	13.3 (0.525)	50	0	Axial

8.0 Data Analysis and Results

Sections 8.1 through 8.5 describe results from the phased-array ultrasonic examinations of the five DMW specimens evaluated in this study. Each section highlights a specimen and reports on the length and depth sizing of flaws and calculated SNR for that specimen. Section 8.6 summarizes the findings as viewed by combining all the flaws together.

Data were acquired primarily at 1.5 MHz with both raster and line scan data formats. Supplemental data were acquired at 2 MHz when the specimen configuration and material would allow it. For example, with limited axial access to the weld, the smaller footprint of the 2-MHz probe was helpful as in specimen 8C-036. When the material supported the higher frequency, data were acquired at 2 MHz for better resolution in flaw characterization.

8.1 Specimen 8C-032

Specimen 8C-032 consists of a SA508 nozzle welded to a 316 SS safe end welded to an A312 TP304L pipe containing four circumferentially oriented TFCs implanted in the nozzle butter material.

Data were acquired from both the carbon steel and austenitic sides of the weld, but only the data from the austenitic safe-end side of the weld will be reported, as this side provides typical access for field inspections (nozzle tapers generally exclude access to these welds from the carbon steel side). The data show that all four TFCs were detected at 1.5 MHz. Figure 8.1 shows the data from flaw 2 and is representative of the data from the other three flaws. A strong reflection from the near-side counterbore is seen in the left of the top-view and side-view images. The flaw response is marked in the side view and shows both a corner response and a response from the upper portion of the flaw. Flaw depth is determined from both the corner and upper flaw response signals. In the side view, the flaw signal is gated and this vertically gated region is displayed in the end view. The complete set of data images from this specimen is shown in Appendix A.

Signal-to-noise ratios were calculated from the gated end-view images. The peak corner response in the image and the mean noise response at the same part path represented the signal and the noise levels respectively. SNRs were in the 13–17 dB range for line scans and in the 16–19 dB range for raster data at 1.5 MHz. Flaw signals are more completely defined in the raster data so a higher SNR is reasonable.

Line scan data was also acquired at 2 MHz and these show finer resolution but more scattering of the flaw signal. Figure 8.2 provides examples of line scan data from 2 MHz (top) and 1.5 MHz (bottom) PA probes. The 2-MHz flaw response was not as well separated from the geometrical responses as is the 1.5-MHz data. In the 1.5-MHz data on the bottom of the figure, the flaw signal is sandwiched between two geometrical reflectors in the side view. The flaw signal is gated by the vertical lines in the side view with results shown in the end view. For the 2-MHz data on top, the flaw signal is not as cleanly gated, or separated from the two geometrical signals and results in a lower SNR. This effect is due to offset in the beam focusing and the axial position of the probe relative to the flaw. These two line scan data sets show the importance of raster data for flaw characterization, in that raster data inherently provides many axial positions. Line scan data, on the other hand, represent only one axial position and that position may not be optimum for signal discrimination and characterization.

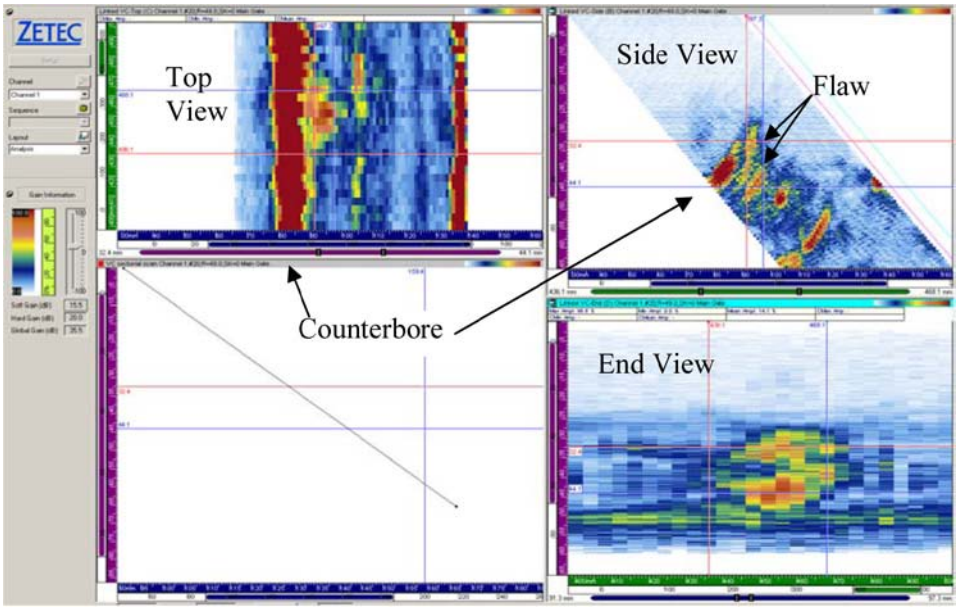

Figure 8.1. Flaw 2 from DMW Specimen 8C-032 at 1.5 MHz

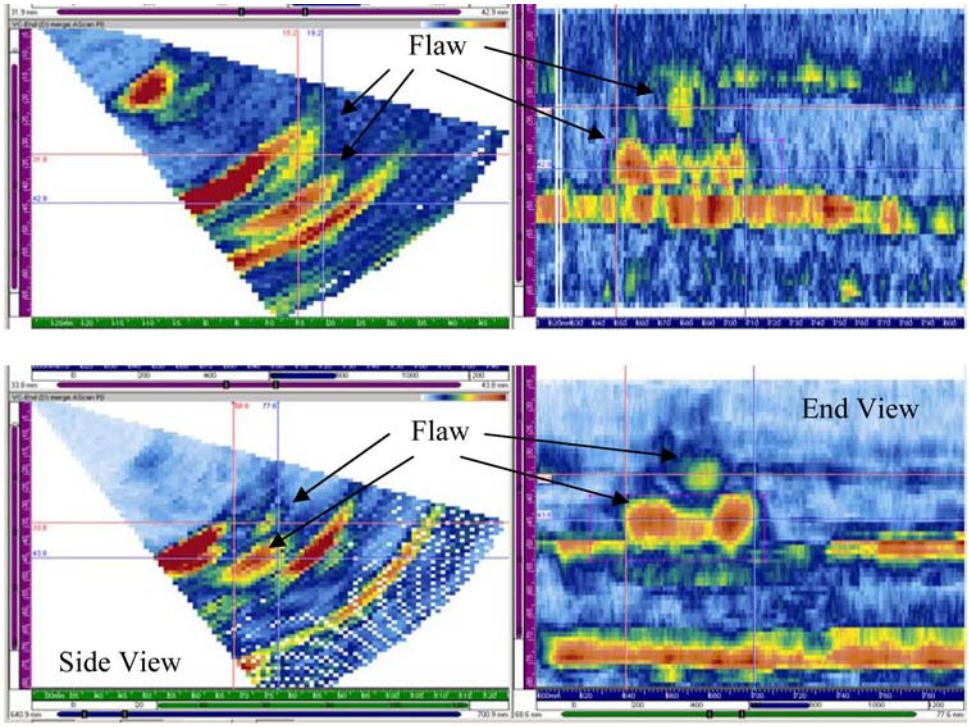

Figure 8.2. Flaw 3 from Specimen 8C-032 at 2 MHz on the Top and at 1.5 MHz on the Bottom. The 1.5-MHz inspection showed better separation between flaw and geometrical signals.

SNRs, which are determined from the flaw corner response, were similar, or slightly lower at 2 MHz as compared to 1.5 MHz. The SNRs were in the 8–18 dB range. All four flaws were detected at 2 MHz from the austenitic pipe side of the DMW.

The length and depth sizing results are shown in Figure 8.3 and Figure 8.4. All data oversized flaw 3 and undersized flaw 4 in length. The deeper flaw, flaw 3, at 60% through-wall, was undersized in depth in all the data sets. In both the 1.5- and 2-MHz probes, the beam is well-defined and has a strong response at 45° giving a good detection of the corner signal. At higher angles, the beam is still well-formed but is less sensitive as shown previously in Figure 5.5 for the 1.5-MHz probe-simulated beam at 60°. This contributes to the lack of detection of the very upper portion (close to the OD) of deeper flaws.

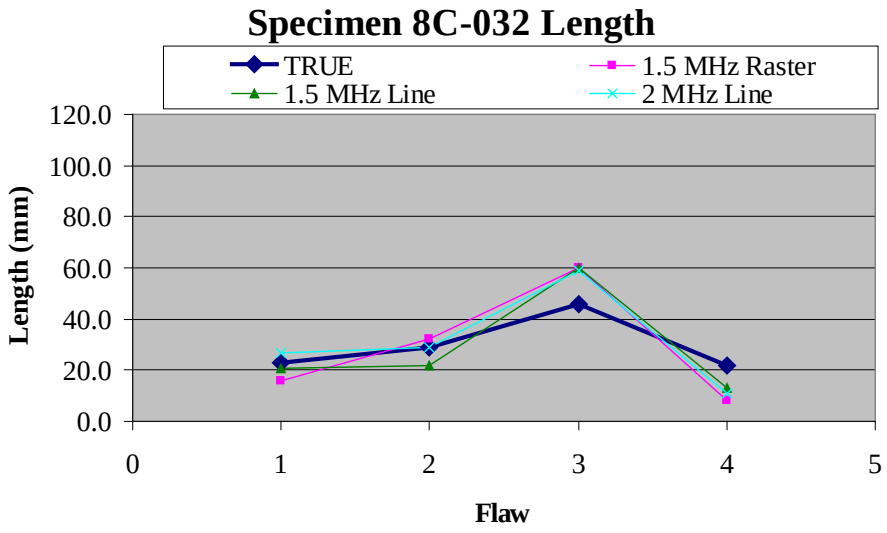

Figure 8.3. Length Sizing Results on Specimen 8C-032

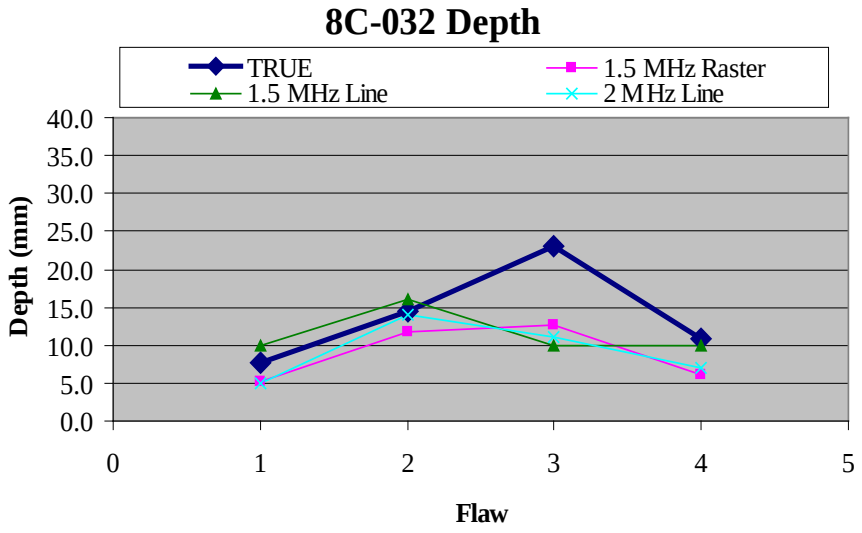

Figure 8.4. Depth Sizing Results on Specimen 8C-032

8.2 DMW Specimen 9C-023

Specimen 9C-023 is a shutdown cooling pipe DMW salvaged from WNP-3 and was ultrasonically examined prior to crack insertion to establish a material baseline. No problem areas were found in the material. This specimen was sent to FlawTech as an already-welded assembly so the TFCs were implanted into the weld region following an excavation process. The weld profile was not known so the axial position for flaw implantation in the weld/butter region was estimated. The flaw implantation required first excavating a region, then inserting the crack coupon, and adding weld filler material around the coupon. The excavation area is reported to be only 2.5 mm (0.100 in.) beyond the crack coupon. When the excavation area is in the weld or butter regions, it should not be ultrasonically visible as the filler material should be acoustically similar to the weld/butter material. Data from this specimen show that an area suspected to be the excavation region was detected and was typically much longer than the crack. The data is discussed below in more detail. Other PNNL DMW specimens, 8C-036, 8C-032, and 9C-034, were fabricated at FlawTech from two separate pieces, such as a cast pipe to a carbon steel nozzle section. For these three specimens, the weld and butter dimensions are fully known and the crack coupon was placed into the weld or butter region as the two specimen ends are joined. No excavation region is needed and none is detected.

The majority of the ultrasonic data collected from the four TFCs in specimen 9C-023 show reflections from a possible excavation area. This is represented in the data by a semicircular reflection in the upper portion of the flaw that extends to the back wall or ID surface. This leads to over sizing of the flaws in length and depth. For example, flaw 1 data from the WSS side of the weld in Figure 8.5 is length sized at 64.3 mm if only the corner response at the −6 dB points are used, noted by the vertical lines in the end view. The reported flaw length is 70.0 mm (2.76 in.). Taking into account the semicircular reflection, which appears to be part of the flaw response, leads to a 114.5-mm (4.5-in.) flaw length as shown in Figure 8.6, also noted by the vertical lines in the end view. This error in length is much greater than a few millimeters and leads one to believe that a large excavation area was used to implant this crack.

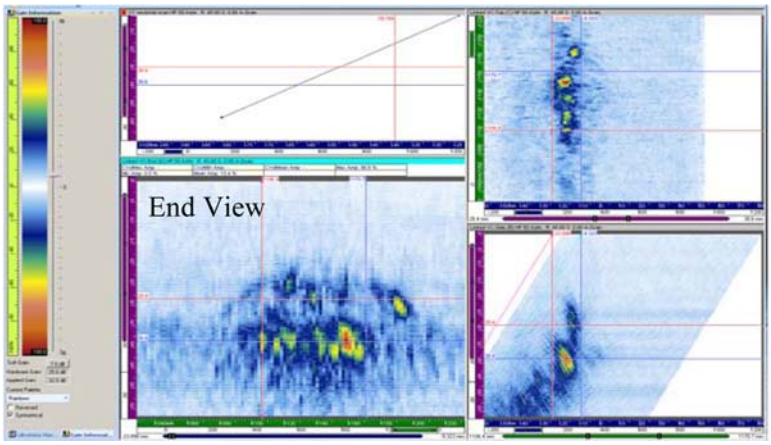

Figure 8.5. Flaw 1 Data on Specimen 9C-023, Obtained from the WSS Side at 1.5 MHz. Vertical markers in the end view show the flaw length as determined at the −6 dB level.

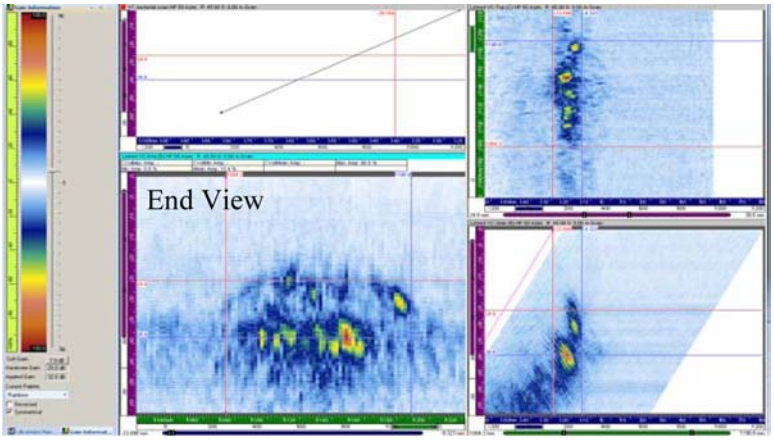

Figure 8.6. Flaw 1 Data on Specimen 9C-023, Obtained from the WSS Side at 1.5 MHz. Vertical markers show the assumed excavation area in the end view.

Depth sizing is also problematic. Flaw 2, shown in Figure 8.7, is reported to be 6.7-mm deep but sizes in the 10–13 mm range. Flaws 1–3 generally size in the 10–14 mm range, which appears to be the excavation region. Only flaw 4, Figure 8.8, is sized lower at 6-mm to 8-mm deep. Its reported depth is 4.1 mm. This flaw, however, is greatly oversized in length. The reported length is 57.4 mm and it is ultrasonically sized at 109–115 mm.

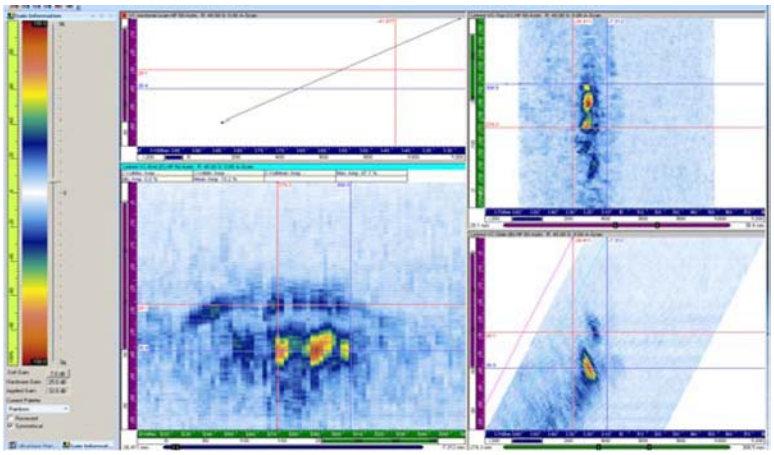

Figure 8.7. Data from Flaw 2 in Specimen 9C-023, Obtained from the WSS Side at 1.5 MHz.

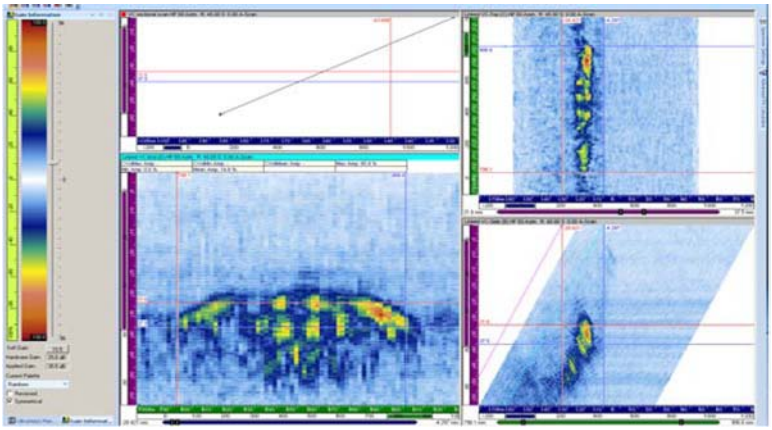

Figure 8.8. Flaw 4 in Specimen 9C-023, from the WSS Side of the Weld at 1.5 MHz

The axial positions of the flaws were also considered to investigate the possibility that the flaws were implanted in the carbon pipe rather than the weld or butter region. In this case, the filler material-to-carbon pipe interface would likely produce a strong acoustic reflection. The axial positions of the four flaws were in the 16–19 mm range from the approximated weld center line towards the carbon side of the specimen. Because the 9C-023 weld profile is unknown, it is estimated to be similar to the other DMW specimens in this study. For example, specimen 9C-034 has a butter region 10.2-mm (0.4-in.) wide and a weld crown width of approximately 30 mm. Therefore, the weld centerline to edge of butter region is approximately 25.2 mm (10.2 + 30.0/2). Assuming these dimensions are applicable to specimen 9C-023, the 16–19 mm axial positions from the approximated weld center line of the 9C-023 flaws would place them in the weld or butter region as desired.

In summary, specimen 9C-023 contains four implanted TFCs. The flaws were supposed to be implanted in the weld/butter region of an already-assembled specimen with a minimal excavation and fill technique. The axial flaw location measured from the ultrasonic data show that the flaws were likely placed in the weld/butter region as desired, but this is based on an estimated weld center line and weld profile, which may not represent the as-built conditions. The data also show that the assumed excavation area is detected and is large. These excavation reflections interfere with the crack reflections leading one to size the excavation area rather than the crack in most situations. This contributes to a large over-sizing in length and unreliable depth information. Due to this problem, the sizing data will not be included in this study but flaw detection results will be considered. All four flaws were detected and the excavation areas do not significantly influence detection.

Specimen 9C-023 was ultrasonically evaluated at 1.0, 1.5, and 2.0 MHz with line scan data and with raster data at the two higher frequencies. Raster data were acquired primarily from the austenitic side of the weld while line scan data were acquired from both the WSS side and the carbon steel side of the weld. In all data sets, the flaws were detected. The data images for this specimen are displayed in Appendix B.

8.3 DMW Specimen 8C-091

Specimen 8C-091 is a DMW PZR surge nozzle specimen that was sent to FlawTech for flaw implantation in the already-assembled state. The specimen contains two HIP'ed EDM notches and two TFCs placed in the butter region as best estimated because the actual weld dimensions are unknown. The

flaw excavation region was not as obviously detected in this specimen as it was in the previously discussed specimen 9C-023.

The OD weld region was machined flat prior to the ultrasonic examinations as there was a large weld crown in place that prohibited full contact of the probe wedge with the specimen. This machining operation left a step approximately at the OD nozzle-to-butter interface. Because of this step, the raster data was shortened in the scan (pipe axial) direction, and line scan data access was not as close to the weld center line as desired. The acquired data were considered valid because the data images showed that the flaw regions were still fully insonified. The corner responses were detected at 55° typically, but higher angles, up to 65° and 70°, were required to detect the responses from the upper portions of the flaws. In other specimens, the raster scan stroke extends well over the weld center line at the OD surface, allowing both the base of a flaw and its upper region to be insonified at 45° to 55°. The line scan data on specimen 8C-091 seemed to adequately capture the flaw region with both corner responses and upper flaw responses being insonified.

Flaws 1–4 were detected in the 1.5-MHz raster data. Flaw 1 was marginally detected by the line scan data, and this is a result of the machined step on the surface that prohibited closer access to the weld center line. SNRs for the raster data were in the 13–20 dB range with lower values of 11–16 dB for the line scan data. Flaws 2 and 3 were inspected with 1- and 2-MHz probes also. The 2-MHz data was fairly broken up or scattered, indicating that this frequency was too high for this particular DMW material and weld configuration. The two SNR values at 2 MHz were 12 and 9 dB for flaws 2 and 3, respectively. The 1-MHz data showed a more contiguous response and had SNR values of 11 and 15 dB for the two flaws. Flaw 2 images at 1, 1.5, and 2 MHz are shown in Figure 8.9 through Figure 8.11 for comparison of the effect of probe frequency on flaw response. The 2-MHz image contains more noise. Both the 1- and 1.5-MHz data show a better flaw detection. All PA-UT imaged data acquired on DMW mock-up specimen 8C-091 can be found in Appendix C.

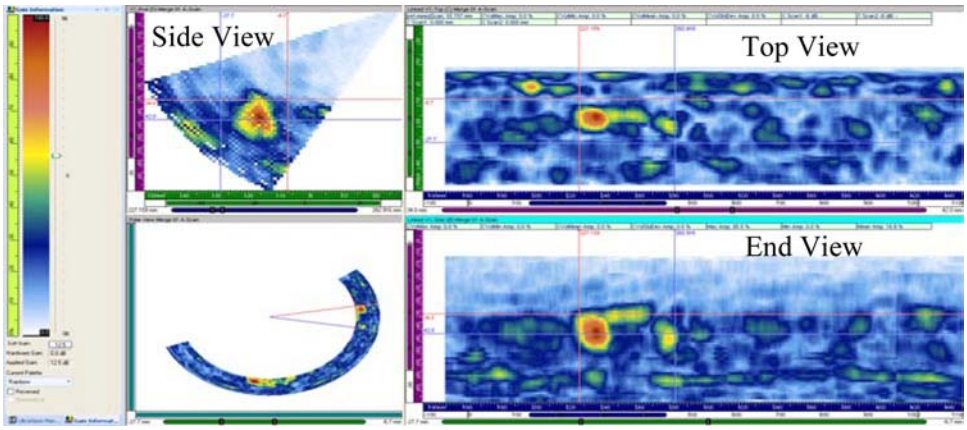

Figure 8.9. Flaw 2 in Specimen 8C-091 at 1 MHz

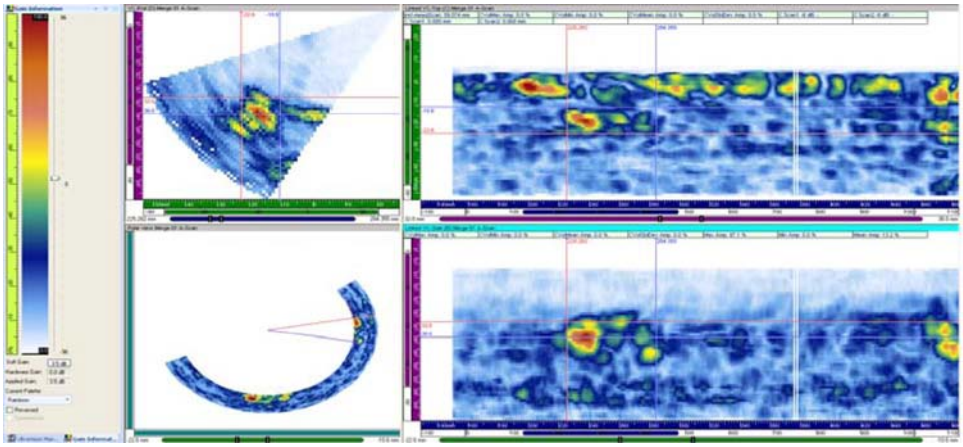

Figure 8.10. Flaw 2 in Specimen 8C-091 at 1.5 MHz

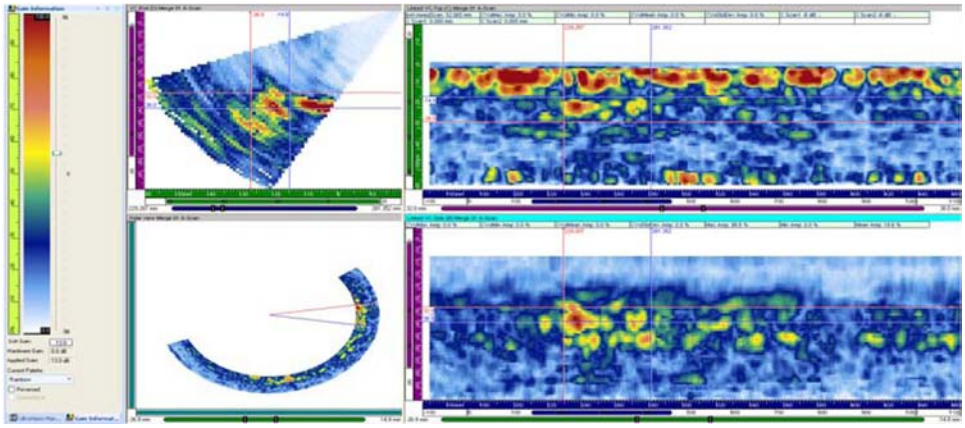

Figure 8.11. Flaw 2 in Specimen 8C-091 at 2 MHz

Length and depth sizing information is displayed in Figure 8.12 and Figure 8.13, respectively. Flaw 1 was marginally detected and length-sizing from the 1.5-MHz line scan data was not very accurate. Depth sizing of flaw 1 with 1.5-MHz line scan data, however, is close to the true state. Due to the limited access in the axial direction, the raster data sets were shortened, and line scans were not taken as close to the weld center line as desired. Higher angles were needed to capture the flaw response and the probe is less sensitive at higher angles as is shown in Figure 5.5 and discussed previously. A refracted angle of 55° was typically used in the raster data analysis on this specimen. The near-45° response is preferred and in other specimens is the primary angle used for flaw detection. At this angle, the beam is well formed, has good sensitivity, and performs well in capturing the flaw corner response.

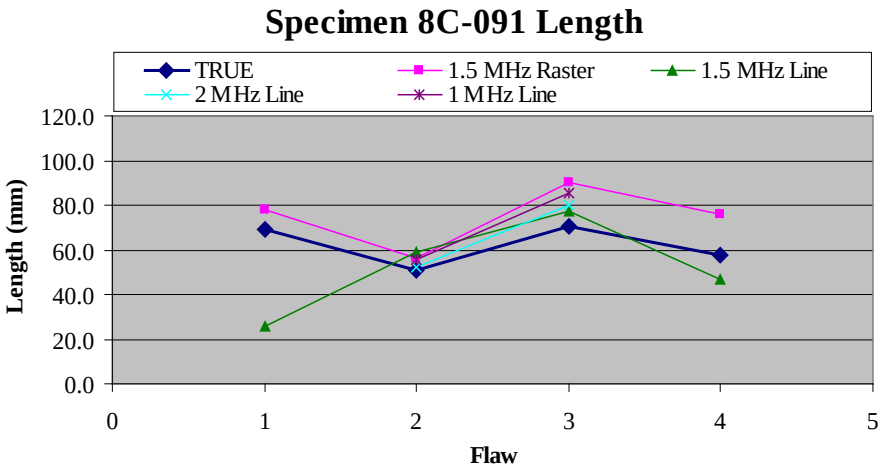

Figure 8.12. Length Sizing Results on Specimen 8C-091

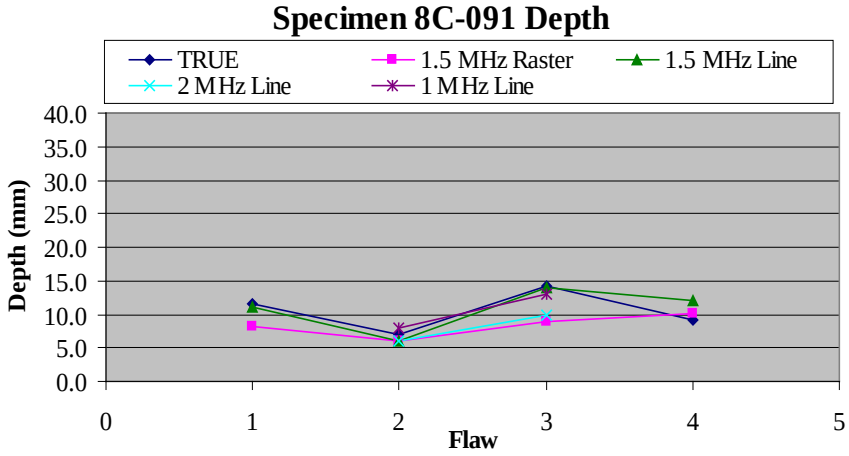

Figure 8.13. Depth Sizing Results on Specimen 8C-091

Flaw 3 is consistently oversized in length with the 1.5-MHz raster data performing the worst. A possible explanation for the length over-sizing of flaw 3 could be that the excavation area is being partially detected. Flaw 4 is equally over-sized and both flaws 3 and 4 are implanted TFCs whereas flaws 1 and 2 are HIP'ed EDM notches. Note that the length sizing of flaws 1 and 2 are closer to true state. On the other hand, the data images do not clearly show the semicircular region as was seen in specimen 9C-023, so the present assumption is that data from the two TFCs, flaws 3 and 4, are valid. Figure 8.14 displays data for both flaws 2 and 3. Again flaw 2 is a HIP'ed EDM notch whereas flaw 3 is a TFC.

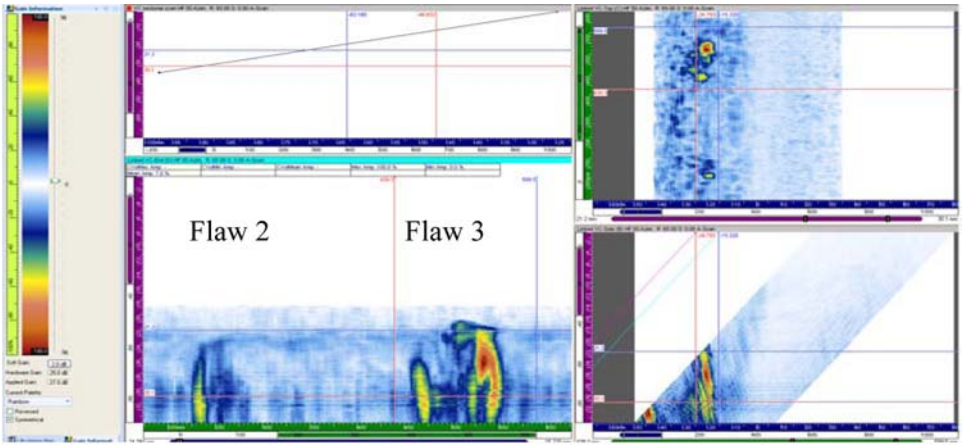

Figure 8.14. Specimen 8C-091 Flaw 2 on the Left, an EDM Notch, and Flaw 3 on the Right, a TFC. Data were acquired at 1.5 MHz.

8.4 DMW Specimen 9C-034

Specimen 9C-034 contains a DMW between a 516 Gr70 carbon steel nozzle and a CASS pipe. The nozzle side butter and weld are Inconel 82/182. Four TFCs were implanted in the weld butter region with flaw depths ranging from 13% to 31% through-wall. The flaws are vertical (i.e., no tilt) and are circumferentially oriented. The specimen was first ultrasonically examined with the weld crown in place. It was determined that the presence of the weld crown limited the data acquisition so the crown was removed and the specimen rescanned. Both the before and after weld crown removal data sets will be discussed, but the emphasis will be on the after-weld crown removal data. With a brief comparison, one can see the need for weld crown removal. Data was acquired from the CASS side of the weld. All PA-UT imaged data acquired on DMW mock-up specimen 9C-034 can be found in Appendix D.

8.4.1 With Weld Crown

In the as-welded condition, the specimen was examined at 1, 1.5, and 2 MHz with line scans and with raster scans at 1.5 MHz. The 31% through-wall flaw, flaw 2, was detected in both 1.5-MHz raster and line scans. The flaw signal was on the edge of the scanned area at 45° but at 60° the corner signal was fully detected as shown in Figure 8.15 in the side view. The upper portion of the flaw was not insonified so no depth information is available. Flaws 1 and 3 with depths of 13% and 19% through-wall were marginally detected. Figure 8.16 shows the flaw 3 corner response data at 55°. The flaw response is on the edge of the scanned aperture so again the upper portion of the flaw was not insonified. Higher angles did not improve the flaw detection. Flaw 4 at 26% through-wall in depth was not detected.

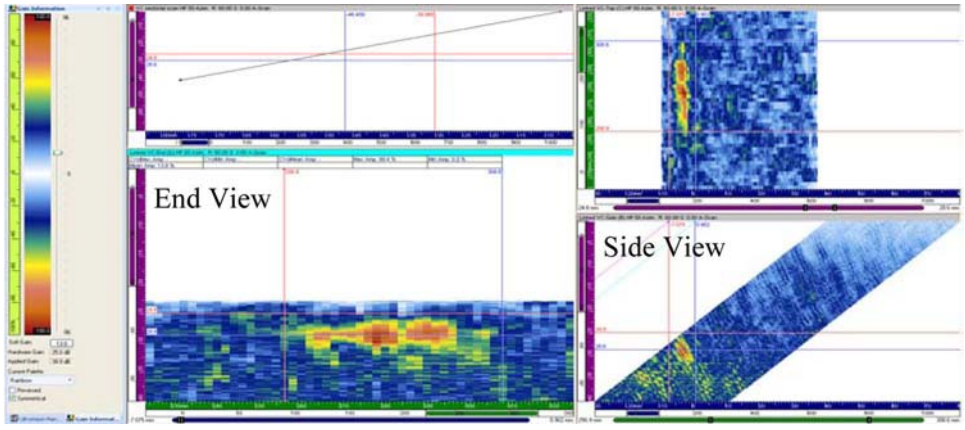

Figure 8.15. Specimen 9C-034 Flaw 2 at 1.5 MHz as Observed from the CASS Side of the Weld was Detected Before Weld Crown Removal at 60°

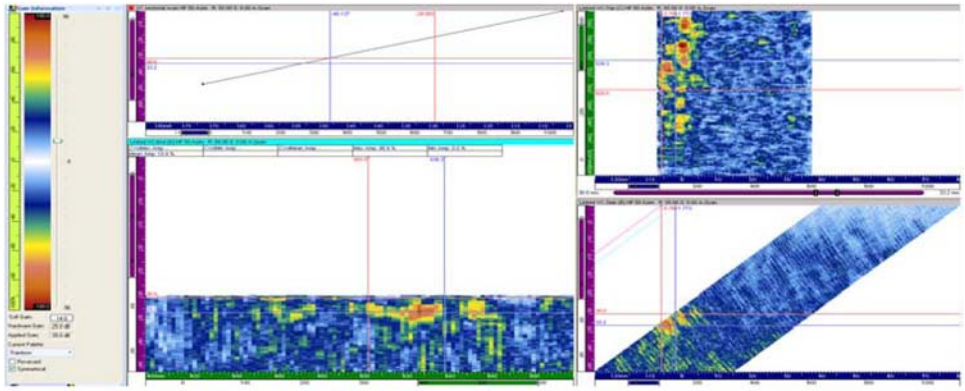

Figure 8.16. Specimen 9C-034 Flaw 3 at 1.5 MHz and 55° as Observed from the CASS Side of the Weld, with a Marginal Detection Before Weld Crown Removal

Examining the specimen with a 1-MHz probe did not improve the detection as the larger probe footprint prevented proper access to the flaw. Limited 1-MHz line scan data showed that flaw 2 was detected but flaws 3 and 4 were not detected. Line scan data at 2 MHz was also acquired for comparison and because of the smaller probe footprint, but the flaw signals were greatly disrupted leading to marginal or no flaw detections.

8.4.2 Weld Crown Removed

Line scan and raster data were acquired at both 1.5 and 2 MHz after the weld crown was removed from specimen 9C-034. All four flaws were readily detected at both frequencies. Figure 8.17 shows the flaw 2 response at 1.5 MHz. A weld root signal was detected and is marked in the side-view image below. The flaw response is to the left of the root signal and is gated by the two vertical lines. The end view on the left shows the gated region; and from this end view, the flaw is characterized for length, depth, and SNR. The root signal was evident in all of the 1.5- and 2-MHz data, both line and raster data. It provided a consistent fiduciary response that assisted the data analysis.

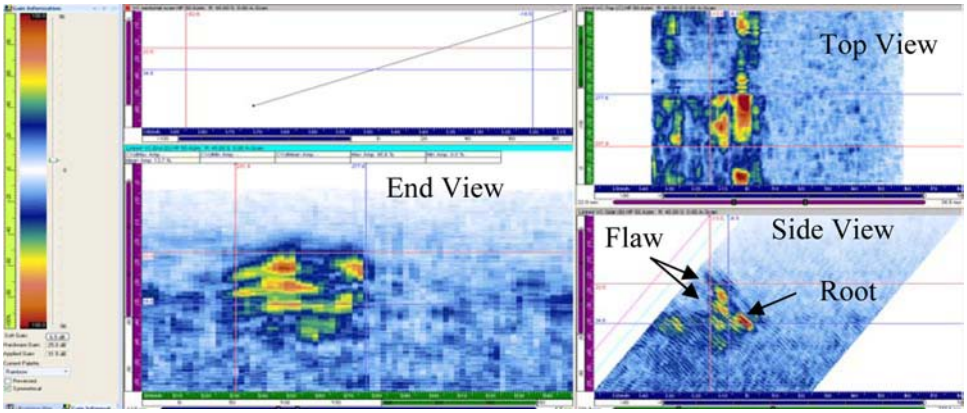

Figure 8.17. Specimen 9C-034 Flaw 2 at 1.5 MHz as Observed from the CASS Side of the Weld After Weld Crown Removal was Detected

Sufficient access to the butter region containing the flaw was provided by removing the weld crown. Because the entire flaw region was insonified, both a flaw response and a response from the prominent weld root were evident in the data. The strong weld root reflector in the data served as a reference point in the data itself. This greatly simplified signal discrimination. The flaw responses were also very good with raster data SNRs in the 15.5–18.3 dB range at 1.5 MHz and in the 14.4–19.2 dB range at 2.0 MHz. Figure 8.18 depicts the response from flaw 2 at 2 MHz. Figure 8.19 and Figure 8.20 show the 1.5- and 2-MHz responses from flaw 3.

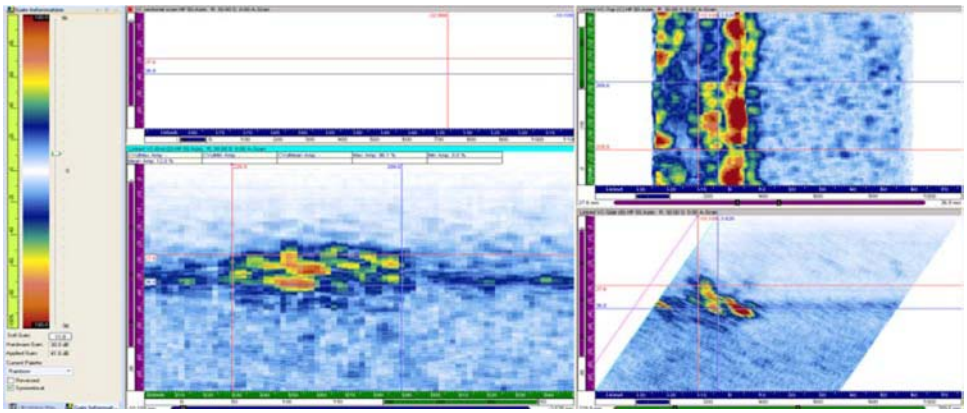

Figure 8.18. Specimen 9C-034 Flaw 2 at 2 MHz as Observed from the CASS Side of the Weld After Weld Crown Removal was Detected

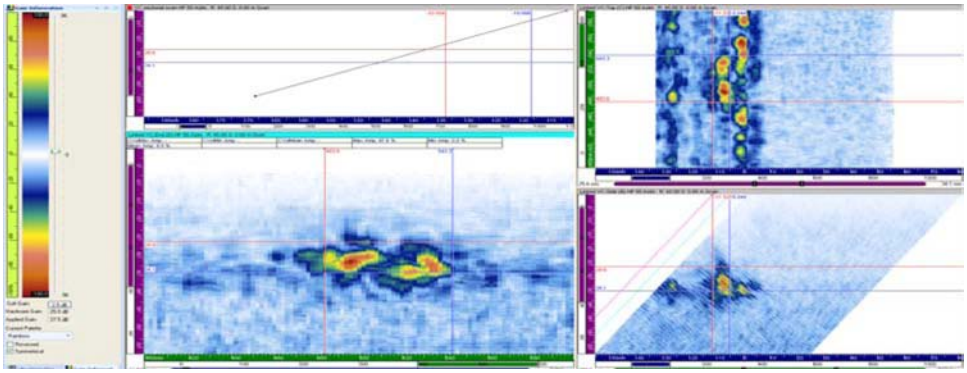

Figure 8.19. Specimen 9C-034 Flaw 3 at 1.5 MHz as Observed from the CASS Side of the Weld After Weld Crown Removal was Detected

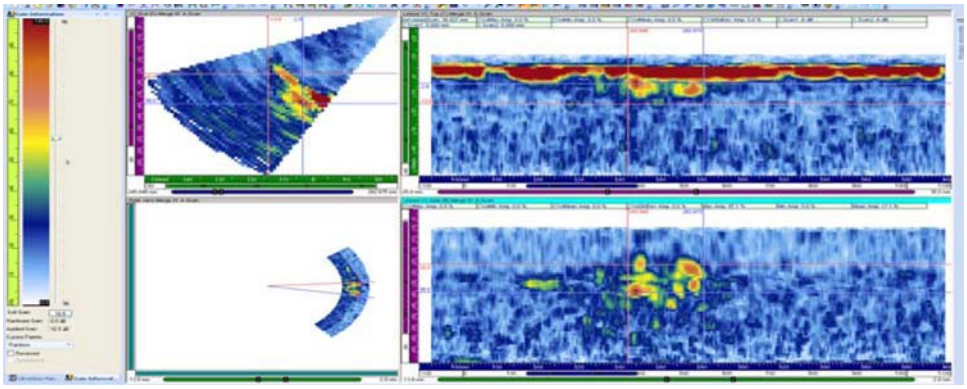

Figure 8.20. Specimen 9C-034 Flaw 3 at 2 MHz as Observed from the CASS Side of the Weld After Weld Crown Removal was Detected

A sizing comparison of the data acquired after weld crown removal is displayed in Figure 8.21 for length and Figure 8.22 for depth. Both line and raster data are displayed for 1.5 and 2 MHz. The length sizing is worst for flaw 4 at 1.5-MHz line scan data and 2-MHz raster data. The error is 19 and 18 mm, respectively. Depth sizing in the raster data is good and within 2.2 mm at both frequencies.

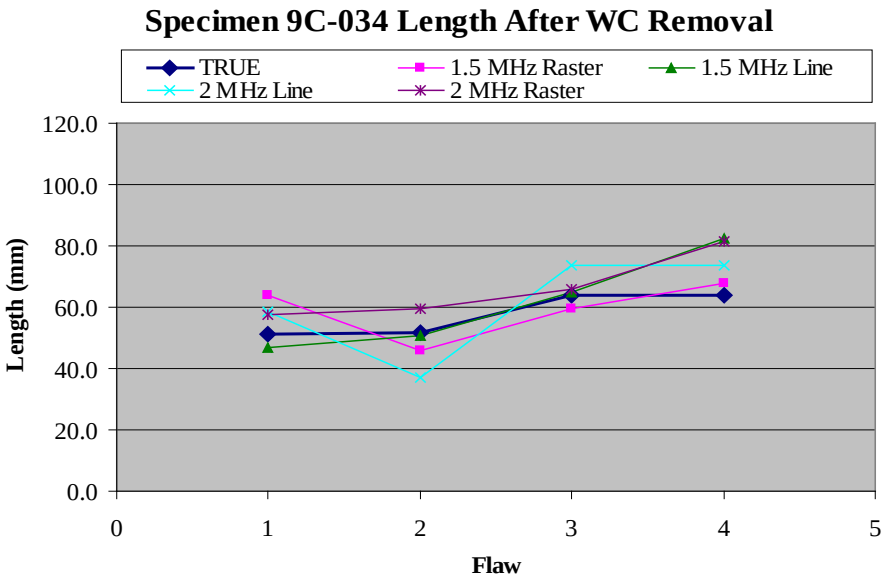

Figure 8.21. Length Sizing Results on Specimen 9C-034

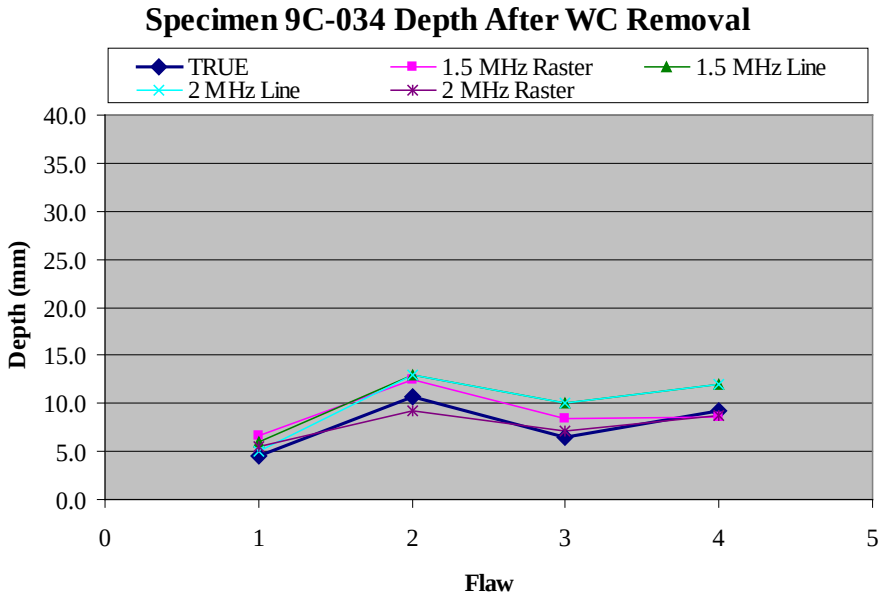

Figure 8.22. Depth Sizing Results on Specimen 9C-034

8.5 DMW Specimen 8C-036

8.5.1 8C-036 After HIP

Specimen 8C-036 is a nozzle-to-stainless steel safe end-to-pipe configuration and was fabricated at FlawTech. It contains four TFCs and four HIP'ed EDM notches. Two of the EDM notches are axially oriented while the other six flaws are circumferential in orientation. Flaws 3, a TFC, and 4, an EDM

notch, have similar dimensions. Flaws 5 and 6 are also paired as a TFC and an EDM notch, respectively, with similar dimensions. This specimen was evaluated both before and after the HIP process was applied. Only the post-HIP data is discussed in this report. The sample was inspected with 1.5- and 2.0-MHz PA probes in the line scan mode from both sides of the weld for the circumferential flaws and from one side for the axial flaws. Raster data was acquired primarily at 2 MHz in part because of the smaller footprint of the probe, which gave better access on the sloped and limited length (in the axial direction) surface. The primary reason for the 2-MHz raster data inspection was, however, the improved signal response. Inspected from the WSS side of the weld, the SNR range for 2-MHz line scan data was 13–18 dB and the range for raster data was 12–22 dB. The SNR range for 1.5 MHz was similar or lower with the line scan data at 14–20 dB and the raster data at 12–15 dB. The raster data in either frequency gives better signal definition and hence better SNR as compared to the line scan data. Data obtained from the WSS side of the weld in general showed a geometrical reflector (counterbore) as the probe was moved towards the weld, followed by the flaw response. Figure 8.23 displays the 2-MHz data from flaw 2. In the data analysis, the flaw signal was separable from the geometrical reflector, making flaw signal detection straightforward. All six circumferential cracks were detected from the WSS side of the weld. The two axial cracks were detected as well. All PA-UT imaged data acquired on DMW mock-up specimen 8C-036 can be found in Appendix E.

Note that inspection surface on specimen 8C-036 was angled by approximately 10°. The effect on the data analysis is that a 30° refracted angle is really 40°. With this in mind, the majority of the raster files were analyzed at 35°, which translated to a real 45°.

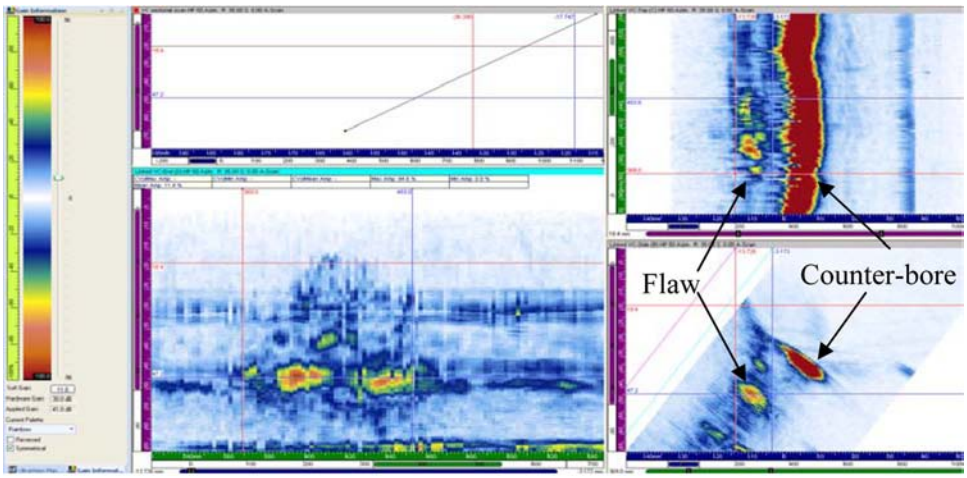

Figure 8.23. Data Acquired at 2 MHz from Flaw 2 as Observed from the WSS Safe End Side of the Weld

Raster data obtained from axial flaw 8 at 1.5 MHz is shown in Figure 8.24. The flaw was not examined at any other frequency because the flaw was clearly detected at 1.5 MHz and PNNL currently only has a wedge contoured for axial flaw inspections for the 1.5-MHz probe. The SNRs for the two axial flaws, flaw 7 and 8, were 20 and 17 dB for raster data and 15 and 12 for line scan data, respectively.

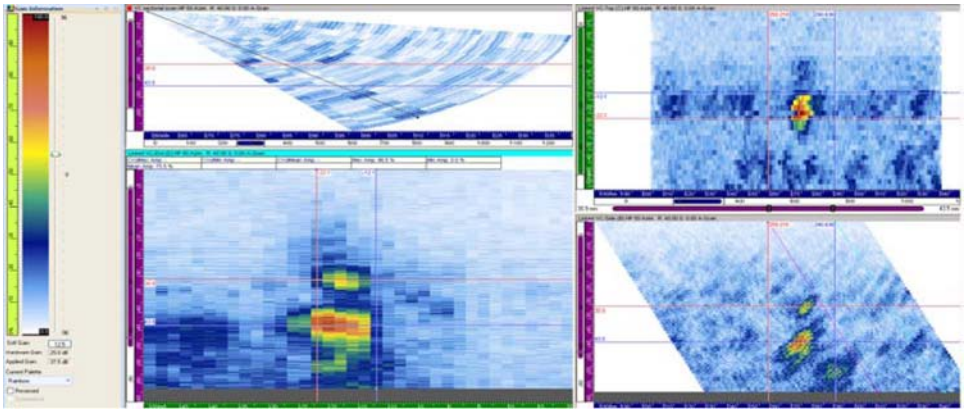

Figure 8.24. Data Acquired at 1.5 MHz from Axial Flaw 8 in Specimen 8C-036

Length and depth sizing information is displayed in Figure 8.25 and Figure 8.26. The outlier in length is from flaw 5 for both the raster and line data at 1.5 MHz. Both data sets captured a noise signal that was included in the length sizing at the −6 dB level. The 2-MHz data did not detect this extraneous signal.

The depth sizing is again problematic for the deeper flaws 5 and 6 but not for flaw 2. The 2-MHz raster data was reviewed again for flaws 4, 5, and 6 with slightly better results obtained at higher angles. At 50° on flaw 4, an upper portion of the flaw was visible and sized to 12 mm. During the previous analysis at 35°, no depth information was evident. Flaw 5 was resized to 14.9-mm deep at a 45° refracted angle and flaw 6 was resized to 17.3-mm deep at 55° refracted. Because this data was obtained after true state was known, it will not be used in the summary analysis in the next section.

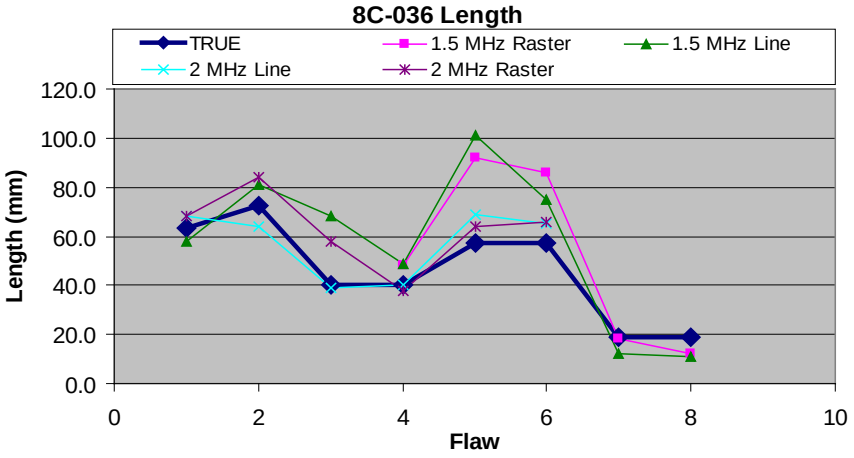

Figure 8.25. Length Sizing Results on Specimen 8C-036

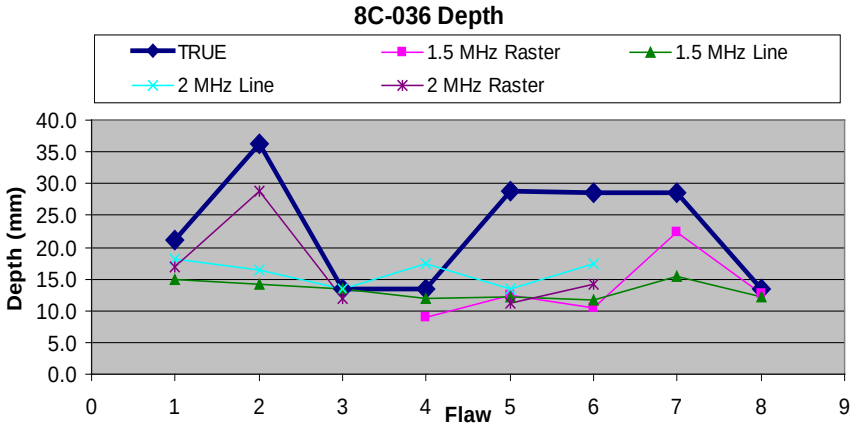

Figure 8.26. Depth Sizing Results on Specimen 8C-036

8.6 Summary of Results

The data are summarized in the following three tables in this section for 1.5- and 2-MHz raster and line scan data. Table 8.1 displays length sizing results, Table 8.2 depth sizing, and Table 8.3 SNR values. The blank locations indicate that there were no data acquired for that specific flaw. For instance, the tables show that there were no 2-MHz raster data acquired on specimens 8C-032 or 8C-091. All of the flaws were detected from the acquired data sets with only one exception. Flaw 1 in specimen 8C-091 was marginally detected with the 1.5-MHz line scan data. It was easily detected with the 1.5-MHz raster data. The marginal detection was due to axial position constraints in the data acquisition.

Length sizing information is summarized in Table 8.1. Line scan data were acquired with a circumferential step of 1 mm, whereas raster data were acquired with a circumferential index of 2 mm or more. With this in mind, one might expect the line scan data to be more accurate in length determination, but the data do not show this. Errors are lower for the raster data. Raster data sets more fully define the flaw response, whereas line scan data capture the flaw response from only a single axial position and this axial position may not be optimum. A conclusion from these data is that line scans are very good for detection, but raster scans are better for flaw characterization. The 2-MHz raster data also out performs the 1.5-MHz raster data in length sizing. When the material supports a higher frequency, the resolution will be improved as the data clearly show.

The ASME Section XI Boiler and Pressure Vessel Code, Appendix VIII, requires that the acceptable length sizing RMSE is within 19.1 mm (0.75 in.) and depth sizing is within 3.2 mm (0.125 in.). Both the 1.5- and 2-MHz data sets pass this requirement for length sizing.

The depth sizing table (Table 8.2) shows the calculated RMSE for the data listed by frequency and type of scan, raster or line. As previously discussed with the deeper flaws, the very upper portion of the flaw, the part nearest the OD surface, is not detected. With the data shown, none of the inspections pass the 3.2-mm (0.125-in.) the ASME Code requirement. By including the four deepest flaws in the RMSE calculations (three 75% TW flaws and one 95% TW flaw), cumulative sizing results for all the inspections do not pass the ASME Code RMSE acceptance limit of 3.2 mm (0.125 in.). However, if these four deeper data points are removed from the analyses, RMSE values for the 1.5-MHz raster and line scan data are

2.9 mm and 2.4 mm, respectively. Under these conditions, the 1.5-MHz line scan and raster data would be within the ASME Code-acceptable 3.2-mm limit for depth sizing.

Table 8.1. Summary DMW Length Sizing Data

			Length (mm)				
Specimen	**Specimen Flaw**	**Flaw**	**True State**	**1.5-MHz Raster**	**1.5-MHz Line**	**2-MHz Line**	**2-MHz Raster**
8C-032	1	1	22.9	16.0	21.0	27.0	
	2	2	28.9	32.0	22.0	29.0	
	3	3	45.9	60.0	60.0	59.0	
	4	4	21.6	8.0	13.0	11.0	
8C-091	1	5	69.1	78.1	26.1		
	2	6	50.8	56.0	59.1	52.1	
	3	7	70.6	90.1	77.1	80.1	
	4	8	57.6	76.1	47.1		
9C-034	1	9	51.2	63.7	46.8	58.7	57.7
	2	10	51.5	45.7	50.7	36.9	59.7
	3	11	63.9	59.7	64.7	73.7	65.7
	4	12	63.8	67.6	82.6	73.7	81.6
8C-036	1	13	63.1		58.1	68.1	68.0
	2	14	72.4		81.0	64.0	84.0
	3	15	40.1		68.0	39.0	58.0
	4	16	40.0	48.0	49.0	40.0	38.0
	5	17	57.4	92.0	101.0	69.0	64.1
	6	18	57.2	86.0	75.0	65.0	66.0
	7	19	19.1	18.0	12.0		
	8	20	19.1	12.0	11.0		
RMSE				**14.2**	**17.0**	**16.2**	**10.2**

A final consideration is that of data quality and this is characterized by the SNR, which is summarized in Table 8.3. Flaw detection and discrimination was not an issue in these specimens and specifically not in specimen 9C-034 once the weld crown was removed. As stated previously, the raster data better defines a flaw and shows as a higher SNR by approximately 3 dB over the line scan data at either frequency.

Recall that flaws 3 and 4, and 5 and 6, were paired TFC and EDM notch types in specimen 8C-036, with flaws 3 and 4 having similar dimensions in length and depth, as did flaws 5 and 6. Flaw 3 and 5 were TFCs while 4 and 6 were HIP'ed EDM notches. The paired SNRs are similar at 1.5 MHz but show a difference at 2 MHz in response from a TFC and a HIP'ed EDM notch of similar dimensions, with the notch response being stronger. The SNR values at both 2-MHz line and raster data are greater for the EDM notches than the TFCs; by 4 dB for line data and 7 dB or more for raster data. Further observation of the data shows that the corner response of the EDM notches is greater than the response of the TFCs by approximately 6 dB in the raster data. See Appendix E, specifically E.3–E.6, for data images.

Table 8.2. Summary DMW Depth Sizing Data

			Depth (mm)				
Specimen	**Specimen Flaw**	**Flaw**	**True State**	**1.5-MHz Raster**	**1.5-MHz Line**	**2-MHz Line**	**2-MHz Raster**
8C-032	1	1	7.7	5.1	10.0	5.0	
	2	2	14.4	11.7	16.0	14.0	
	3	3	23.0	12.7	10.0	11.0	
	4	4	10.8	6.0	10.0	7.0	
8C-091	1	5	11.7	8.1	11.0		
	2	6	7.0	6.1	6.0	6.0	
	3	7	14.1	8.9	14.0	10.0	
	4	8	9.2	10.2	12.0		
9C-034	1	9	4.5	6.7	6.0	5.00	5.5
	2	10	10.7	12.5	13.0	13.0	9.2
	3	11	6.5	8.5	10.0	10.0	7.2
	4	12	9.2	8.6	12.0	12.0	8.7
8C-036	1	13	21.1		17.3	10.9	17.0
	2	14	36.2		23.9	26.0	28.8
	3	15	13.4		18.4	10.9	11.9
	4	16	13.3	8.9	15.2	8.7	
	5	17	28.8	12.4	21.7	21.7	11.1
	6	18	28.6	10.5	22.8	21.7	14.2
	7	19	28.6	22.3	22.0		
	8	20	13.3	12.7	14.0		
RMSE				**7.0**	**5.2**	**5.8**	**8.8**

Table 8.3. DMW Signal to Noise Ratio Summary

			SNR (dB)			
Specimen	**Specimen Flaw**	**Flaw**	**1.5-MHz Raster**	**1.5-MHz Line**	**2-MHz Line**	**2-MHz Raster**
8C-032	1	1	17.0	16.7		
	2	2	15.6	13.4		
	3	3	16.2	13.1		
	4	4	18.5	15.0		
8C-091	1	5	13.5	10.7		
	2	6	13.9	13.8	12.4	
	3	7	19.8	16.3	9.4	
	4	8	16.1	12.3		
9C-034	1	9	15.5	14.7	15.3	15.4
	2	10	16.2	12.2	13.7	14.4
	3	11	17.9	15.2	16.6	19.2
	4	12	18.3	14.3	16.2	17.8
8C-036	1	13		14.9	18.1	19.8
	2	14		14.2	16.4	15.0
	3	15		13.5	13.5	12.4
	4	16	14.5	12.0	17.3	21.6
	5	17	13.7	12.2	13.3	14.1
	6	18	13.8	11.8	17.3	21.2
	7	19	19.7	15.3		
	8	20	16.8	12.1		
Average			**16.0**	**13.4**	**14.4**	**17.1**

9.0 Discussion and Conclusions

A technical evaluation of a phased-array ultrasonic inspection method was conducted to evaluate detection and sizing performance for inspection of small-bore, DMW piping components. A set of flaws, including both thermal fatigue cracks and hot isostatically pressed EDM notches were inserted into five DMW mock-up specimens. PA-UT flaw responses from these flaws were used to evaluate detection and characterization performance. This effort included technical assessments and confirmatory research that addressed:

- The use of sound-field modeling to more effectively modify inspection parameters and enhance the inspection outcomes;
- The use of PA-UT methods and advanced probe design to enhance detection and characterization of circumferentially and axially oriented flaws in smaller-bore DMW mock-up specimens;
- An analysis of flaw detection, length sizing, depth sizing, and signal-to-noise ratio for all flaws in all specimens, as a function of various inspection parameters.

The DMW mock-up specimens used in this study were either salvaged from a cancelled NPP that had never been in an operational state, or were fabricated from new and/or vintage materials. For those specimens that were salvaged, historical information and details associated with metals composition were only partially available. Where CASS materials were used, these materials were polished and chemically etched to visually highlight (enhance) the microstructures of the pipe parent material used in the fabrication of the DMW mock-up. This work focused on confirmatory research in applying and evaluating phased-array ultrasonic methods for gauging inspection and flaw characterization performance in these challenging components.

The anticipated inspection challenges (based upon work conducted in the literature, recent events at NPPs, and operating experience described by industry on smaller-bore DMW components) drove the efforts to employ more effective PA probes for application to smaller-bore, relatively thin-walled DMW component inspections. Previous work in developing effective probe matrix designs for far-side austenitic weld examinations and examination of CASS materials was employed in this work and the evolution of the PA-UT inspection approach has been well documented in previous PNNL reports to the NRC. Lessons learned from developing PA probes with improved penetration and resolution for CASS PZR surge lines were important to the efforts reported here. The inspection challenge for DMWs is defined by the array of complex component configurations, metallurgical interfaces, grain growth pattern variations, and ID/OD geometry/access issues. These factors became key elements in driving the determinations for probe type and inspection frequency. The probes applied in this evaluation were chosen to have adequate focusing apertures (with minimal footprints), higher bandwidths, and improved beam steering and lateral skewing capabilities. The 1.5-MHz probe employed in this study was originally designed for far-side examinations of austenitic welds in WSS piping, but performed well on these DMW mock-up specimens. Finally, both the 1.0-MHz and 2.0-MHz PA probes were originally designed for evaluating inspection effectiveness of PA methods on components with inlays, onlays, and overlays; however, these probes also performed well with regard to detection and flaw characterization in these materials.

The PA-UT examination approach used on the DMW component mock-ups focused on acquiring data as a function of inspection frequency (2.0 MHz, 1.5 MHz, and 1.0 MHz), inspection angle (30° to 70° in 1° increments), and by employing both raster and line scan data acquisition. Data were acquired from both sides of the welds; however, the focus in this document was to evaluate inspection performance by assessing the data taken from the austenitic of the DMW configuration, as this is the side where an inspector typically has access in the field. The data analysis conducted here provided quantitative information regarding detection and sizing performance against the true state, and a qualitative assessment of the general capabilities of PA-UT for effective flaw localization/positioning versus true state. Additional metrics used for the analysis included SNR and RMSE for length and depth sizing. Also, a comparison of detection and sizing performance for line scan versus raster scan data was also conducted, to determine if inspection performance is significantly enhanced by performing more rigorous and time-consuming raster scans over simple line scans. Finally, a qualitative assessment of the effect of angular flaw tilt (from the normal to the ID surface) was conducted.

The detection and sizing data showed that all of the implanted cracks in all five DMW mock-up specimens were detected from the austenitic pipe of the DMWs. While most of the data were acquired at inspection frequencies of 1.5 and 2.0 MHz, and the focus of the analysis was also at these frequencies, it was shown that 1.0-MHz data also provided suitable penetration and resolution for effective flaw detection, without compromising data quality or results. However, because the higher frequencies provide a smaller wavelength, thereby enhancing resolution, the focus of the analysis remained on the results from the 1.5- and 2.0-MHz inspection frequencies. The results reported here showed that longitudinal mode, transmit-receive matrix PA probes over this frequency range, can provide optimal and effective sound fields for detection and characterization of circumferential and axial flaws in smaller-bore DMW components. The flaw depths chosen for the implanted TFCs and HIP'ed EDM notch cracks employed in this study ranged from approximately 10% through-wall to 95% through-wall, corresponding to an approximate range of 4.1 mm (0.16 in.) to 36.2 mm (1.43 in.) in depth. Flaw lengths ranged from approximately 19.1 mm (0.75 in.) to 72.4 mm (2.85 in.). This set of flaw dimensions (depths and lengths) provided a wide spectrum of sizes from which to assess the inspection performance and evaluate resolution and sensitivity of the PA-UT approach in these components. With regard to flaw positioning, approximately 75% of the flaws were positioned in the Inconel 82/182 buttering of the DMWs, while approximately 25% of the flaws were positioned in the weld material. The two axial flaws spanned both butter and weldment zones. PA-UT results were compared against true-state data for all flaws, and RMSE was computed as a metric for both length sizing and depth sizing of the flaws in this study. Also, signal-to-noise measurements were made and SNR values were computed and documented for all flaws and scanning scenarios (at 1.5 and 2.0 MHz).

A primary metric used for determination of the effectiveness and utility of the inspection approach is to compare the composite length sizing and depth sizing results from the evaluation against the ASME Code Section XI acceptance criteria for both length and depth sizing. The length sizing criterion calls for an RMSE less than 19.05 mm (0.75 in.), while the depth sizing criterion calls for an RMSE less than 3.81 mm (0.125 in.). Length and depth sizing measurements were made by a single analyst using a standard −6 dB drop, flaw sizing criteria documented in previous work on CASS and far-side austenitic weld inspection evaluations (Anderson et al. 2003; Anderson et al. 2007). While much of the data were straightforward and easily sized at the −6 dB level, some data required interpretation due primarily to either noncontiguous signals or artifact "remnants" resulting from ultrasonic responses from the crack implantation (excavation) process. Thus, sizing error due to human factors has been significantly

reduced. Regarding detection capability, all flaws were detected in this evaluation across all five DMW mock-up specimens.

Signal-to-noise values were consistently acceptable (> 10 dB), spanning both raster and line scan data at both 1.5- and 2.0-MHz frequencies, indicating that flaw detection was not an issue. Table 8.3 illustrates that SNRs were generally above 12 dB, corresponding to a factor of 4-to-1 signal-to-noise. The data show that flaws are detectable at frequencies up to 2.0 MHz in these DMW mock-up specimens, even in DMW configurations containing CASS pipe segments, where grain sizes can be as large as 41 mm (1.61 in.) and the nominal wall thickness is 33 mm (1.3 in.). The detection and sizing performance is not generally degraded by using a 2.0-MHz inspection. The higher frequency (2.0-MHz probe) was able to detect tip-diffracted energy from some of the cracks in these DMW mock-ups. The SNRs were calculated from the peak signal response and the mean noise response at the same part path in decibels. These calculated values are all very good, indicating minimal attenuation effects on sound field propagation over the frequency range from 1.5 to 2.0 MHz. Flaw detection was consistent and effective for the flaws implanted in these specimens as shown by the relatively high SNRs. Results show that all flaw length sizing fell completely within the Code-allowable limit while depth sizing was outside (over) the Code-allowable limit on all specimens.

Out of 24 total cracks evaluated in this study, 10 of these cracks were implanted at an angle (tilt) to the normal of the ID surface of the component. The range of flaw tilt varied from +2° to +30° from the normal. All flaws with angled orientations were tilted away from the scanning direction of the PA probes as they were scanned from the austenitic side of the DMW, essentially opening the flaw face up to the incident sound field. One might anticipate some level of signal response enhancement due to the tilt angle of the flaw face relative to the sound fields. However, it should also be noted that in reviewing the data provided, there was no correlation to either degradation or enhancement of flaw detection or flaw characterization performance as a function of flaw tilt.

Access limitations became a critical issue with specimen 9C-034, where the weld crown precluded effective coverage by limiting data acquisition with the necessary inspection angles to consistently detect and characterize the implanted flaws. Data were presented and discussed in Section 8.0, comparing and contrasting signal responses before and after weld crown removal. In addition, the ID geometrical conditions and contours also affected the resultant ultrasonic signal responses. Finally, to challenge the inspection even further, this specimen was being examined from the coarse-grained CASS pipe side of the DMW. After initially scanning and analyzing the results, the need for weld crown removal was apparent. From a review of the results, it can be shown that weld crown removal (essentially proper OD surface preparation) can indeed significantly improve ultrasonic inspection results by providing a scanning surface that improves probe coupling and allows suitable access for volumetric weld coverage.

With regard to length sizing (see Table 8.1), line scan data were acquired with a circumferential step of 1 mm, whereas raster data were acquired with a circumferential index of 2 mm or more. It was anticipated that the line scan data might be more accurate in length determination capability; however, the data do not show this. Errors are lower for the raster data. Raster data sets more fully define the flaw response because all steered angles are moved over the flaw during the axial scan motion, whereas line scan data capture the flaw response from only a single axial position (distance from probe to the flaw) and this axial position may not be optimized to allow the best angles to impact the flaw. In addition, the flaws were located in welds, which have dendritic grain structures that may re-direct insonification angles and impact the ability of the affected beams to produce adequate specular reflections from the flaw

extremities. Raster scans provide a better opportunity for each of the UT beams to interact with the flaws. A conclusion from these data is that line scans are very good for detection but raster scans are better for flaw characterization. The 2.0-MHz raster data also out performed the 1.5-MHz data in length sizing. When the material supports a higher frequency, the resolution will be improved as the data indicate. For depth sizing, Table 8.2 shows the calculated RMSE for the data listed by frequency and type of scan, raster or line. As previously discussed in Section 8.0, with the deeper flaws, the very upper portion of these flaws, nearest the OD surface, were not detected. As previously discussed, by including the four deepest flaws in the RMSE calculations (three 75% TW flaws and one 95% TW flaw), cumulative sizing results for all the inspections do not pass the ASME Code RMSE acceptance limit of 3.2 mm (0.125 in.). However, if these four deeper data points are removed from the analyses, RMSE values for the 1.5-MHz raster and line scan data are 2.9 mm and 2.4 mm, respectively. Under these conditions, the 1.5-MHz line scan and raster data would be within the ASME Code-acceptable 3.2-mm limit for depth sizing.

With respect to the evaluations conducted on DMW components in RCS piping, the primary issues requiring more research include gaining a better understanding of the impact and role of the various materials used and component configurations employed across the industry and, more importantly, the effects of inlays, onlays, and overlays used in the mitigation of DMWs affected by PWSCC. This report assesses the issue of smaller-bore DMW configurations; however, the eventual target will be to include an evaluation of thicker-walled DMW configurations, and to focus on evaluating inspection capabilities and performance for larger-bore DMWs that have CASS piping and/or inlays, onlays, or overlays. While advances in phased-array inspection systems continue to improve general capabilities for crack detection and relatively accurate lateral resolution for length sizing, overcoming the main inspection challenges posed by DMWs requires finding the optimal balance between three key factors. Achieving suitable signal-to-noise ratio, obtaining effective penetration of the sound field from the OD, and acquiring optimal resolution for flaw localization and sizing are all critical toward improving flaw detection and sizing capabilities in larger-bore DMW components.

Finally, because this technical evaluation employed only five DMW mock-up specimens, with a limited flaw set, there may be a need to expand this work and evaluate additional specimens, which would provide the basis for a more rigorous and statistically relevant set of recommendations. It may be possible to leverage work and collaborative efforts with the Electric Power Research Institute's NDE Center in Charlotte, North Carolina, to further support additional assessments in this area.

In conclusion, based upon the results of this work, state-of-the-art phased-array inspection approaches are rapidly evolving and the capability to detect cracks in DMW components where the wall thickness is generally less than 50 mm (2.0 in.) has been demonstrated here. While additional questions remain to be answered, PA ultrasonic approaches coupled with advanced signal processing technologies are showing the capability to successfully address this challenging inspection issue.

10.0 References

Ammirato F. 2001. "Examination of Dissimilar Metal Welds and Alloy 600 CRDM Head Penetrations – US Industry Update." Presented at *Workshop on Dissimilar Metal Weld NDE, held at the 16th International Conference on Structural Mechanics in Reactor Technology (SMiRT16)*. August 12–17, 2001, Washington, D.C.

Anderson MT, SL Crawford, SE Cumblidge, KM Denslow, AA Diaz and SR Doctor. 2007. *Assessment of Crack Detection in Heavy-Walled Cast Stainless Steel Piping Welds Using Advanced Low-Frequency Ultrasonic Methods*. NUREG/CR-6933, PNNL-16292, U.S. Nuclear Regulatory Commission, Washington, D.C.

Anderson MT, SE Cumblidge and SR Doctor. 2003. "Applying Ultrasonic Phased Array Technology to Examine Austenitic Coarse-Grained Structures for Light Water Reactor Piping." In *Third EPRI Phased Array Inspection Seminar*. June 9–11, 2003, Seattle, Washington.

ASME. 2008. "Section XI, Rules for Inservice Inspection of Nuclear Power Plant Components; An International Code." In *2007 ASME Boiler and Pressure Vessel Code – An International Code*. American Society of Mechanical Engineers, New York. 2008a Addenda, July 1, 2008.

Diaz AA, AD Cinson, SL Crawford, SE Cumblidge, KM Denslow, M Morra, MS Prowant and MT Anderson. 2008. *Technical Letter Report: Assessment of Ultrasonic Phased Array Testing for Cast Austenitic Stainless Steel Pressurizer Surge Line Piping Welds and Thick Section Primary System Cast Piping Welds*. PNNL-17698, Pacific Northwest National Laboratory, Richland, Washington.

Diaz AA, SR Doctor, BP Hildebrand, FA Simonen, GJ Schuster, ES Andersen, GP McDonald and RD Hasse. 1998. *Evaluation of Ultrasonic Inspection Techniques for Coarse-Grained Materials*. NUREG/CR-6594, PNNL-11171, U.S. Nuclear Regulatory Commission, Washington, D.C.

EPRI. 2005. *Materials Reliability Program: Primary System Piping Butt Weld Inspection and Evaluation Guidelines (MRP-139)*. EPRI Report 1010087, Electric Power Research Institute, Palo Alto, California.

Faidy C, G Martin, S Chapuliot, Y Kayser, N Safa, MF Cipierre, P Gilles, H Keinanen, A Laukkanen, A Sherry, D Lidbury, J Wintle, N Taylor, A Youtsos and G Lenkey. 2003. "Assessment of Aged Piping Dissimilar Metal Weld Integrity (ADIMEW)." Presented at *FISA 2003, Proceedings of the EU Research in Reactor Safety, EC Luxembourg, EURATOM, Brussels (EUR 20281)*. November 10–13, 2003.

Hsiao C-C, N-C Shie, Y-H Wu and S-L Chu. 2008. "Study of Ultrasonic Techniques on the Inspection of NPP Components." Presented at *17th World Conference on Nondestructive Testing*. October 25–28, 2008, Shanghai, China.

Kroning M, A Bulavinov, KM Reddy, F Walte and M Dalichow. 2008. "Improving the Inspectability of Stainless Steel and Dissimilar Metal Welded Joints Using Inverse Phase-Matching of Phased Array Time-Domain Signals." Presented at *17th World Conference on Nondestructive Testing*. October 25–28, 2008, Shanghai, China.

Mayinger W and WJ Metzner. 2001. "Dissimilar Metal Welds (DMW) in German LWR's - Design Types, Disbonding, NDT." Presented at *Workshop on Dissimilar Metal Weld NDE, held at the 16th International Conference on Structural Mechanics in Reactor Technology (SMiRT16).* August 12–17, 2001, Washington, D.C.

NRC. 2008a. *Reactor Coolant System Dissimilar Metal Butt Welds*. NRC Inspection Manual, Temporary Instruction 2515/172, U.S. Nuclear Regulatory Commission, Washington, D.C. Issued: 10/21/2008.

NRC. 2008b. *Regulatory Approach for Primary Water Stress Corrosion Cracking of Dissimilar Metal Butt Welds in Pressurized Water Reactor Primary Coolant System Piping*. NRC Regulatory Issue Summary 2008-25, U.S. Nuclear Regulatory Commission, Washington, D.C. Issued: 10/22/2008.

NRC. 2009. "Reactor Coolant System Weld Issues." *US NRC Online Newsletter*. Available online at: http://www.nrc.gov/reactors/operating/ops-experience/pressure-boundary-integrity/weld-issues/index.html. Issued: June 16, 2009.

Taylor TT. 1984. *An Evaluation of Manual Ultrasonic Inspection of Cast Stainless Steel Piping*. NUREG/CR-3753, PNL-5070, U.S. Nuclear Regulatory Commission, Washington, D.C.

Appendix A

Dissimilar Metal Weld Specimen 8C-032 Phased-Array Data

Appendix A

Dissimilar Metal Weld Specimen 8C-032 Phased-Array Data

1.5-MHz Raster Data on Flaws 1–4 ..... A.2

1.5-MHz Line Scan Data on Flaws 1–4 ..... A.4

2-MHz Line Scan Data on Flaws 1–4 ..... A.6

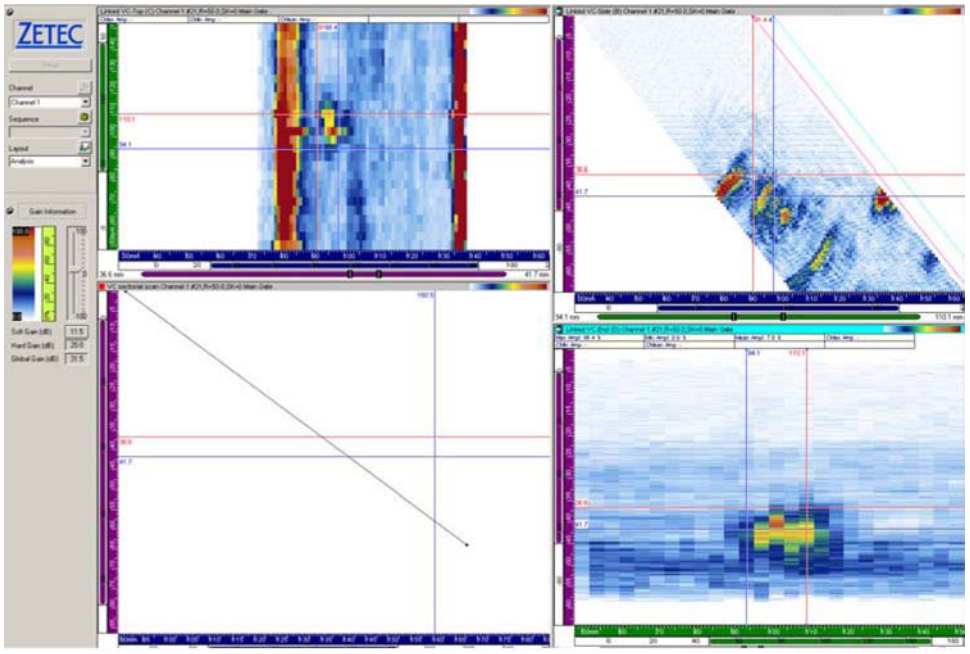

Figure A.1. Specimen 8C-032, Flaw 1 Raster Data at 1.5 MHz

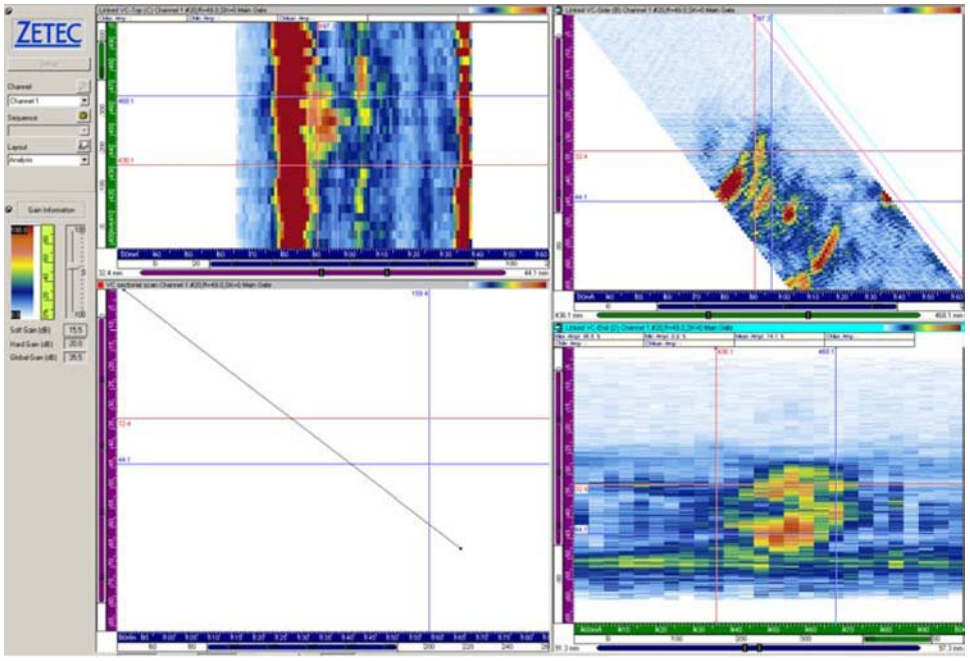

Figure A.2. Specimen 8C-032, Flaw 2 Raster Data at 1.5 MHz

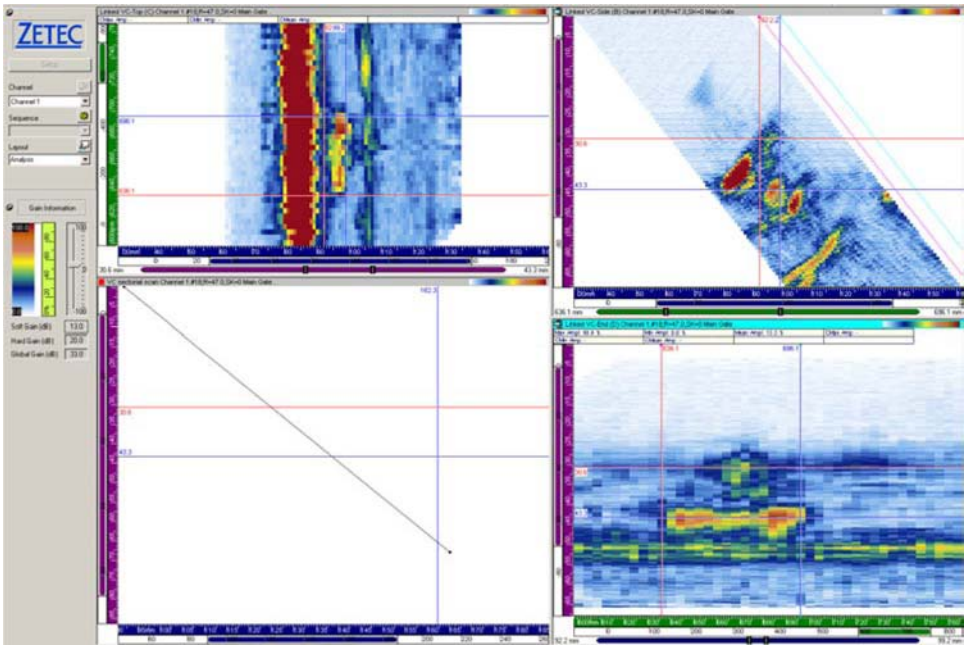

Figure A.3. Specimen 8C-032, Flaw 3 at Raster Data 1.5 MHz

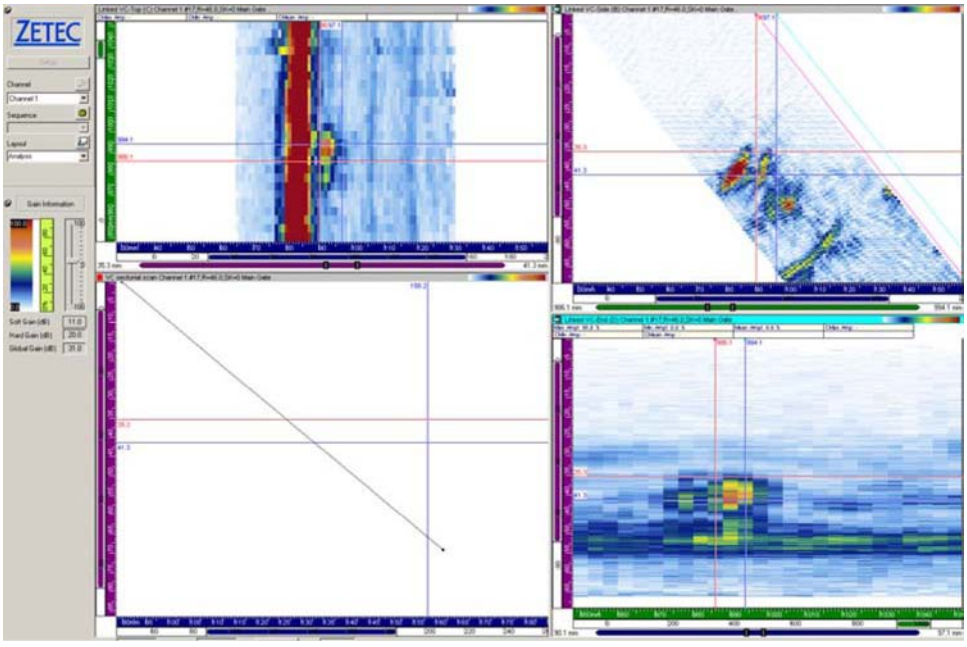

Figure A.4. Specimen 8C-032, Flaw 4 at Raster Data 1.5 MHz

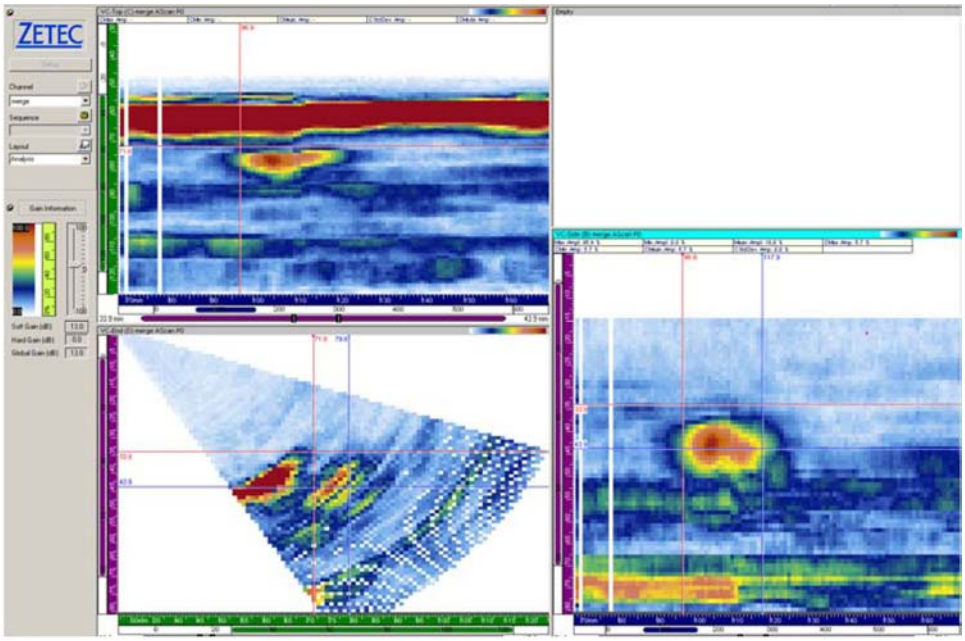

Figure A.5. Specimen 8C-032, Flaw 1 Line Scan Data at 1.5 MHz

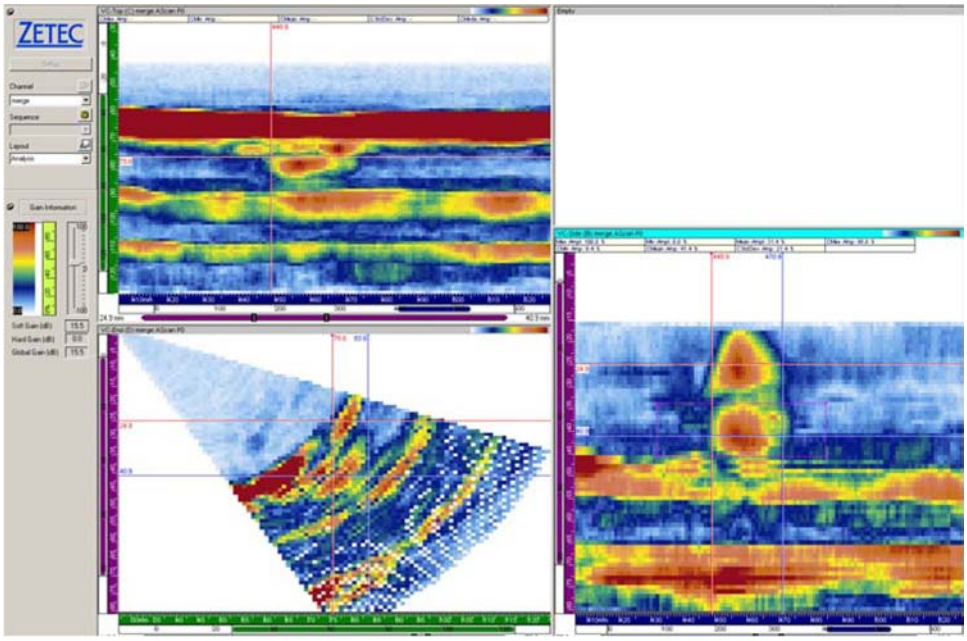

Figure A.6. Specimen 8C-032, Flaw 2 Line Scan Data at 1.5 MHz

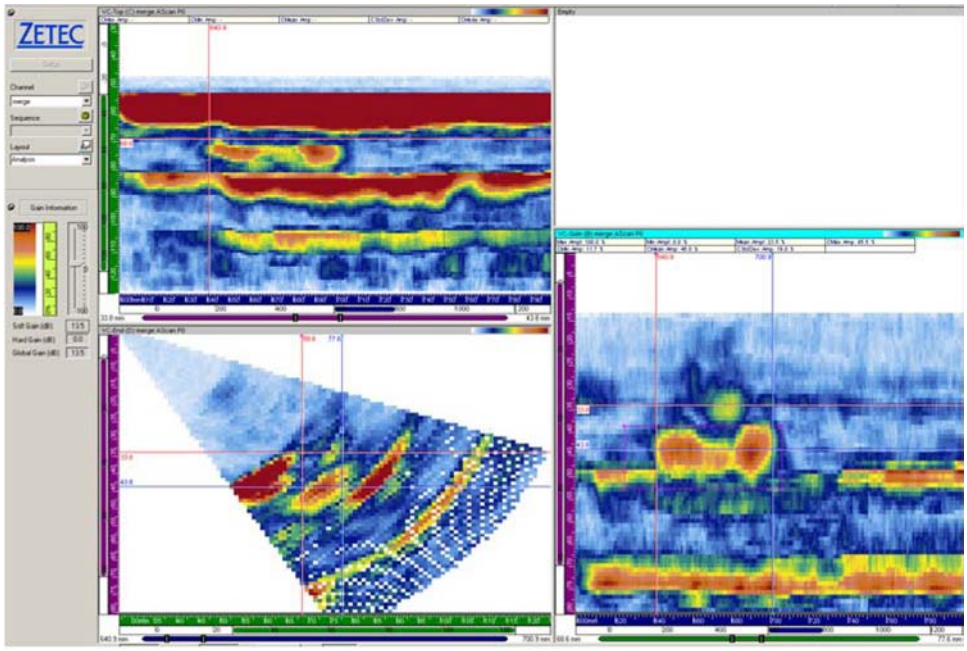

Figure A.7. Specimen 8C-032, Flaw 3 Line Scan Data at 1.5 MHz

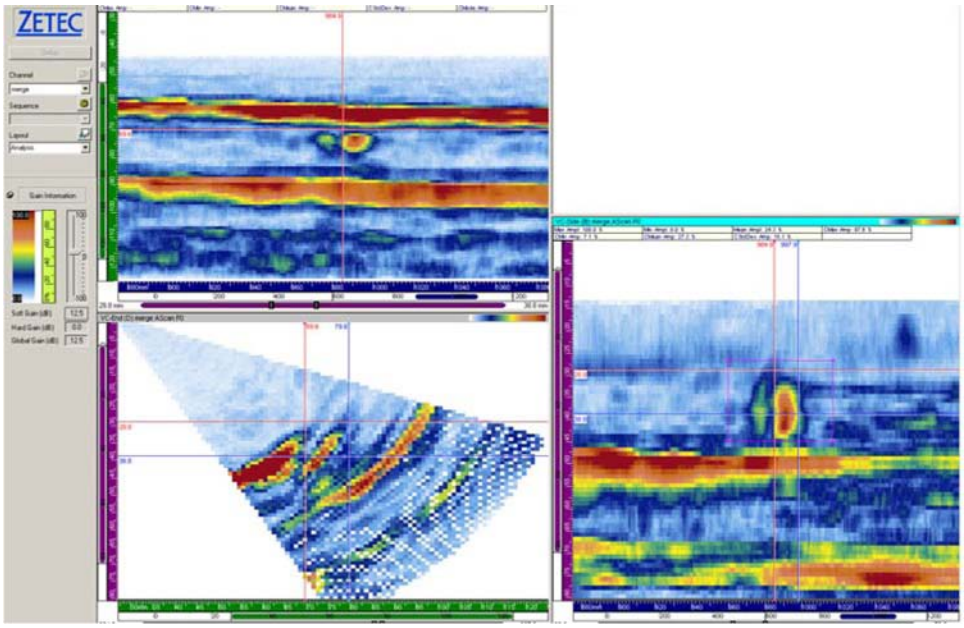

Figure A.8. Specimen 8C-032, Flaw 4 Line Scan Data at 1.5 MHz

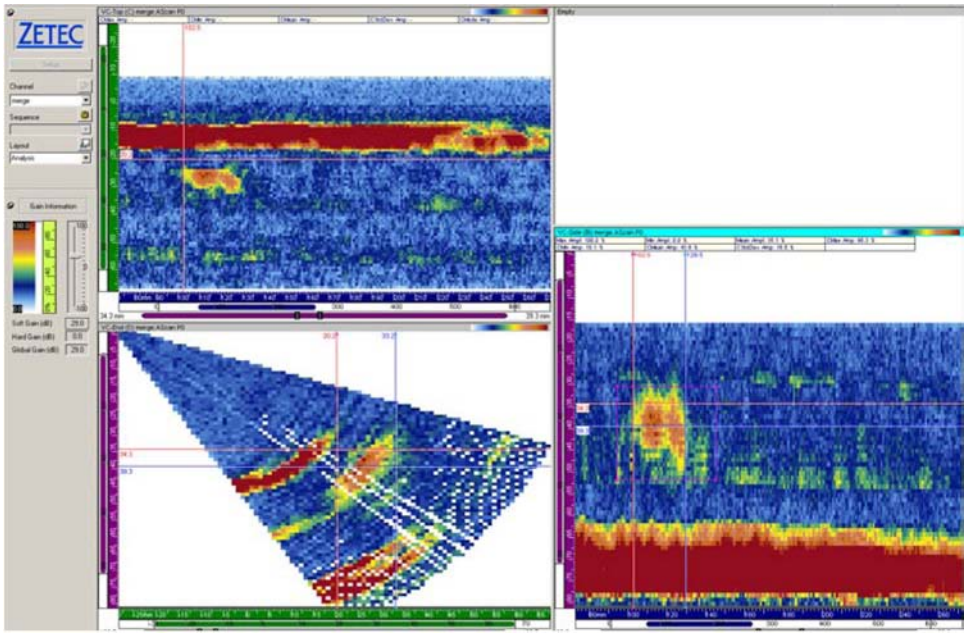

Figure A.9. Specimen 8C-032, Flaw 1 Line Scan Data at 2 MHz

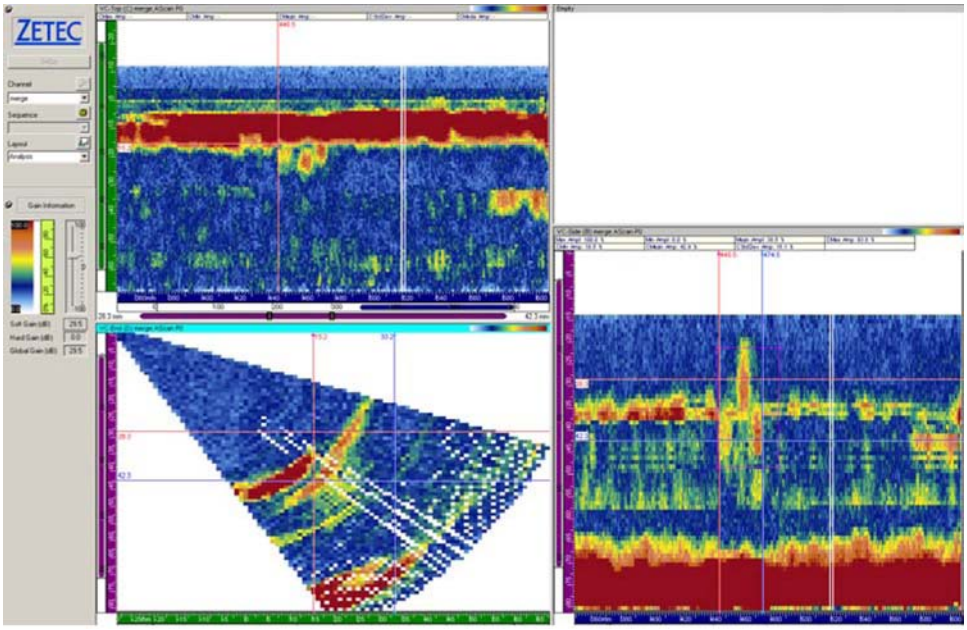

Figure A.10. Specimen 8C-032, Flaw 2 Line Scan Data at 2 MHz

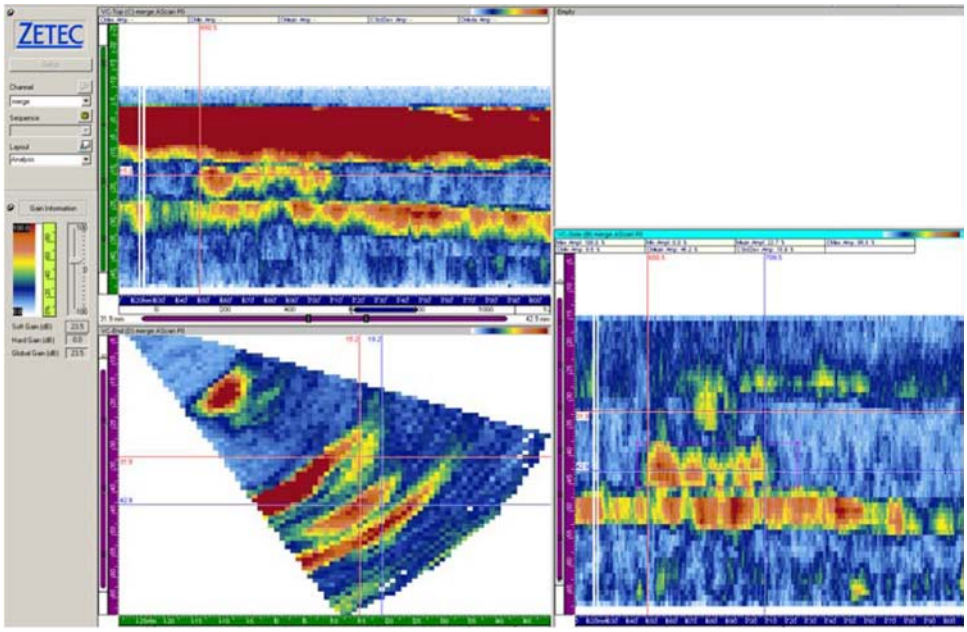

Figure A.11. Specimen 8C-032, Flaw 3 Line Scan Data at 2 MHz

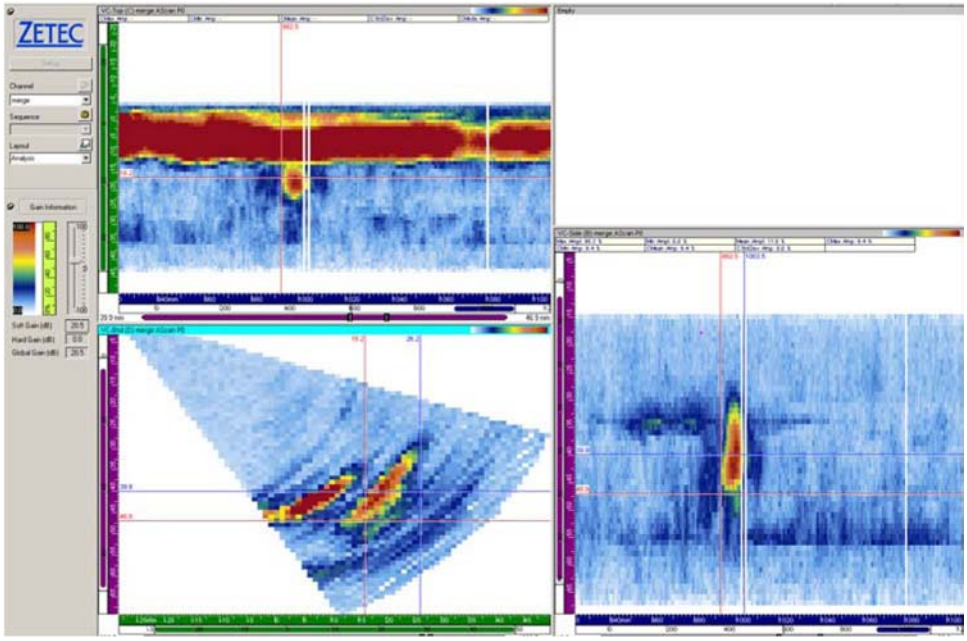

Figure A.12. Specimen 8C-032, Flaw 4 Line Scan Data at 2 MHz

Appendix B

Dissimilar Metal Weld Specimen 9C-023 Phased-Array Data

Appendix B

Dissimilar Metal Weld Specimen 9C-023 Phased-Array Data

1.5-MHz Raster Data on Flaws 1–4 ..... B.2

2-MHz Raster Data on Flaws 1–4 ..... B.4

1.5-MHz Line Scan Data on Flaws 1–4 ..... B.6

1-MHz Line Scan Data on Flaws 1–4 ..... B.8

2-MHz Line Scan Data on Flaws 1–4 ..... B.10

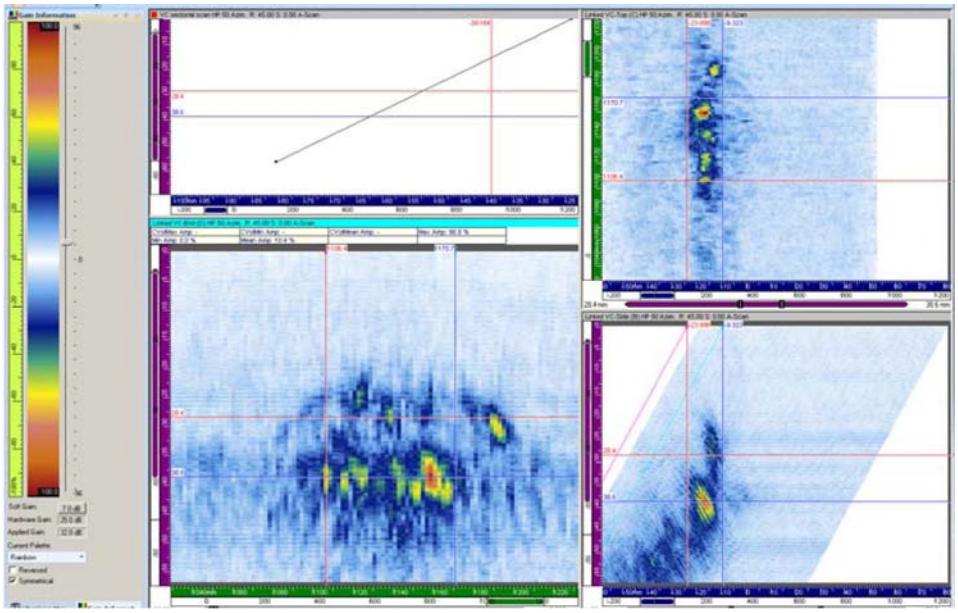

Figure B.1. Specimen 9C-023, Flaw 1 Raster Data at 1.5 MHz

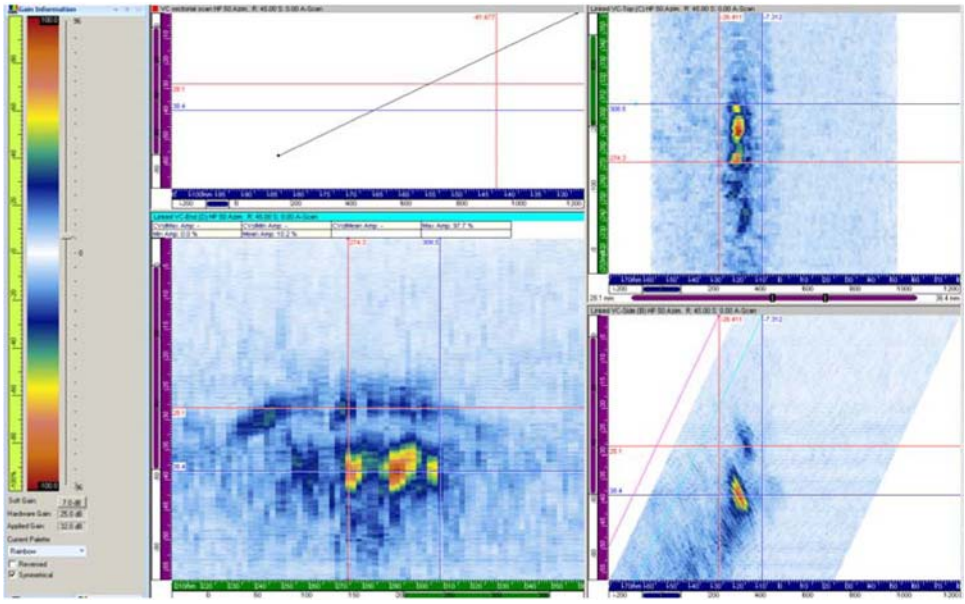

Figure B.2. Specimen 9C-023, Flaw 2 Raster Data at 1.5 MHz

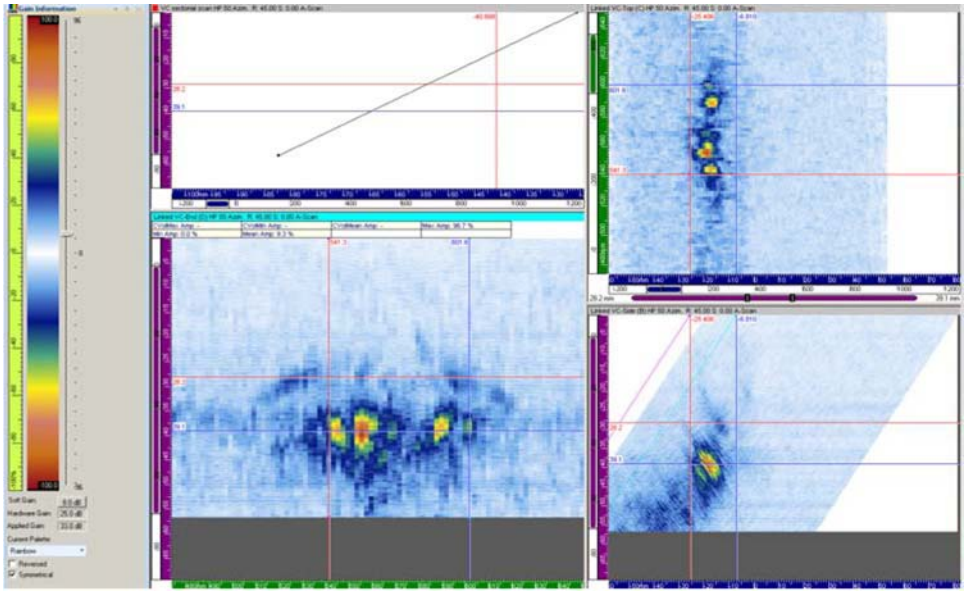

Figure B.3. Specimen 9C-023, Flaw 3 Raster Data at 1.5 MHz

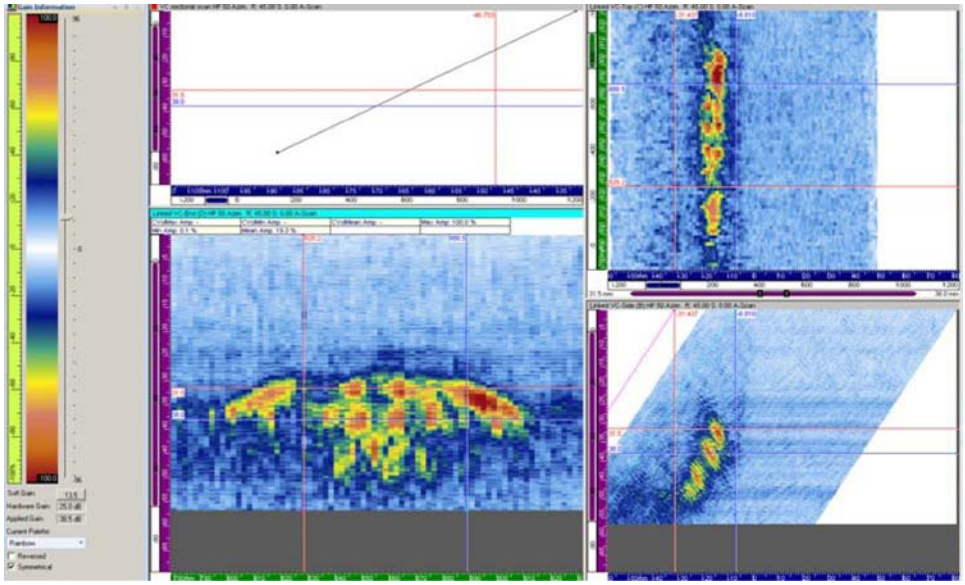

Figure B.4. Specimen 9C-023, Flaw 4 Raster Data at 1.5 MHz

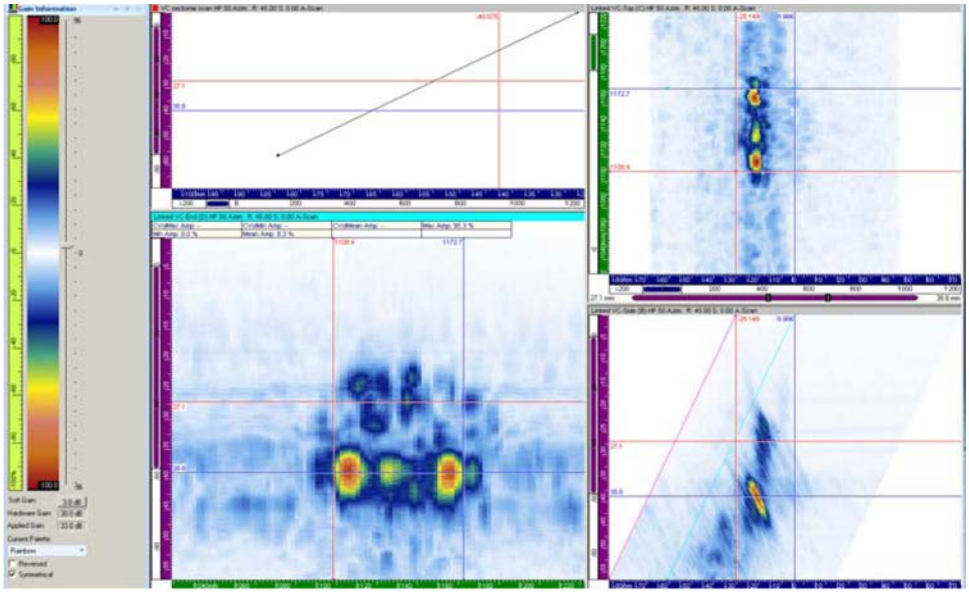

Figure B.5. Specimen 9C-023, Flaw 1 Raster Data at 2 MHz

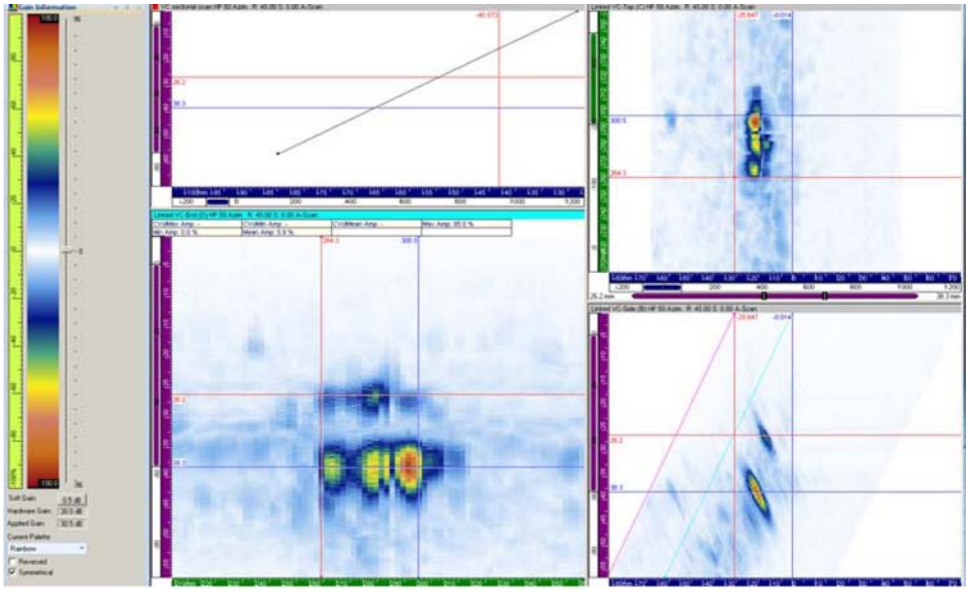

Figure B.6. Specimen 9C-023, Flaw 2 Raster Data at 2 MHz

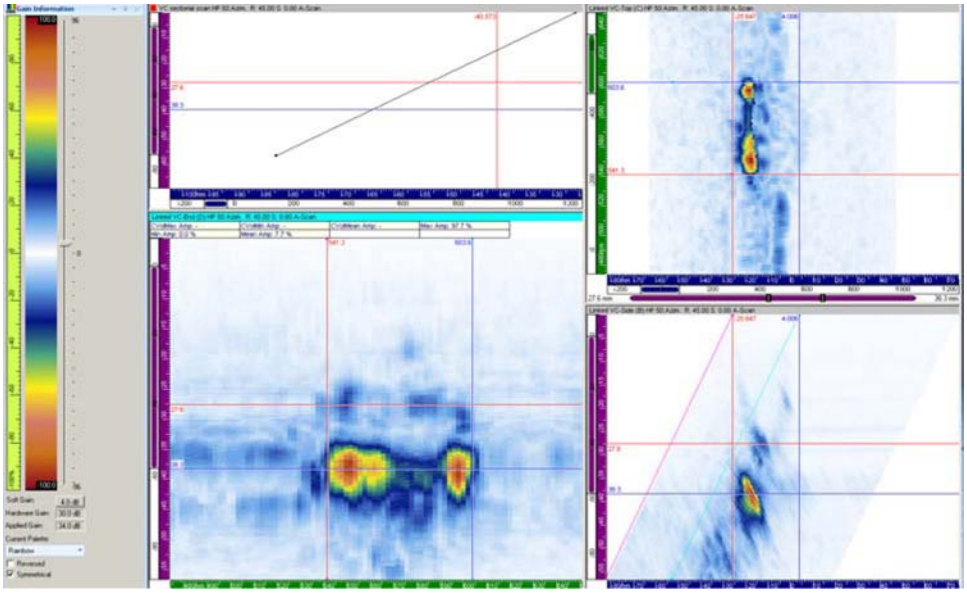

Figure B.7. Specimen 9C-023, Flaw 3 Raster Data at 2 MHz

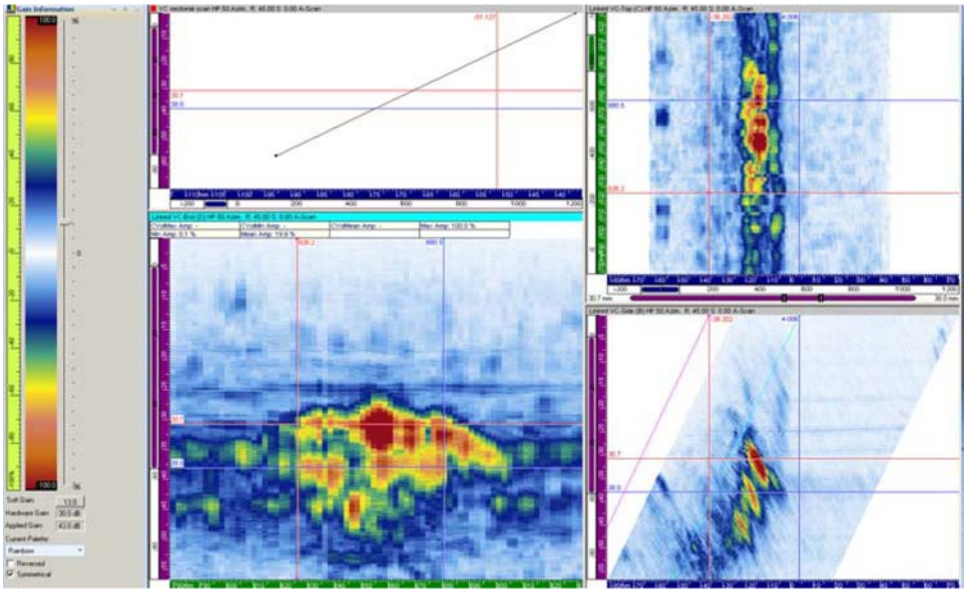

Figure B.8. Specimen 9C-023, Flaw 4 Raster Data at 2 MHz

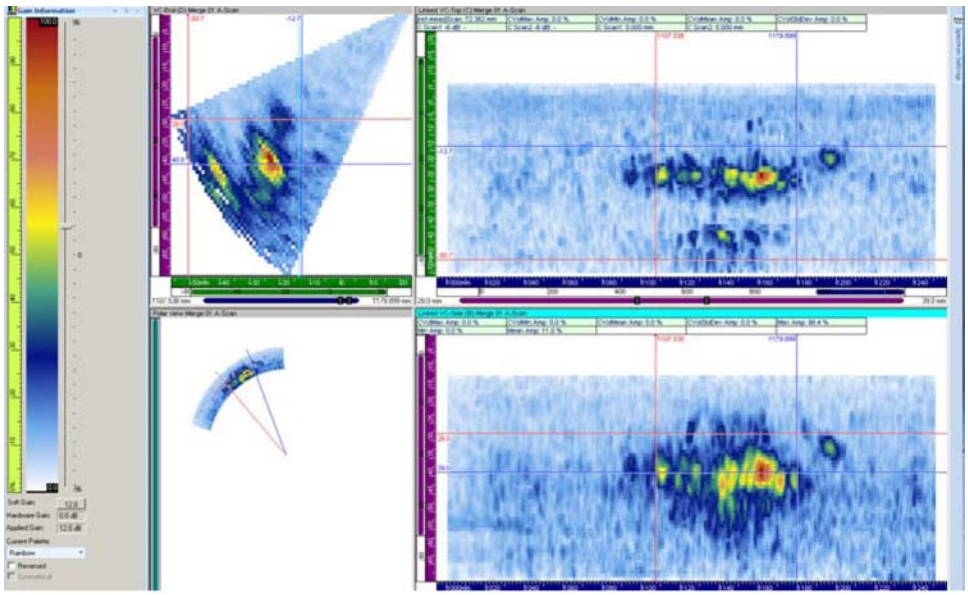

Figure B.9. Specimen 9C-023, Flaw 1 Line Scan Data at 1.5 MHz

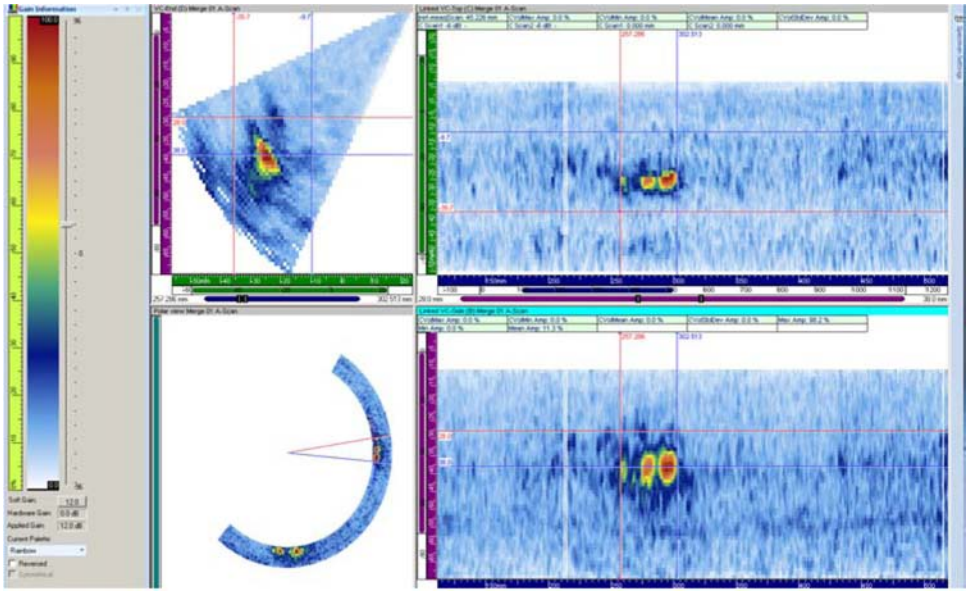

Figure B.10. Specimen 9C-023, Flaw 2 Line Scan Data at 1.5 MHz

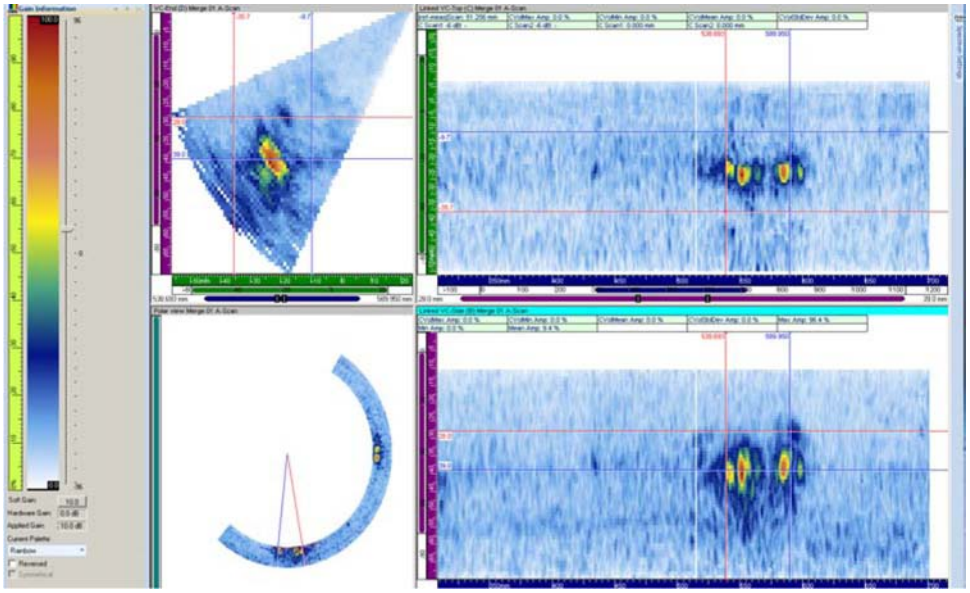

Figure B.11. Specimen 9C-023, Flaw 3 Line Scan Data at 1.5 MHz

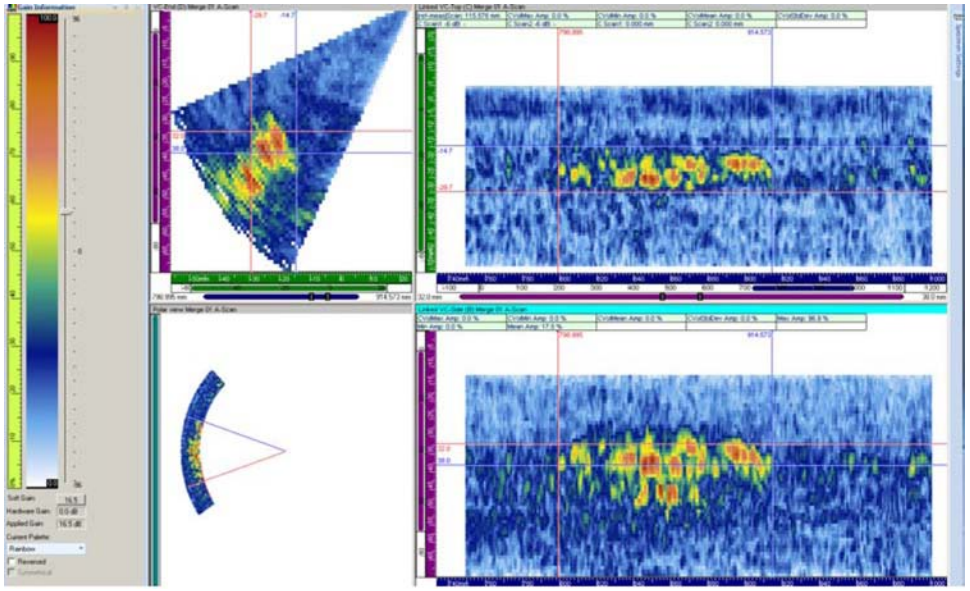

Figure B.12. Specimen 9C-023, Flaw 4 Line Scan Data at 1.5 MHz

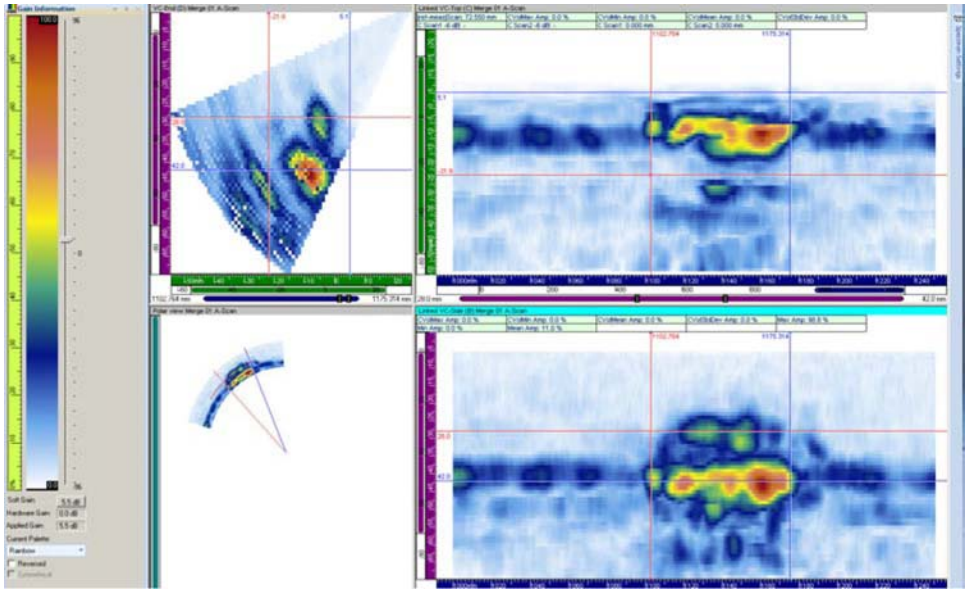

Figure B.13. Specimen 9C-023, Flaw 1 Line Scan Data at 1 MHz

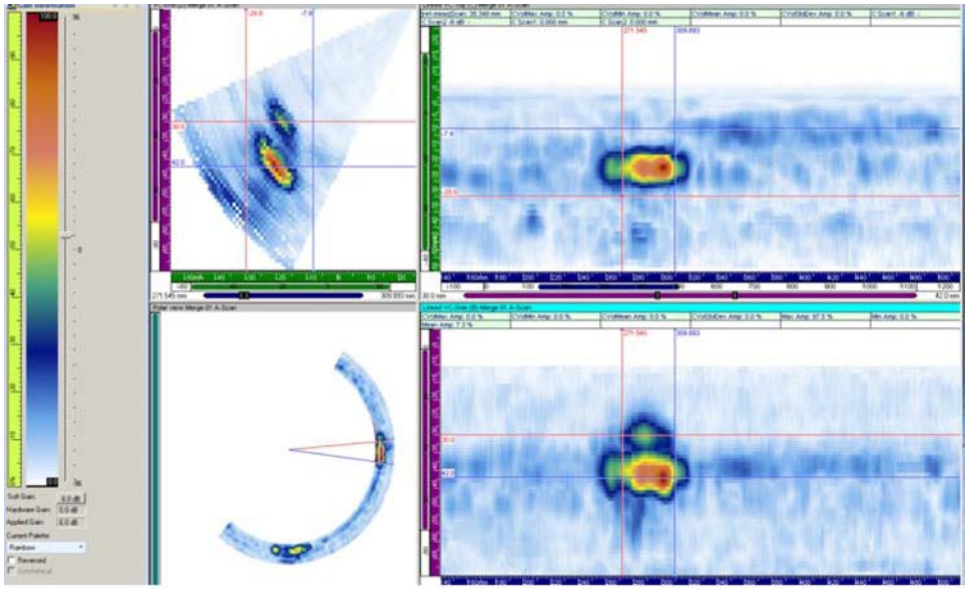

Figure B.14. Specimen 9C-023, Flaw 2 Line Scan Data at 1 MHz

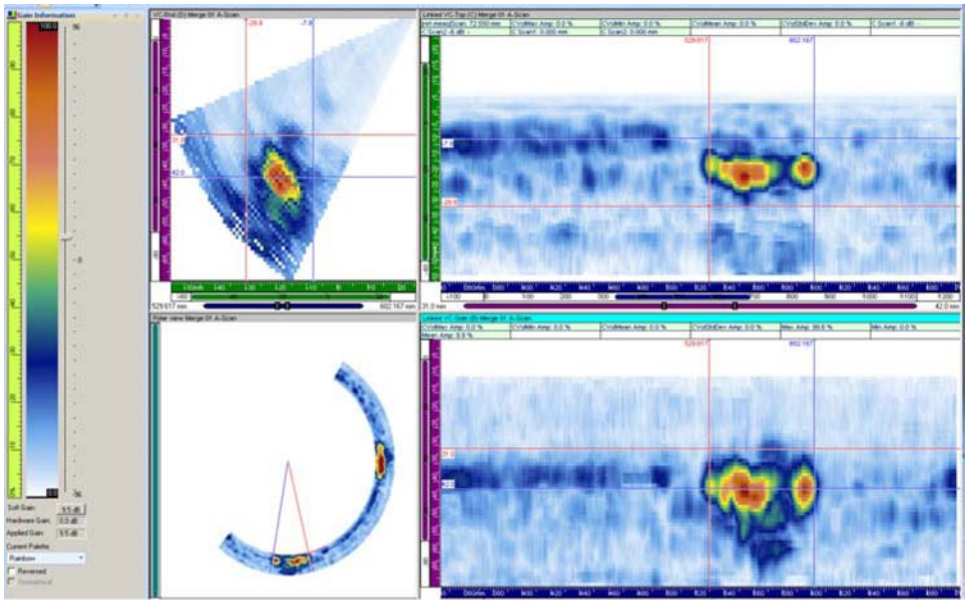

Figure B.15. Specimen 9C-023, Flaw 3 Line Scan Data at 1 MHz

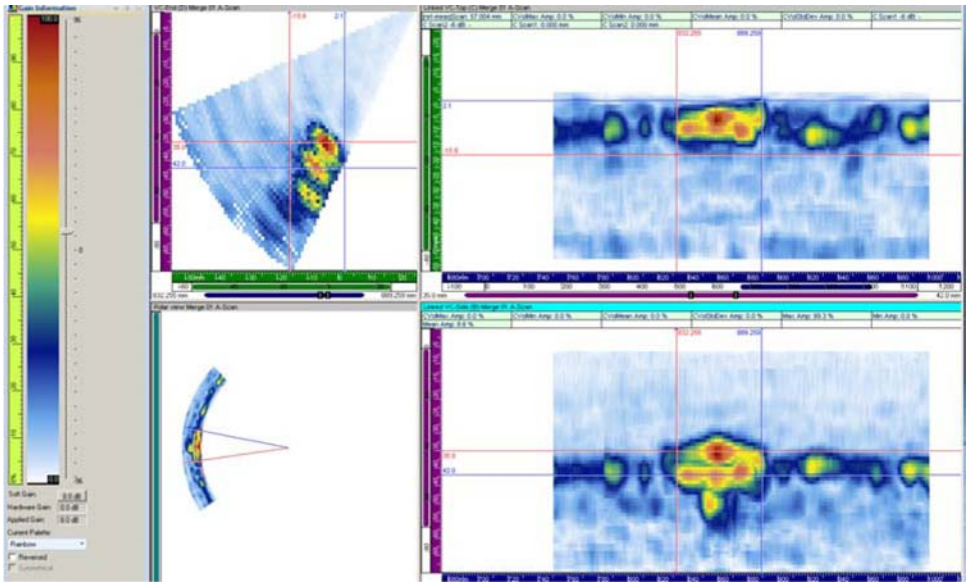

Figure B.16. Specimen 9C-023, Flaw 4 Line Scan Data at 1 MHz

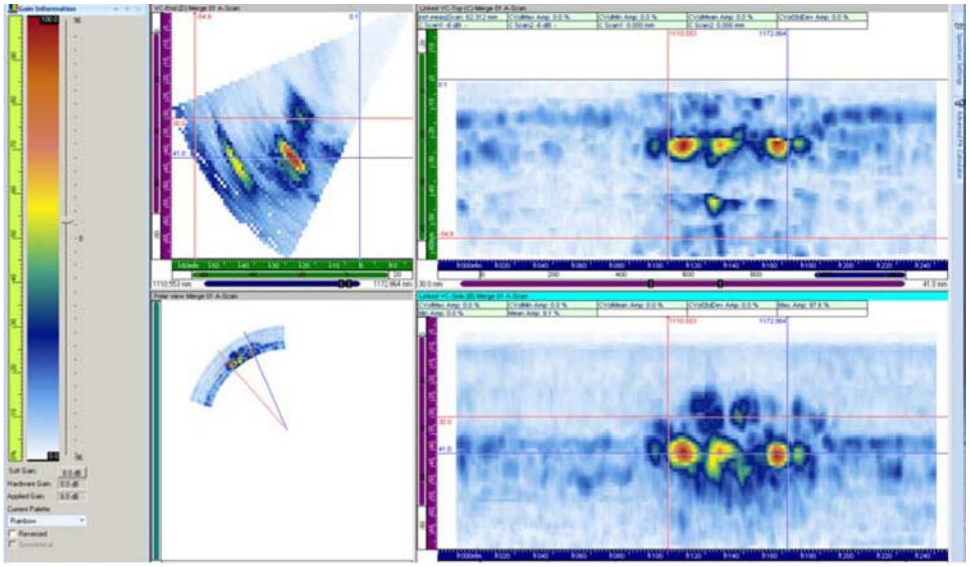

Figure B.17. Specimen 9C-023, Flaw 1 Line Scan Data at 2 MHz

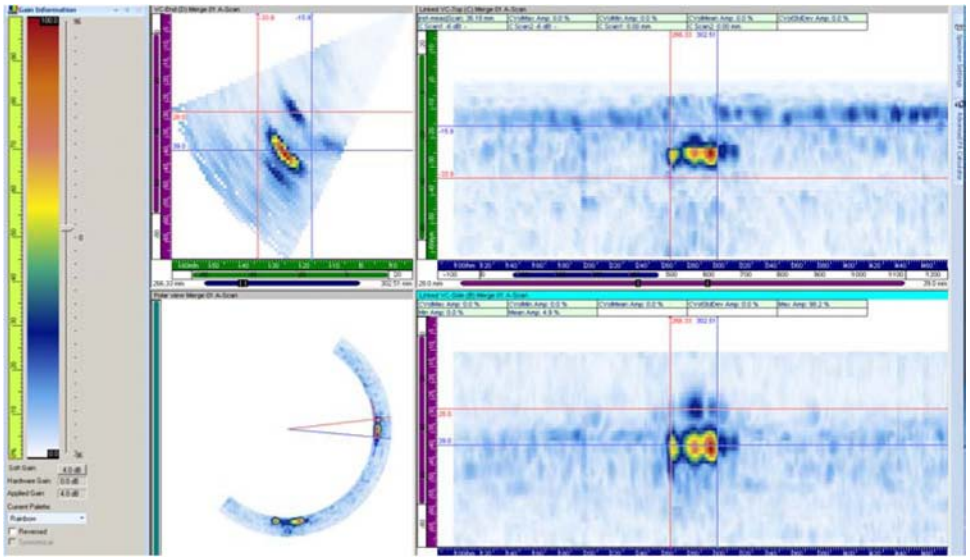

Figure B.18. Specimen 9C-023, Flaw 2 Line Scan Data at 2 MHz

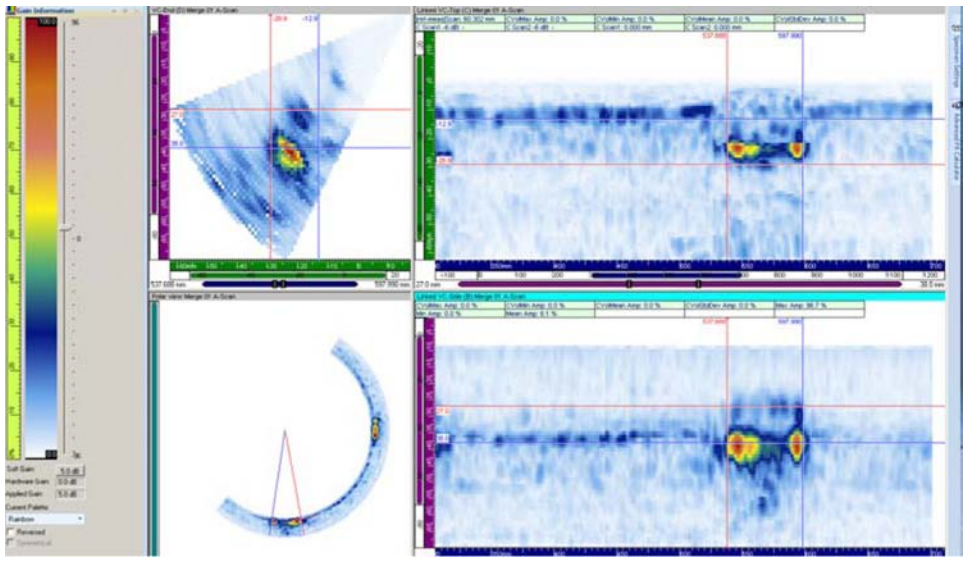

Figure B.19. Specimen 9C-023, Flaw 3 Line Scan Data at 2 MHz

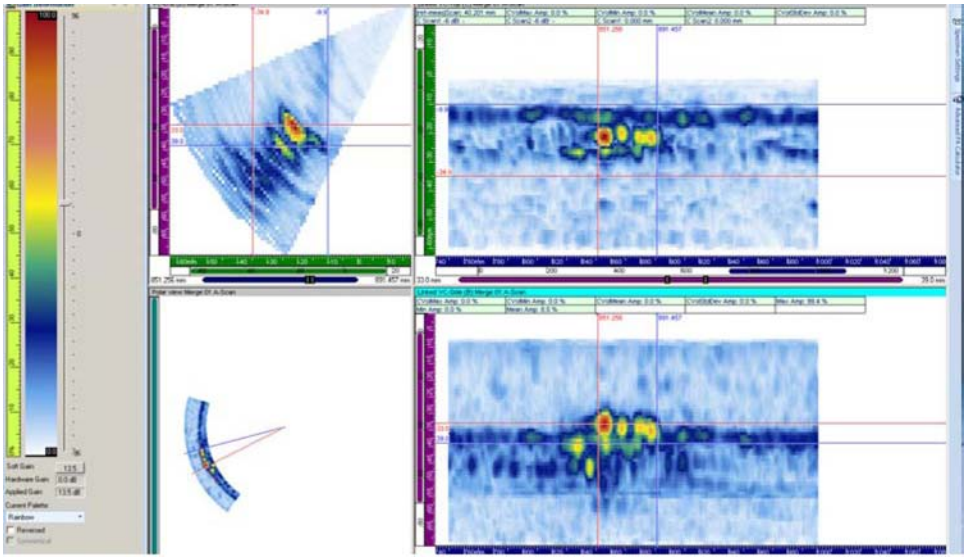

Figure B.20. Specimen 9C-023, Flaw 4 Line Scan Data at 2 MHz

Appendix C

Dissimilar Metal Weld Specimen 8C-091 Phased-Array Data

Appendix C

Dissimilar Metal Weld Specimen 8C-091 Phased-Array Data

1.5-MHz Line Scan Data on Flaws 1–4 ..... C.2

1.5-MHz Raster Data on Flaws 1–4 ..... C.3

1-MHz Line Scan Data on Flaws 2 and 3 ..... C.4

2-MHz Line Scan Data on Flaws 2 and 3 ..... C.5

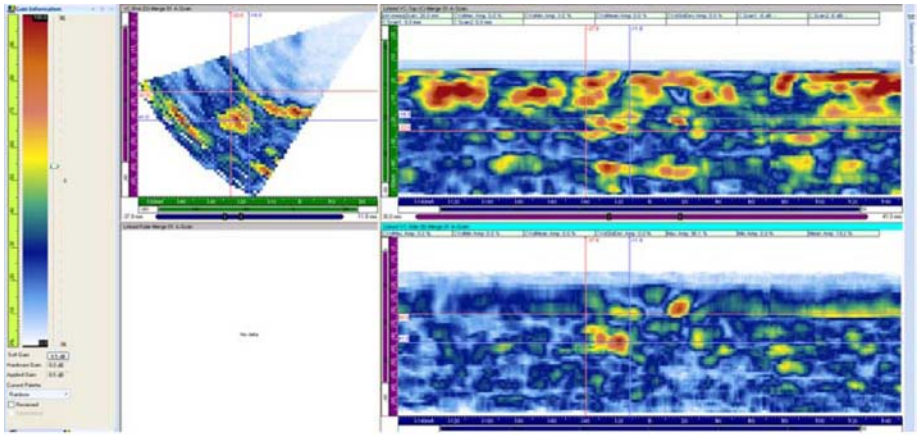

Figure C.1. Specimen 8C-091 Flaw 1 at 1.5 MHz is Marginally Detected in Line Scan Data

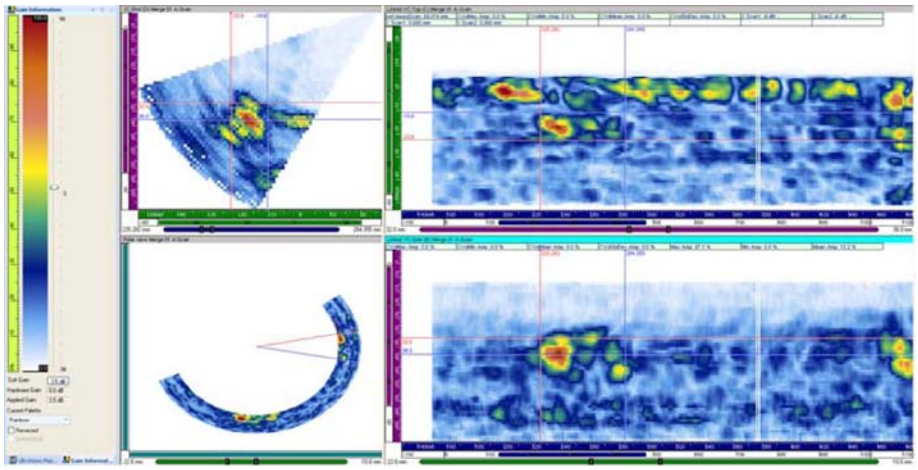

Figure C.2. Specimen 8C-091 Flaw 2 at 1.5 MHz, Line Scan Data

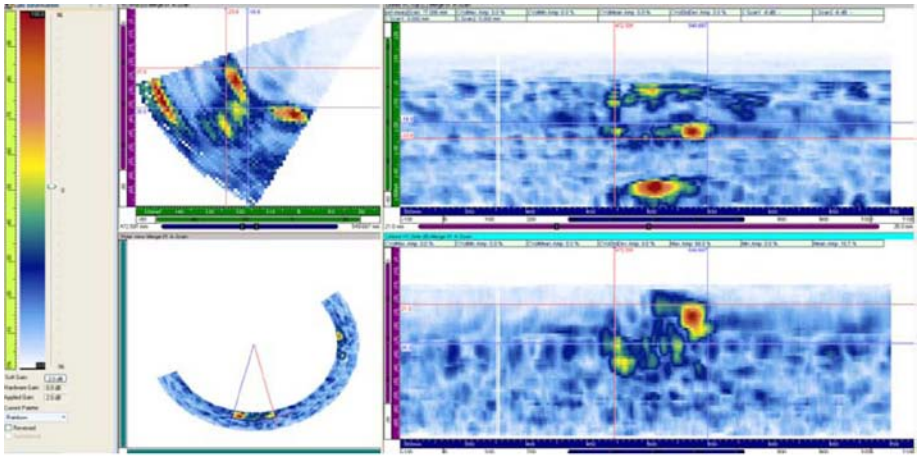

Figure C.3. Specimen 8C-091 Flaw 3 at 1.5 MHz, Line Scan Data

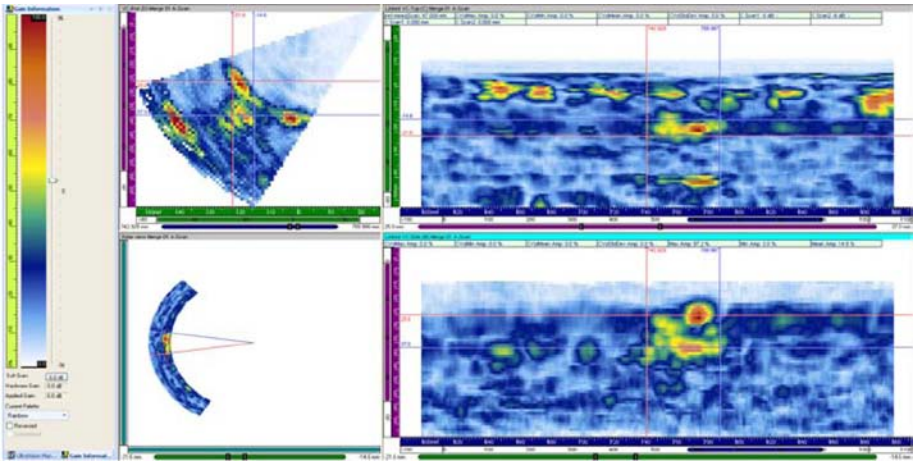

Figure C.4. Specimen 8C-091 Flaw 4 at 1.5 MHz, Line Scan Data

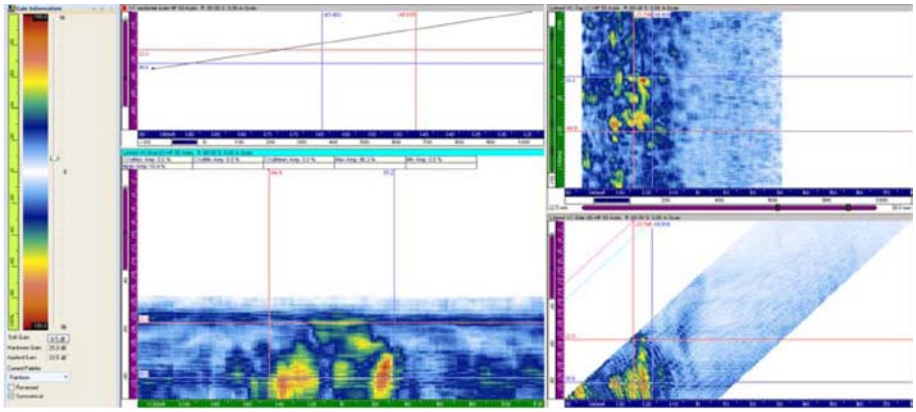

Figure C.5. Specimen 8C-091 Flaw 1, 65 Degree Raster Data at 1.5 MHz

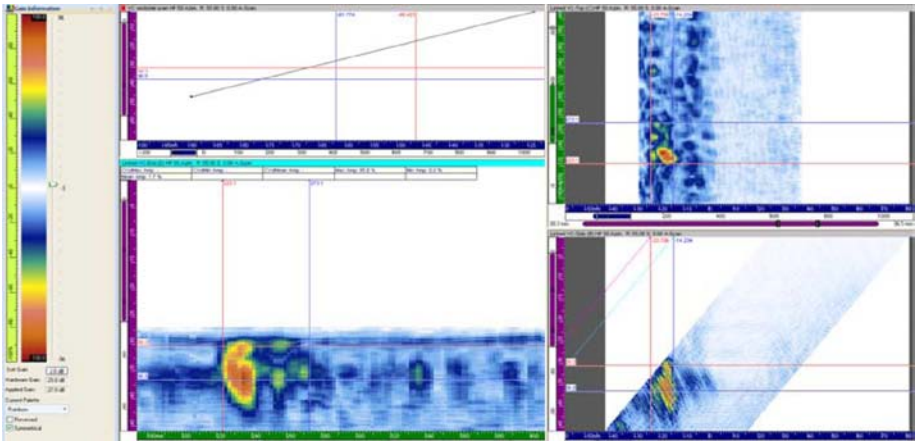

Figure C.6. Specimen 8C-091 Flaw 2, 55 Degree Raster Data at 1.5 MHz

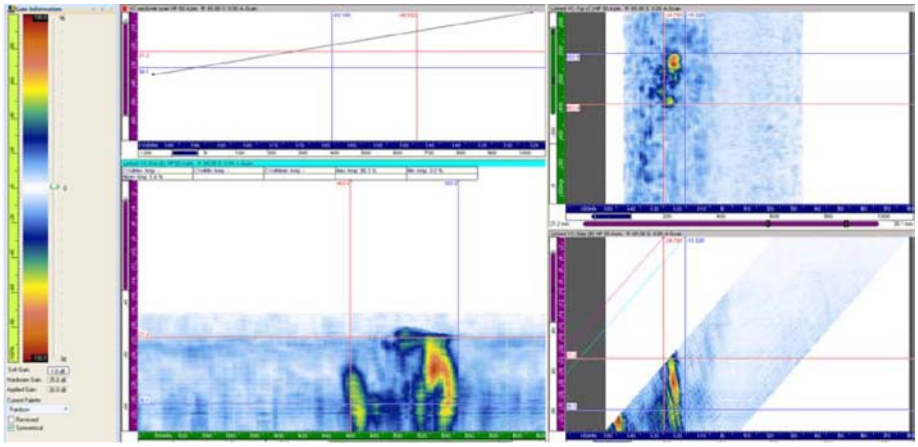

Figure C.7. Specimen 8C-091 Flaw 3, 65 Degree Raster Data at 1.5 MHz

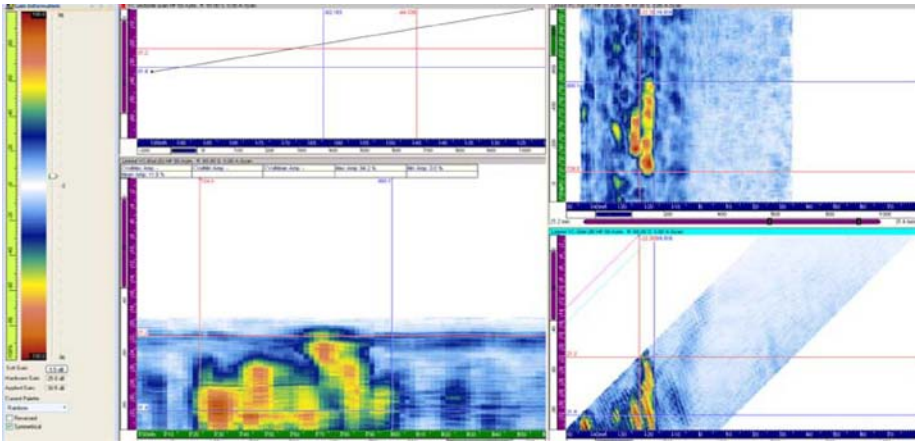

Figure C.8. Specimen 8C-091 Flaw 4, 55 Degree Raster Data at 1.5 MHz

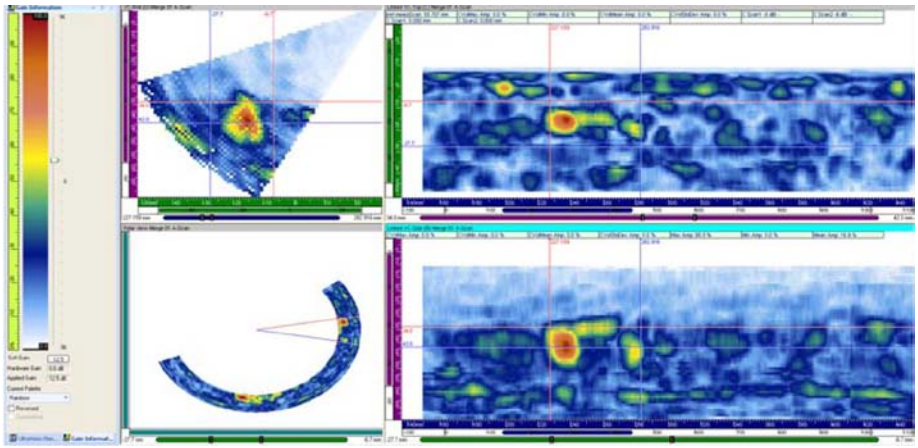

Figure C.9. Specimen 8C-091 Flaw 2 at 1 MHz, Line Scan Data

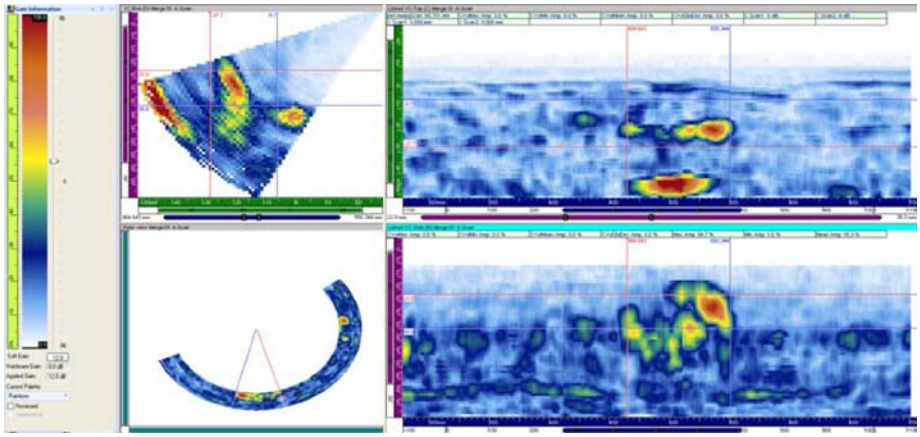

Figure C.10. Specimen 8C-091 Flaw 3 at 1 MHz, Line Scan Data

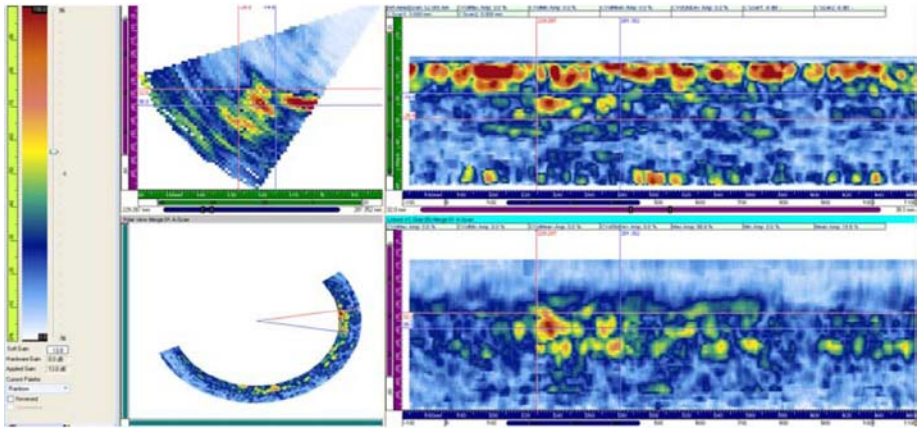

Figure C.11. Specimen 8C-091 Flaw 2 at 2 MHz, Line Scan Data

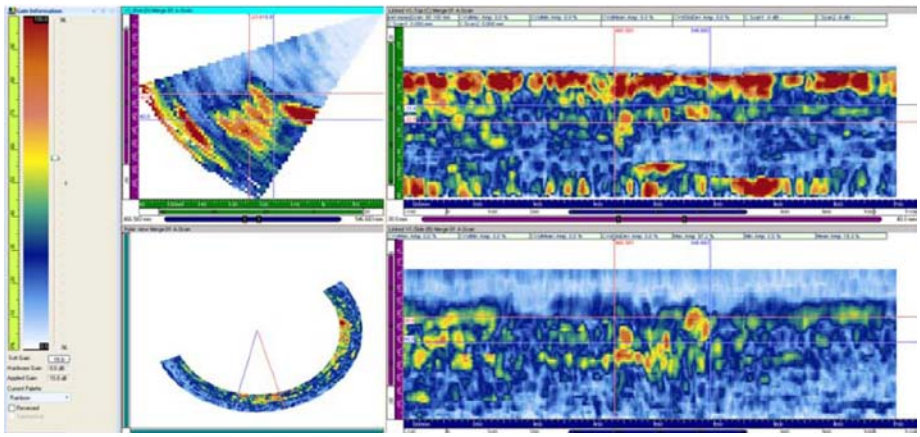

Figure C.12. Specimen 8C-091 Flaw 3 at 2 MHz, Line Scan Data

Appendix D

Dissimilar Metal Weld Specimen 9C-034 Phased-Array Data

Appendix D

Dissimilar Metal Weld Specimen 9C-034 Phased-Array Data

1.5-MHz Raster Data on Flaws 1–4 Before Weld Crown Removal D.2

1.5-MHz Raster Data on Flaws 1–4 After Weld Crown Removal D.3

2-MHz Raster Data on Flaws 1–4 After Weld Crown Removal D.4

1.5-MHz Line Scan Data on Flaws 1–4 After Weld Crown Removal..... D.6

2-MHz Line Scan Data on Flaws 1–4 After Weld Crown Removal..... D.7

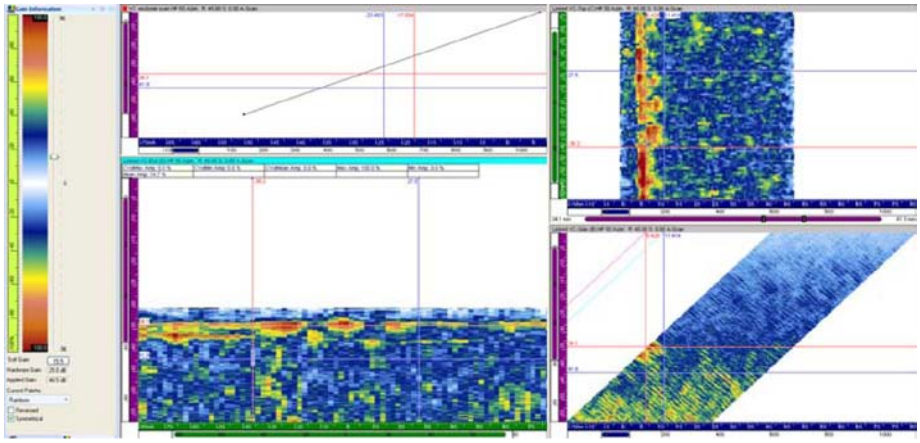

Figure D.1. Specimen 9C-034 Flaw 1 Before Weld Crown Removal at 1.5 MHz, 45 Degrees with a Marginal Detection

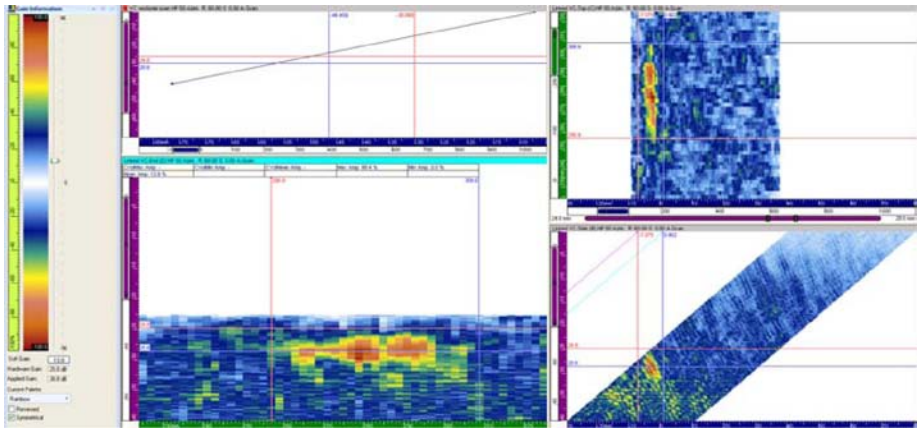

Figure D.2. Specimen 9C-034 Flaw 2 Before Weld Crown Removal at 1.5 MHz, 60 Degrees

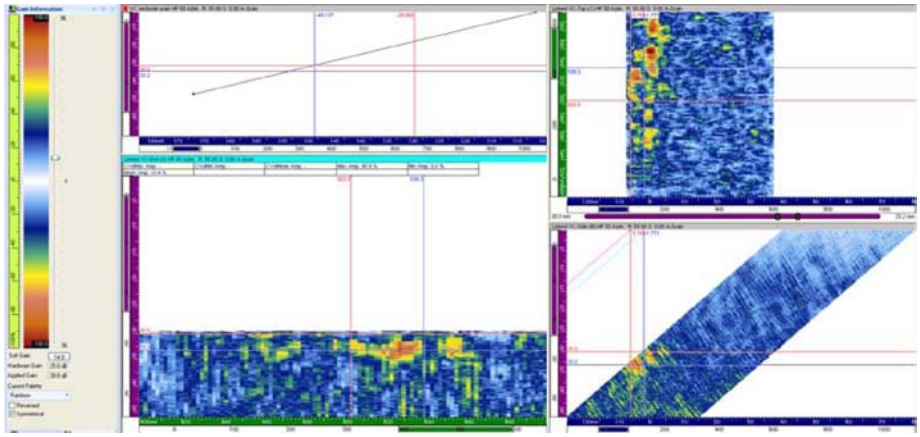

Figure D.3. Specimen 9C-034 Flaw 3 Before Weld Crown Removal at 1.5 MHz, 55 Degrees with a Marginal Detection

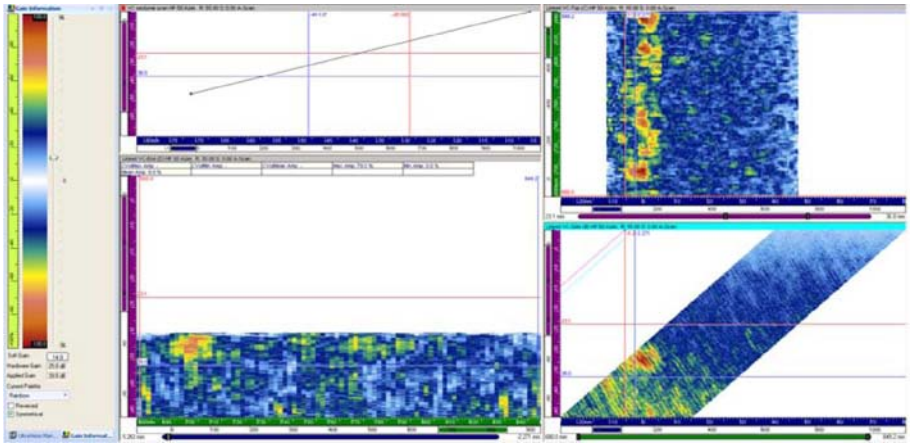

Figure D.4. Specimen 9C-034 Flaw 4 Before Weld Crown Removal at 1.5 MHz, 55 Degrees with a No Detection

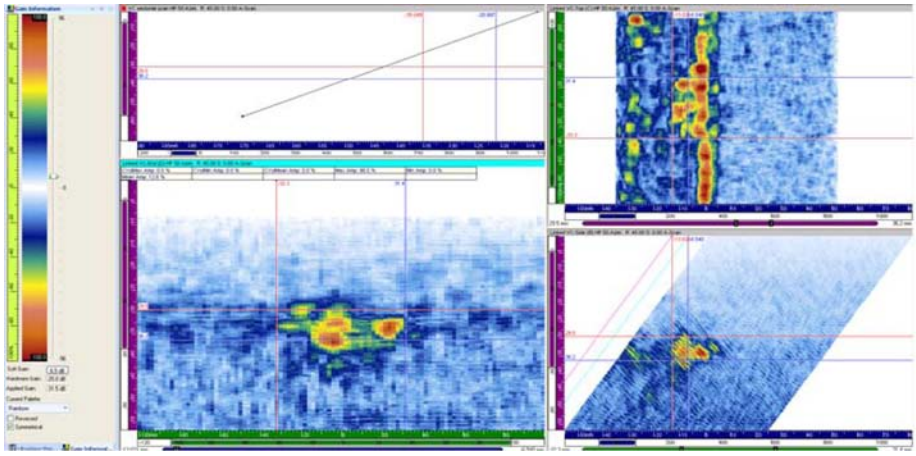

Figure D.5. Specimen 9C-034 Flaw 1 After Weld Crown Removal at 1.5 MHz

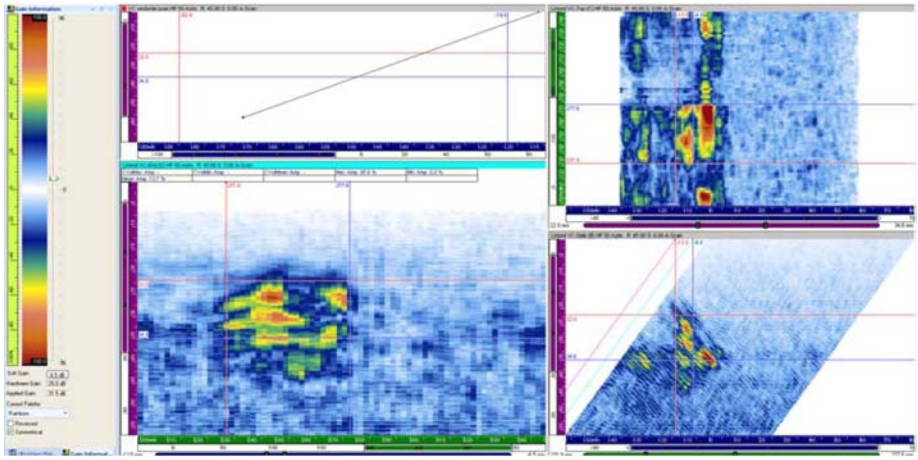

Figure D.6. Specimen 9C-034 Flaw 2 After Weld Crown Removal at 1.5 MHz

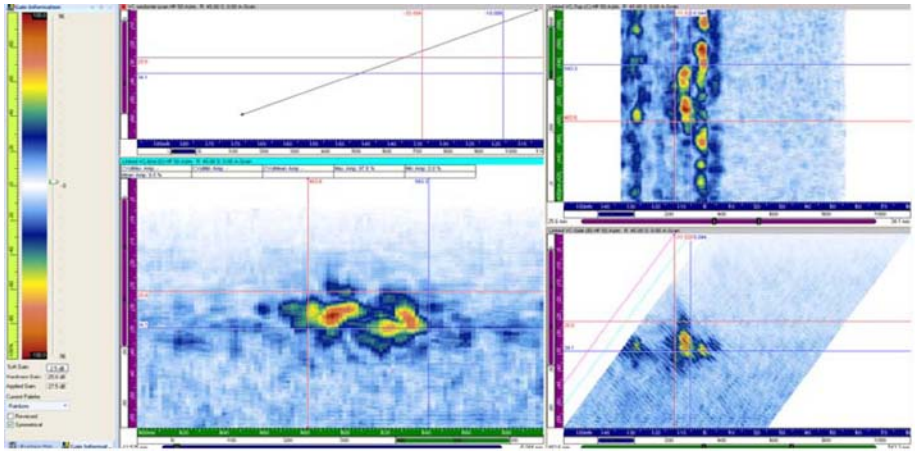

Figure D.7. Specimen 9C-034 Flaw 3 After Weld Crown Removal at 1.5 MHz

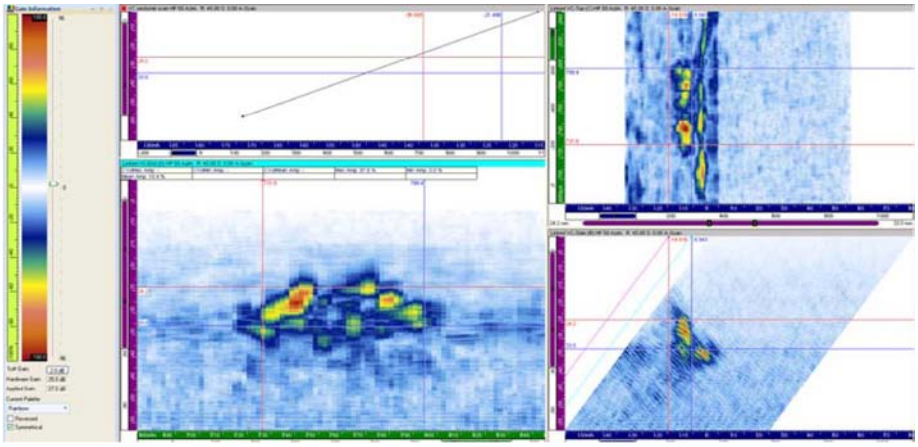

Figure D.8. Specimen 9C-034 Flaw 4 After Weld Crown Removal at 1.5 MHz

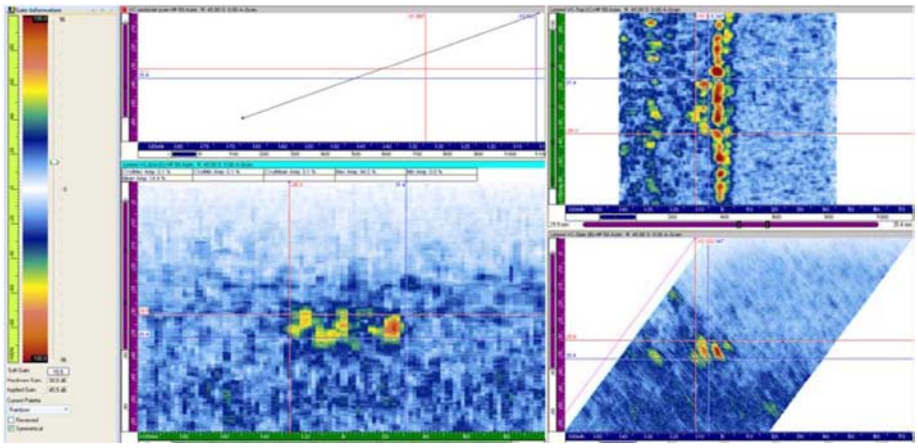

Figure D.9. Specimen 9C-034 Flaw 1 After Weld Crown Removal at 2 MHz

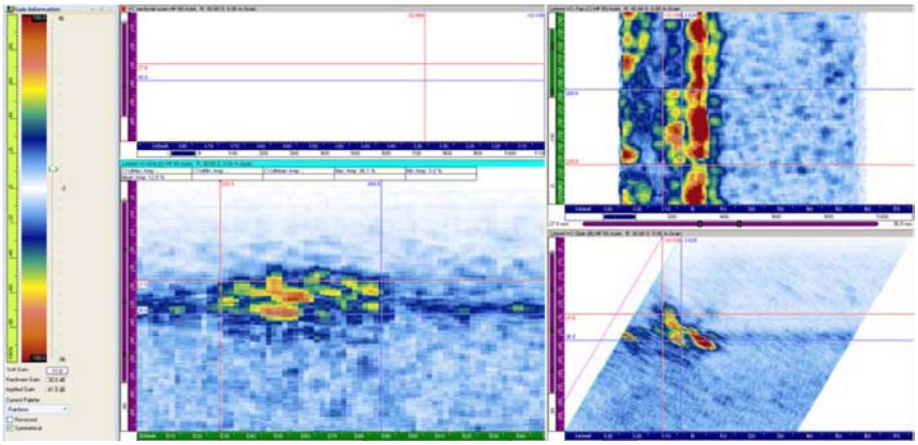

Figure D.10. Specimen 9C-034 Flaw 2 After Weld Crown Removal at 2 MHz

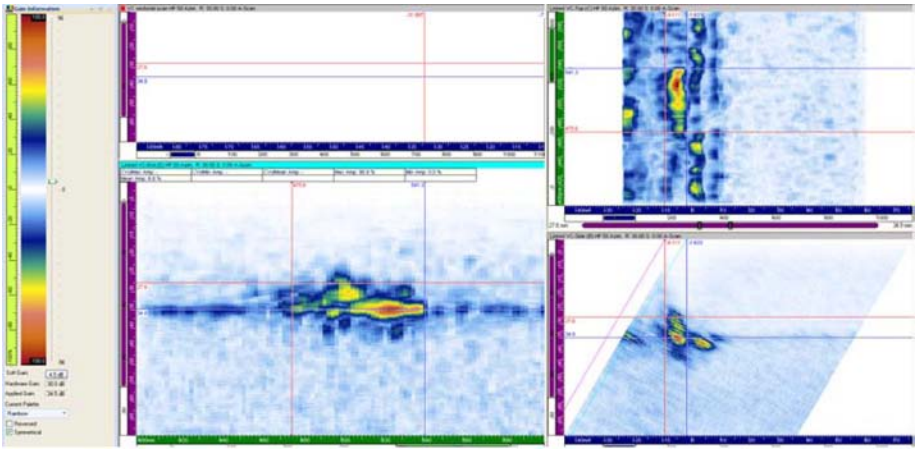

Figure D.11. Specimen 9C-034 Flaw 3 After Weld Crown Removal at 2 MHz

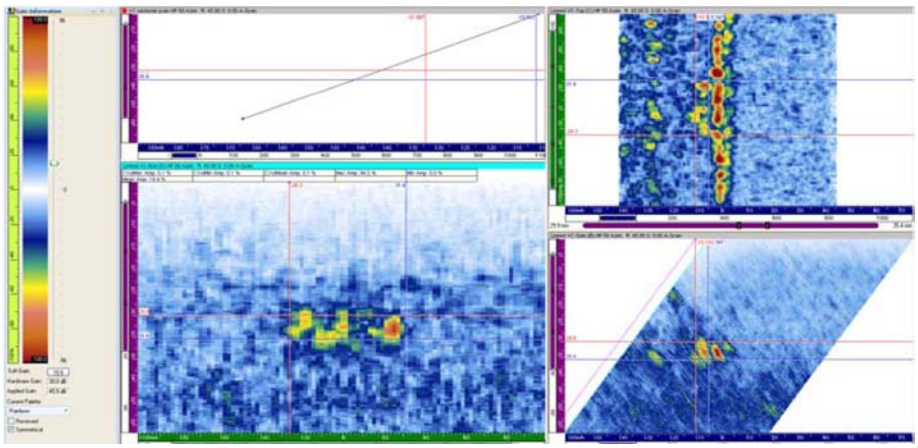

Figure D.12. Specimen 9C-034 Flaw 4 After Weld Crown Removal at 2 MHz

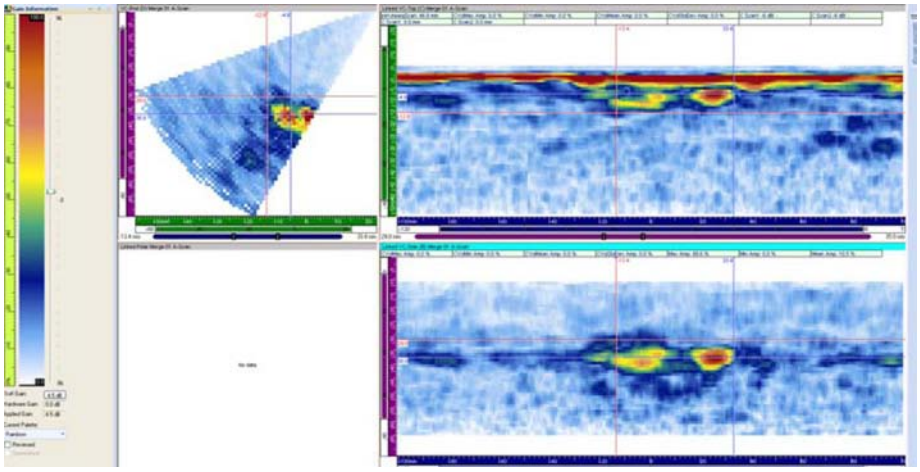

Figure D.13. Specimen 9C-034 Flaw 1 After Weld Crown Removal at 1.5 MHz, Line Scan Data

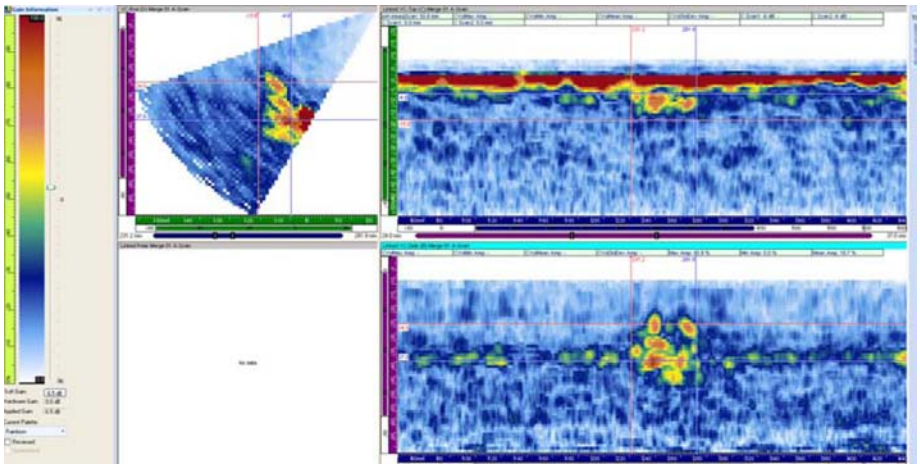

Figure D.14. Specimen 9C-034 Flaw 2 After Weld Crown Removal at 1.5 MHz, Line Scan Data

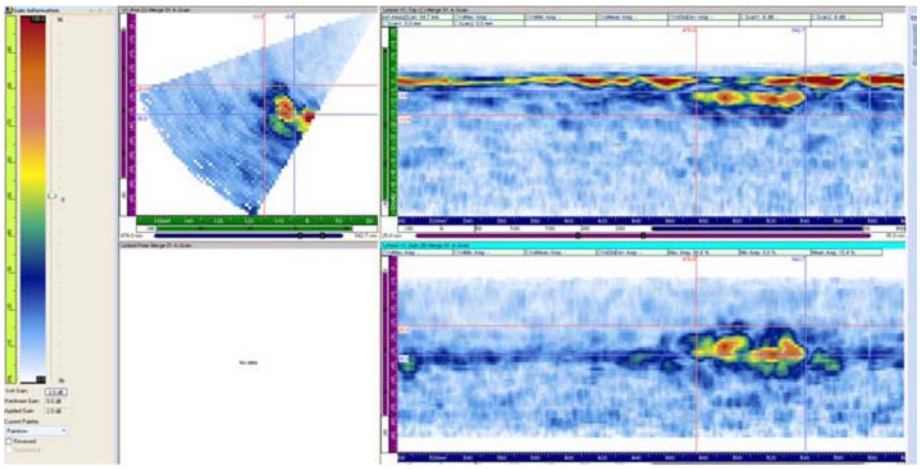

Figure D.15. Specimen 9C-034 Flaw 3 After Weld Crown Removal at 1.5 MHz, Line Scan Data

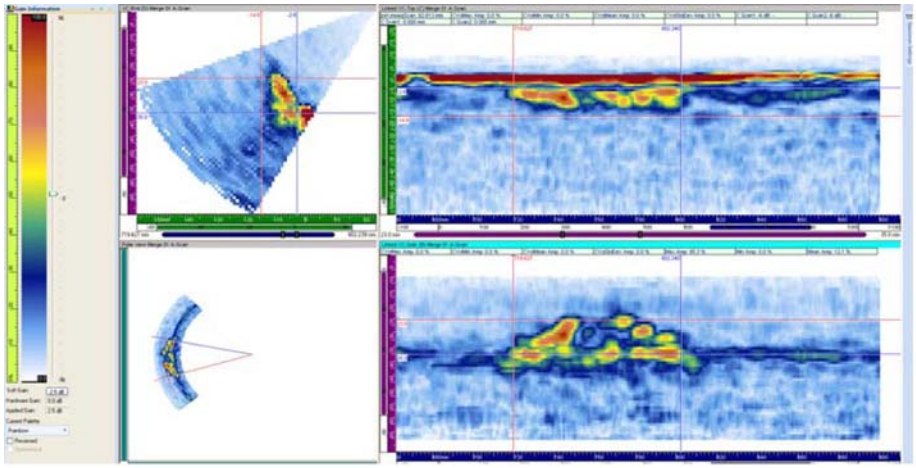

Figure D.16. Specimen 9C-034 Flaw 4 After Weld Crown Removal at 1.5 MHz, Line Scan Data

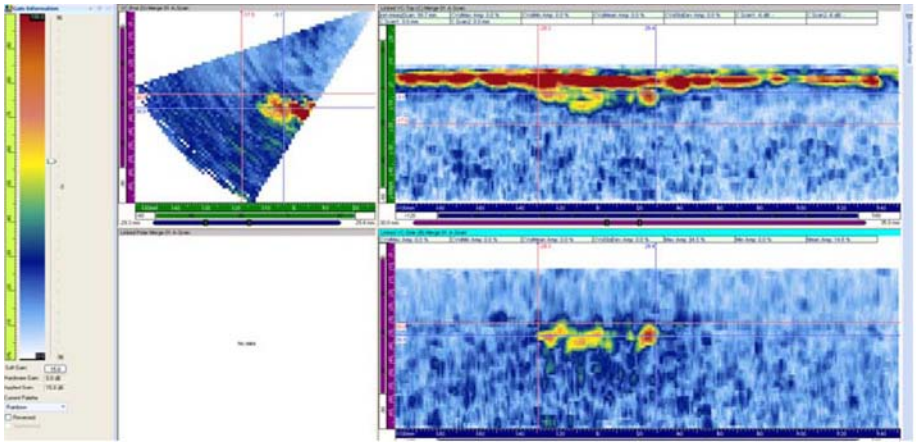

Figure D.17. Specimen 9C-034 Flaw 1 After Weld Crown Removal at 2 MHz, Line Scan Data

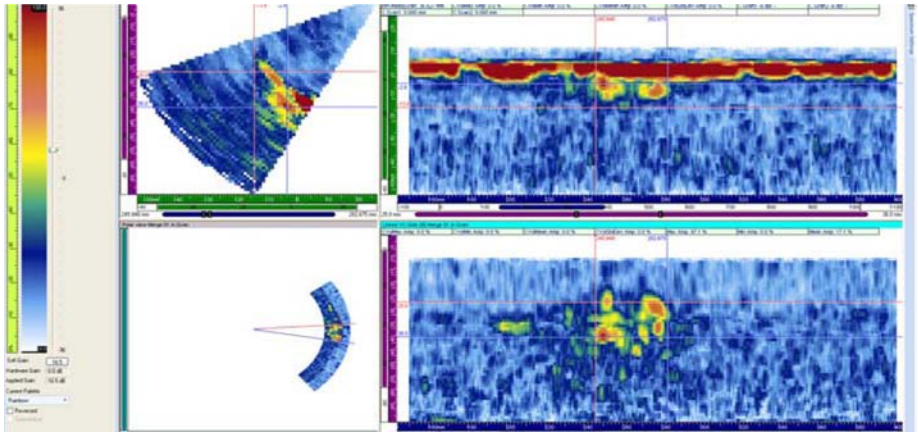

Figure D.18. Specimen 9C-034 Flaw 2 After Weld Crown Removal at 2 MHz, Line Scan Data

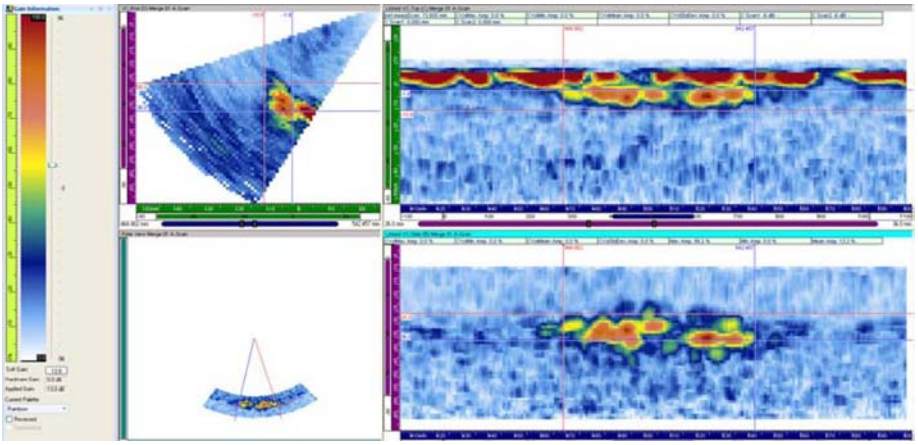

Figure D.19. Specimen 9C-034 Flaw 3 After Weld Crown Removal at 2 MHz, Line Scan Data

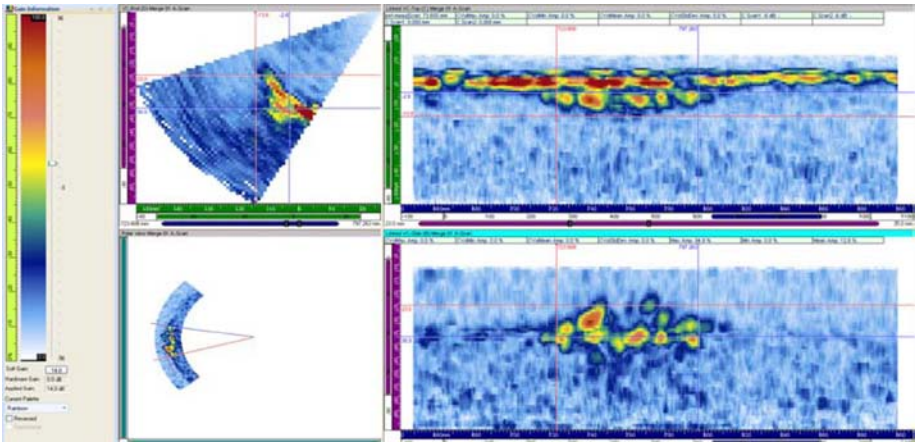

Figure D.20. Specimen 9C-034 Flaw 4 After Weld Crown Removal at 2 MHz, Line Scan Data

Appendix E

Dissimilar Metal Weld Specimen 8C-036 Phased-Array Data

Appendix E

Dissimilar Metal Weld Specimen 8C-036 Phased-Array Data

2-MHz Raster Data on Circumferential Flaws 1–6 ..... E.2

1.5-MHz Raster Data on Axial Flaws 7 and 8 ..... E.4

1.5-MHz Line Scan Data on Flaws 1–8 ..... E.4

2-MHz Line Scan Data on Circumferential Flaws 1–6 ..... E.7

1.5-MHz Raster Data on Circumferential Flaws 4–6 ..... E.9

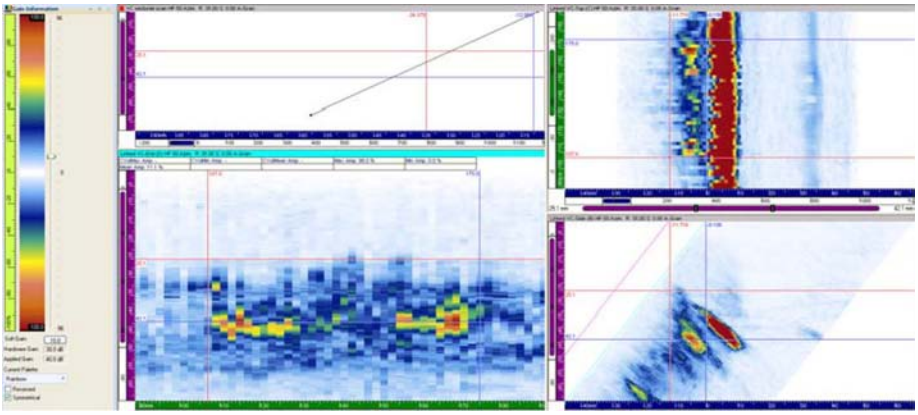

Figure E.1. Specimen 8C-036 Flaw 1 at 2 MHz

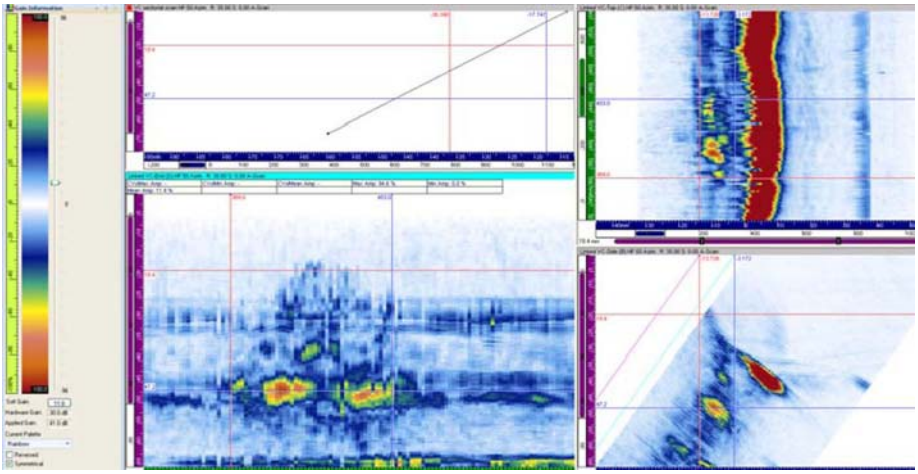

Figure E.2. Specimen 8C-036 Flaw 2 at 2 MHz

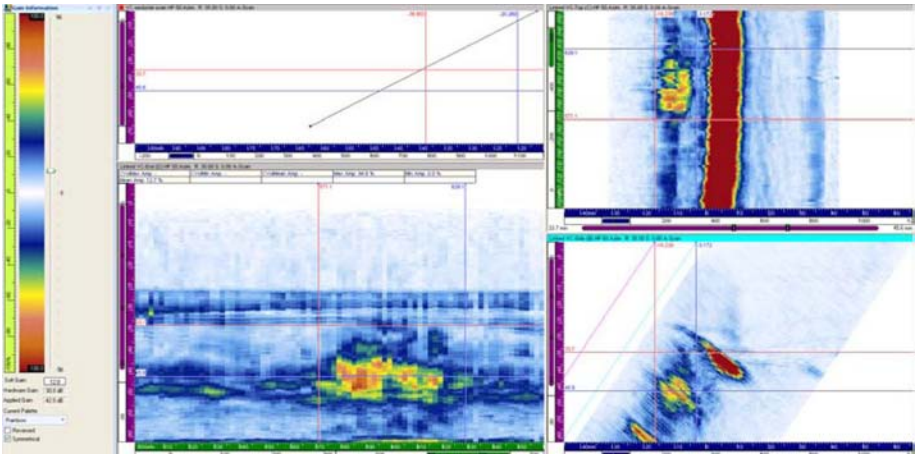

Figure E.3. Specimen 8C-036 Flaw 3 at 2 MHz

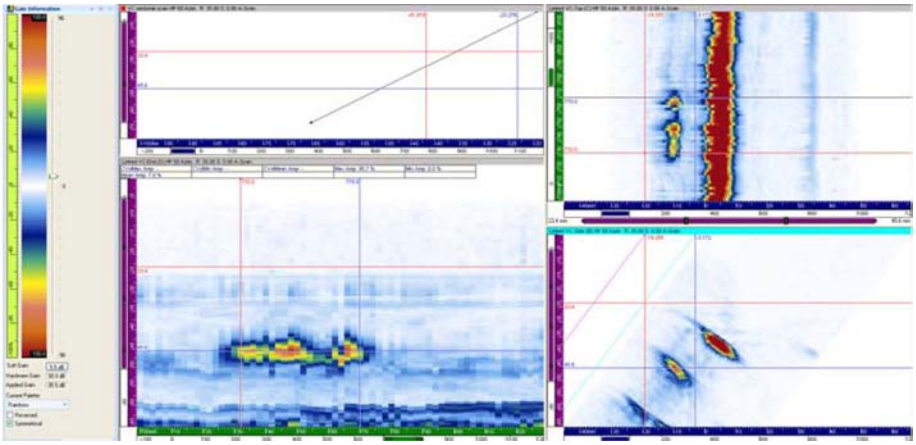

Figure E.4. Specimen 8C-036 Flaw 4 at 2 MHz

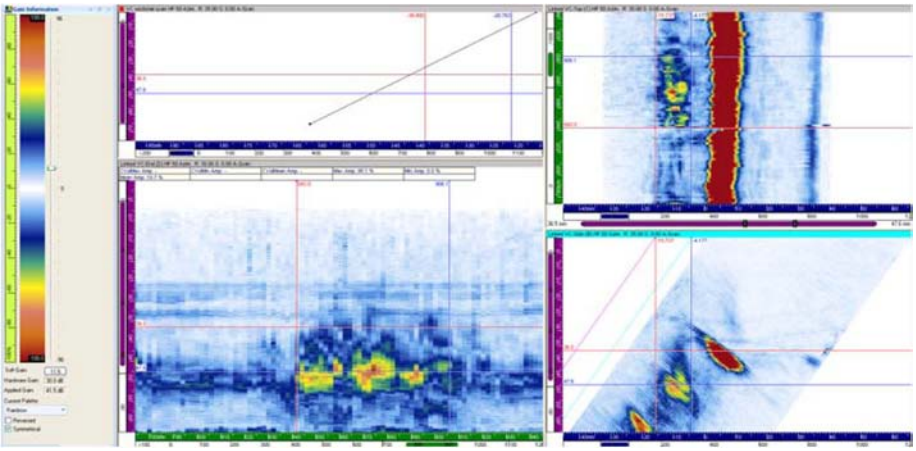

Figure E.5. Specimen 8C-036 Flaw 5 at 2 MHz

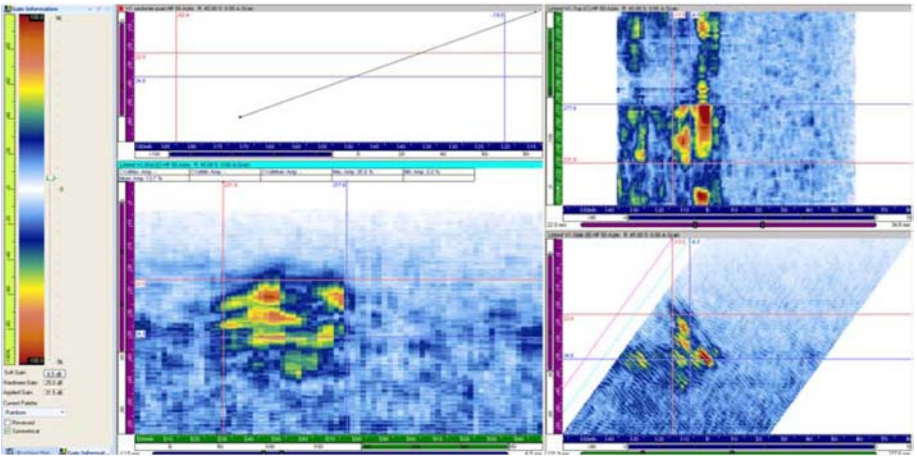

Figure E.6. Specimen 8C-036 Flaw 6 at 2 MHz

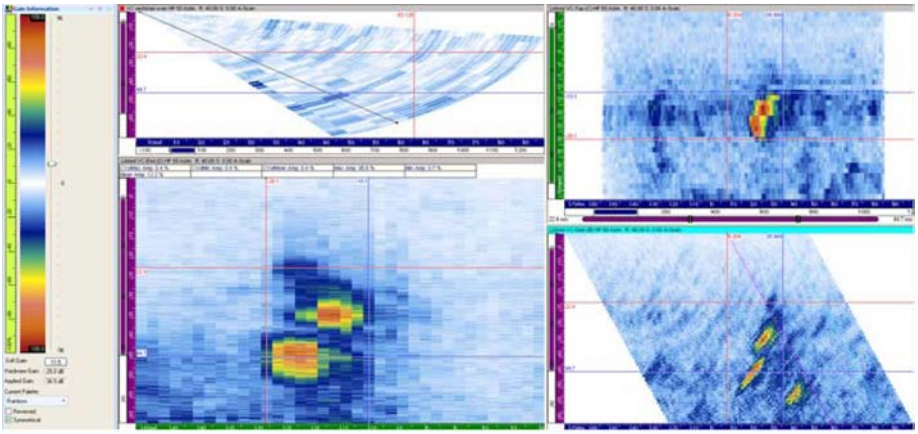

Figure E.7. Specimen 8C-036 Axial Flaw 7 at 1.5 MHz

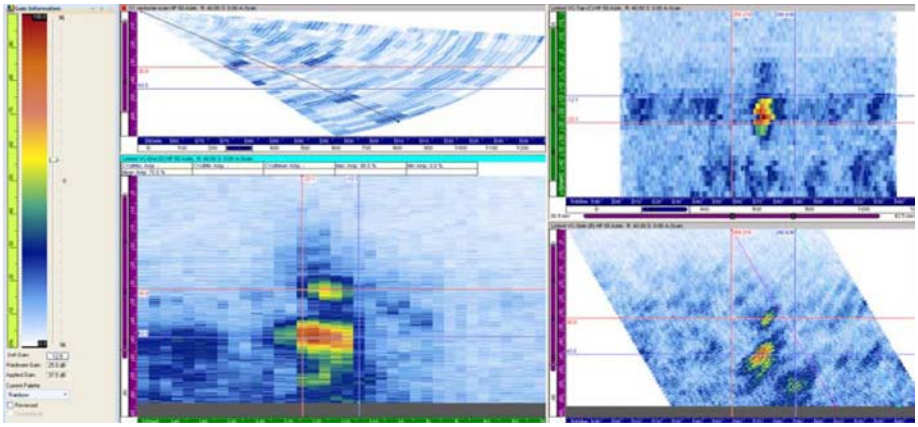

Figure E.8. Specimen 8C-036 Axial Flaw 8 at 1.5 MHz

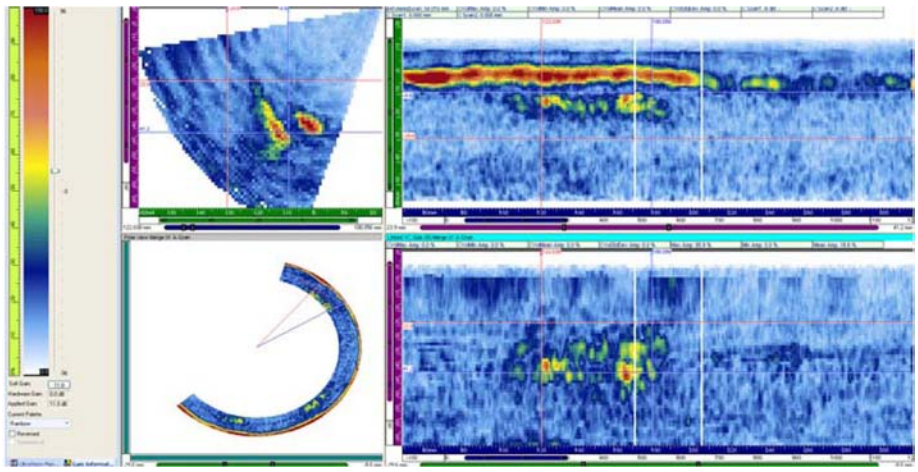

Figure E.9. Specimen 8C-036 Flaw 1 Line Scan Data at 1.5 MHz

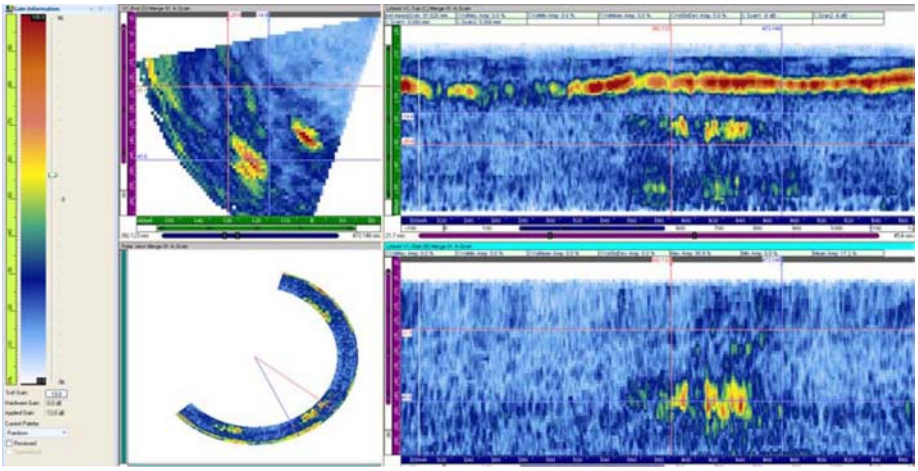

Figure E.10. Specimen 8C-036 Flaw 2 Line Scan Data at 1.5 MHz

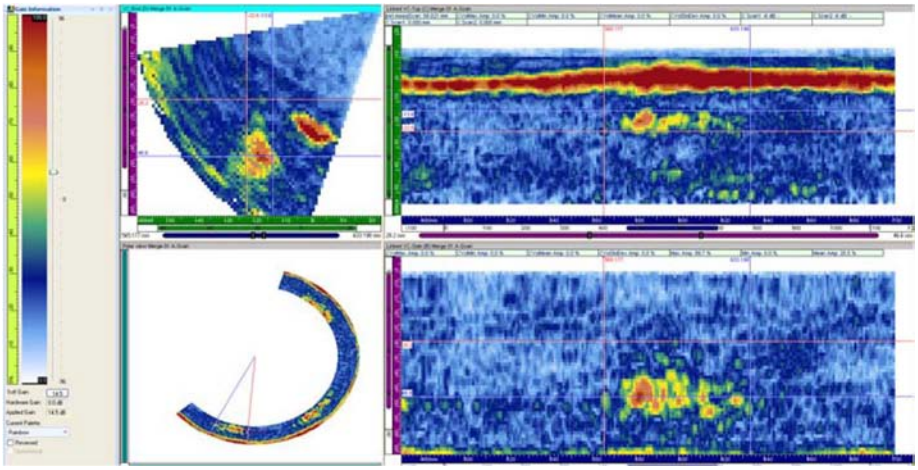

Figure E.11. Specimen 8C-036 Flaw 3 Line Scan Data at 1.5 MHz

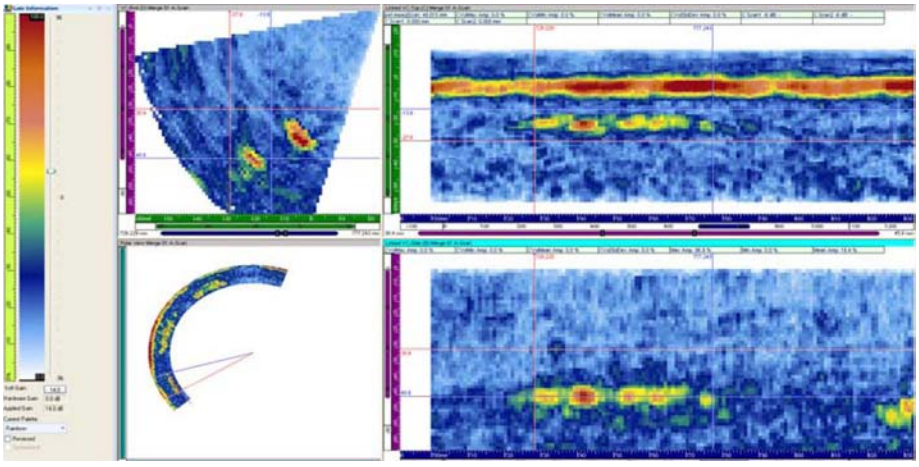

Figure E.12. Specimen 8C-036 Flaw 4 Line Scan Data at 1.5 MHz

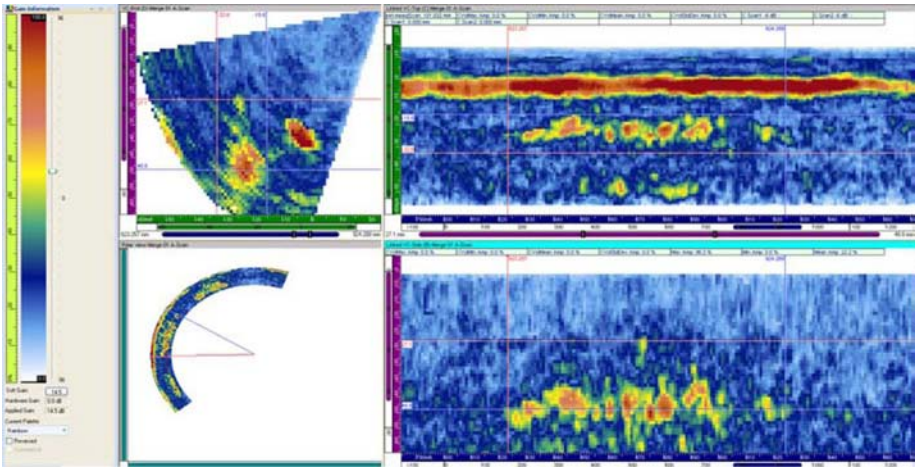

Figure E.13. Specimen 8C-036 Flaw 5 Line Scan Data at 1.5 MHz

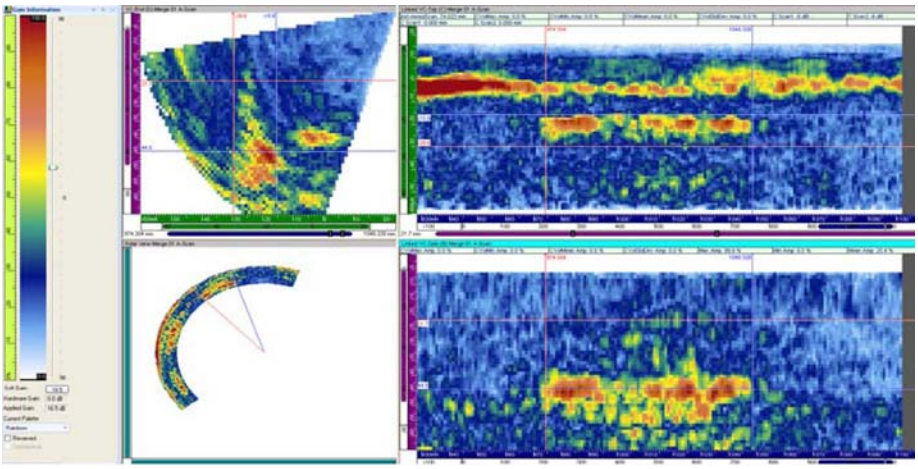

Figure E.14. Specimen 8C-036 Flaw 6 Line Scan Data at 1.5 MHz

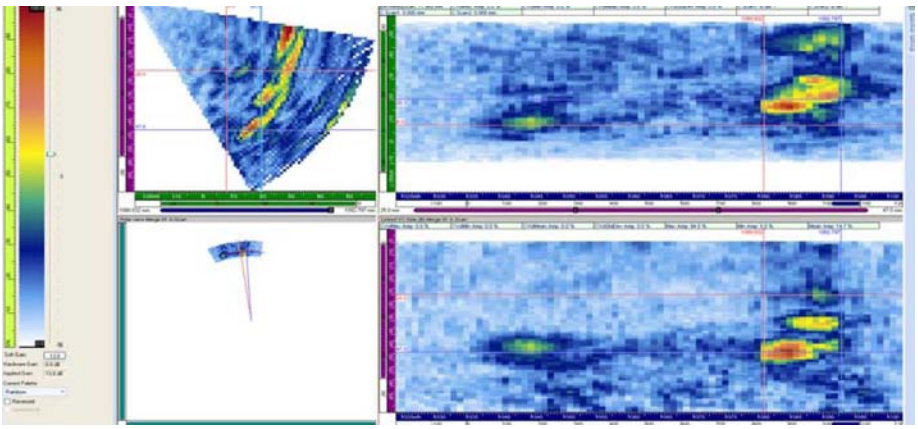

Figure E.15. Specimen 8C-036 Flaw 7 Line Scan Data at 1.5 MHz

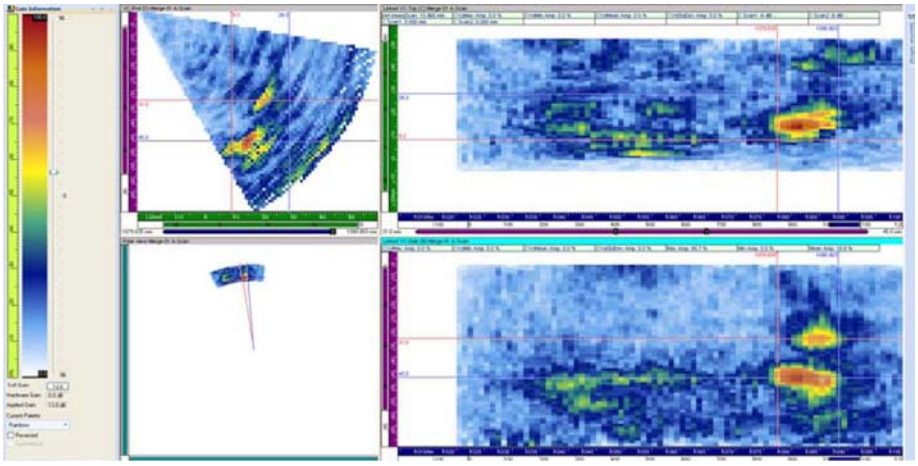

Figure E.16. Specimen 8C-036 Flaw 8 Line Scan Data at 1.5 MHz

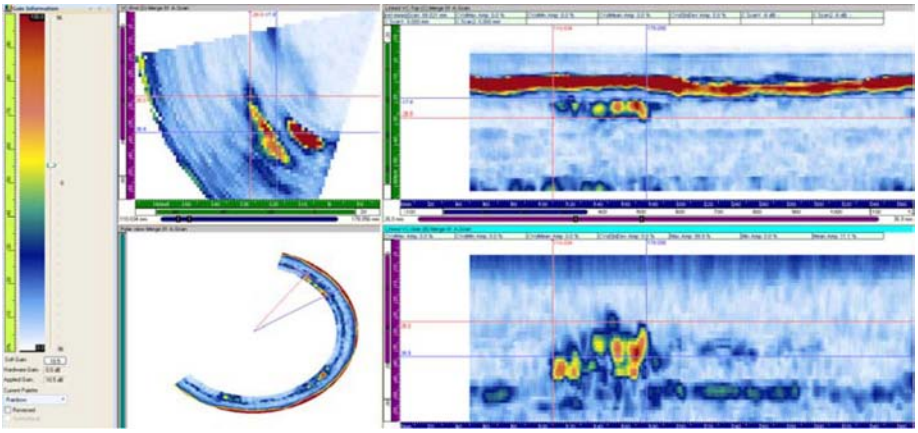

Figure E.17. Specimen 8C-036 Flaw 1 Line Scan Data at 2 MHz

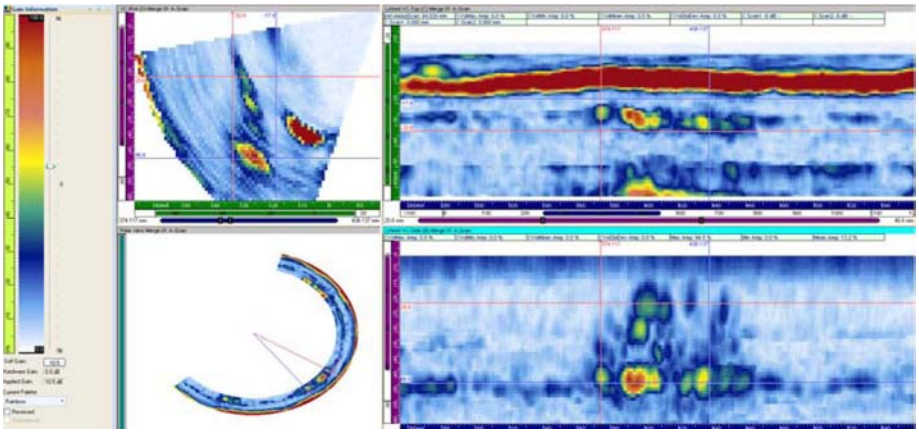

Figure E.18. Specimen 8C-036 Flaw 2 Line Scan Data at 2 MHz

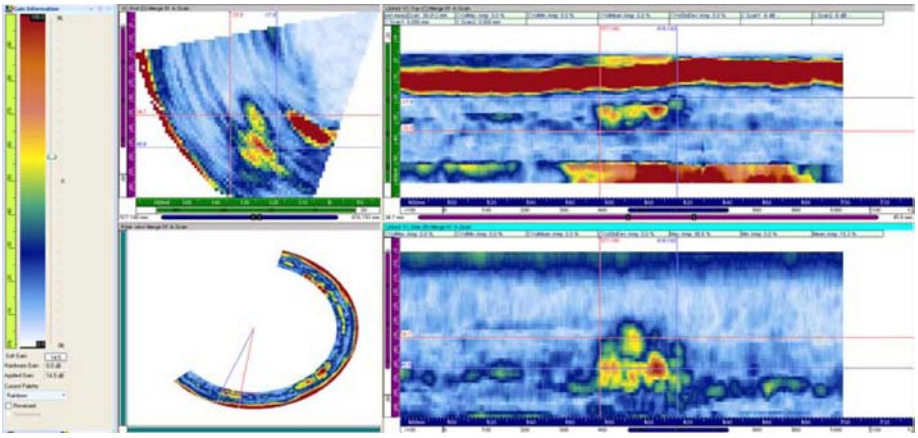

Figure E.19. Specimen 8C-036 Flaw 3 Line Scan Data at 2 MHz

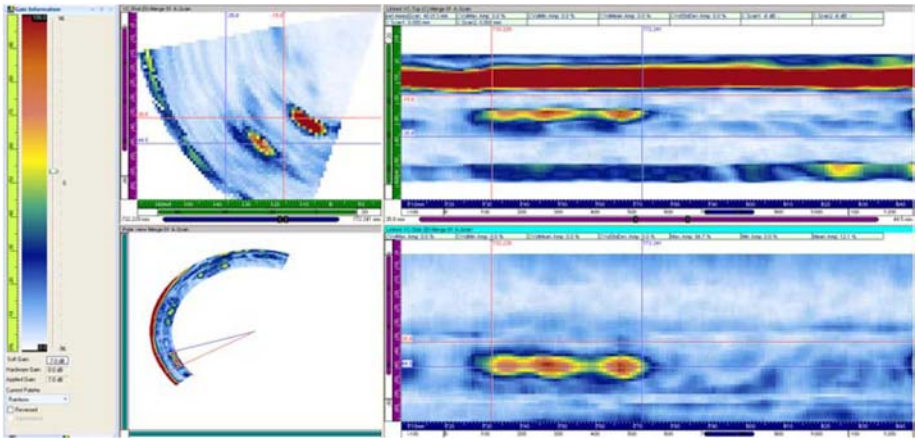

Figure E.20. Specimen 8C-036 Flaw 4 Line Scan Data at 2 MHz

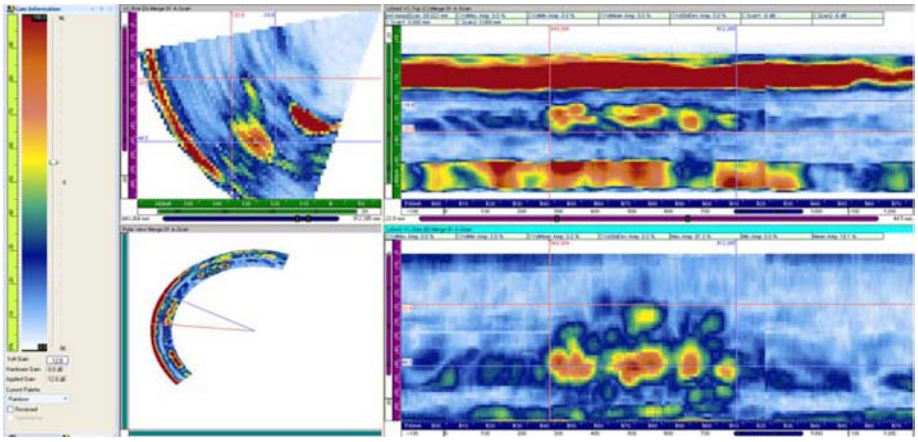

Figure E.21. Specimen 8C-036 Flaw 5 Line Scan Data at 2 MHz

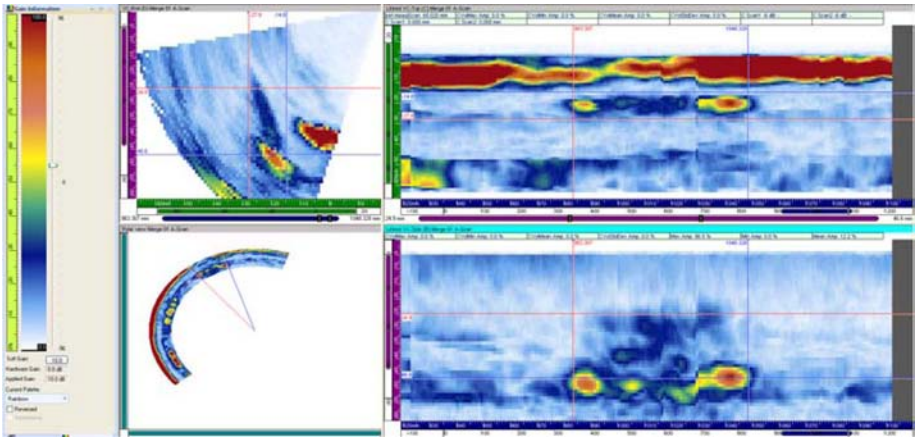

Figure E.22. Specimen 8C-036 Flaw 6 Line Scan Data at 2 MHz

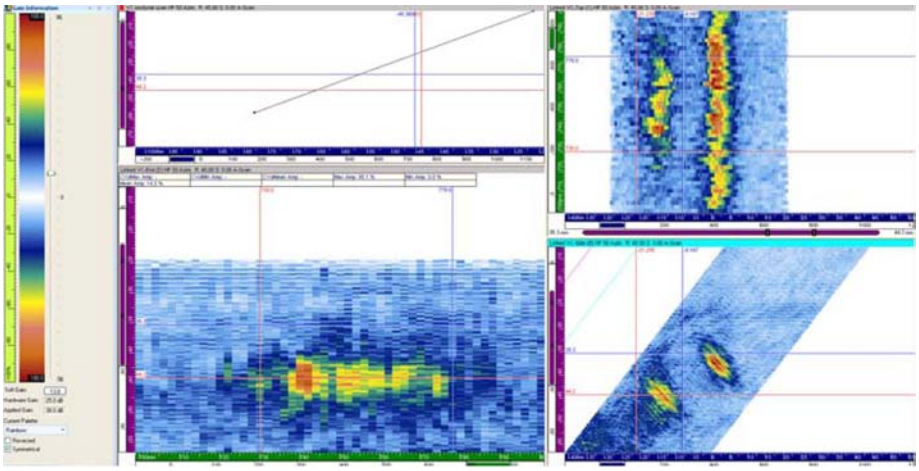

Figure E.23. Specimen 8C-036 Flaw 4 at 1.5 MHz

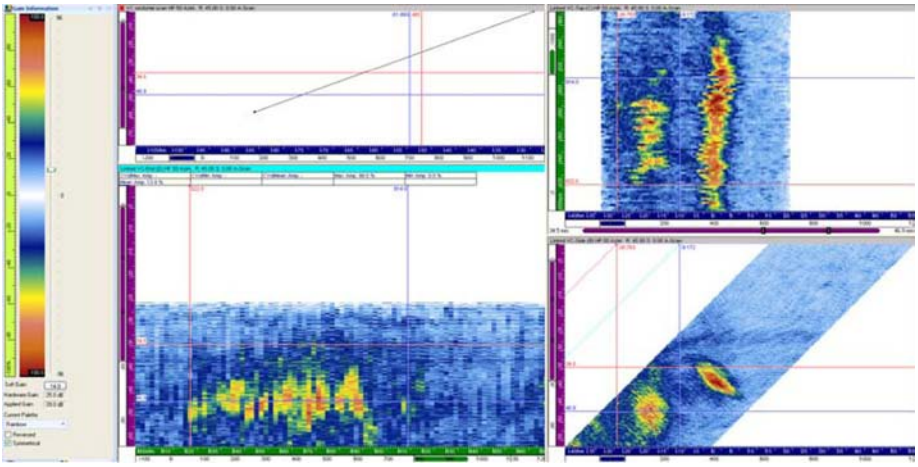

Figure E.24. Specimen 8C-036 Flaw 5 at 1.5 MHz

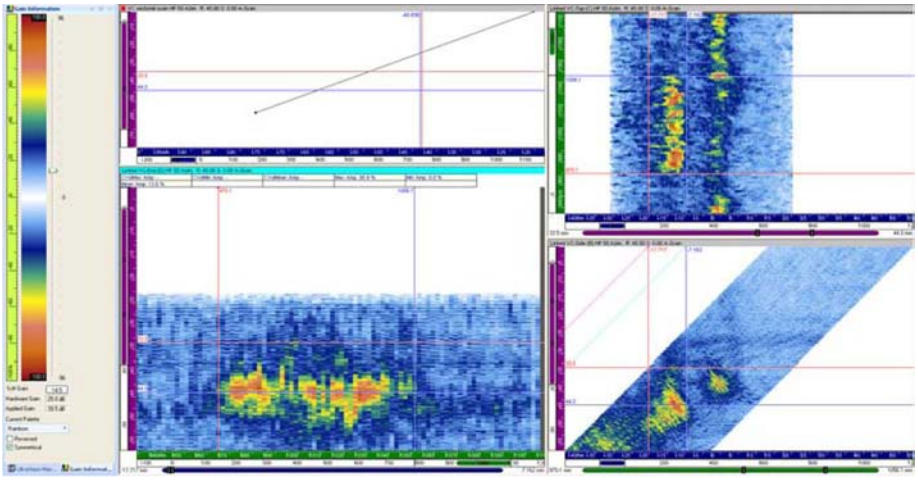

Figure E.25. Specimen 8C-036 Flaw 6 at 1.5 MHz

Pacific Northwest
NATIONAL LABORATORY

U.S. DEPARTMENT OF
ENERGY

Proudly Operated by Battelle *Since 1965*

902 Battelle Boulevard
P.O. Box 999
Richland, WA 99352
1-888-375-PNNL (7665)
www.pnl.gov